Table of contents

1. Introduction

Hearing, or auditory perception, is technically the ability to perceive sound by detecting vibrations, changes in the pressure of the surrounding medium through time, through the ear. But socially - hearing is an important tool for connection people to one another and to the environment around. Every day, we are exposed to variety of sounds. It can be sounds of bird chirping, rustling of leaves, traffic on the road, voices, music. Most environmental sounds are not pure tones, but combinations of various frequencies at various amplitudes and intensities, frequency- and amplitude-modulated sounds. The main task for the brain is to analyse these complex sounds and to identify them as words, song, dog's barking and so on.

The sound information propagates from the cochlea via the auditory nerve to the brainstem auditory nuclei and then projected to the inferior colliculus in the midbrain tectum, which in turn projects to the medial geniculate nucleus, a part of the thalamus where sound information is relayed to the auditory cortex in the temporal lobe. Each relay of the auditory pathway has a complex structure, incorporates several subnuclei with a network of local interconnections; and does a specific work of decoding and integration. So from the lower divisions of auditory pathway auditory cortex receives the profiles of different frequencies and different intensities and recognizes them the as a particular pattern, for example voice or particular musical instrument. Especially sophisticated task is an understanding of speech, which depends on the proper processing of sensory information in the association areas of the temporal lobe and auditory cortex.

The auditory efferent system that comprises several descending pathways originating at the auditory cortex and targets a wide range of subcortical nuclei, is assigned to the range of different functions: balancing of interaural cochlear sensitivity (Darrow et al., 2006), modulation of cochlear responses during selective attention (Terreros and Delano, 2015), neural plasticity during learning of behaviorally relevant auditory tasks (Bajo et al., 2010), protection to acoustic trauma (Maison and Liberman, 2000) and antimasking of auditory stimuli in a noisy environment (Kawase and Liberman, 1993).

During the postnatal development, functional and morphological properties of the brain are continuously shaped by the interactions of genetic and environmental factors. Neural plasticity allows the brain to adapt to changes in the environment from its embryonic stages to the last minute of life. It takes place in our everyday life and determines the functional organization and reorganization of the brain tissues (Yan, 2003). Cortical plasticity, as in other sensory systems, plays important role in the fine tuning of the auditory system. For

example, early musical training leads to an expansion in the representation of complex harmonic sounds in the auditory cortex. Similarly, the early phonetic environment has a strong influence on speech development and, presumably, on the cortical processing of speech (Rauschecker, 1999).

This thesis is aimed to reveal functional properties and developmental plasticity of the auditory cortex in rats, frequently used animal model in the hearing research. Firstly, we compare intrinsic electrical properties of neurons in the core and belt subdivisions of the auditory cortex in rats. Afterwards, we investigate functional role of the cortico-collicular projections on neuronal activity in the inferior colliculus using a reversible AC inactivation. And finally, we study the possible effect of complex acoustic environment presented during the maturation of the auditory system on the responses of adult auditory cortex neurons. We believe that our results will contribute to better understanding about signal processing within the AC circuits and to awareness about the impact of the complex acoustical stimulation during developmental period on the formation of the auditory system.

1.1. Auditory cortex organization

1.1.1. Anatomy of human auditory cortex (AC)

In human the AC is located in the temporal area just below the lateral (Sylvian) fissure, largely involving the transverse temporal (Heschl's) gyrus and the posterior two-thirds of the superior temporal gyrus (Fig. 1) and like other sensory cortices has several subdivisions. The traditional view on the auditory cortex distinguishes between the primary auditory and auditory association cortices (Gelfand, 2010): area 41 (in the classic Brodmann classification system) is the primary site (AI) and Brodmann's area 42 is the auditory association area (AII) - located more rostrally in the temporal lobe. Together, Brodmann's areas 41 and 42 receive projections from the medial geniculate nucleus. The tonotopic organization of the auditory pathway (gradient in the representation of sound frequencies driving the neurons), which arises in the cochlea and keeps thought the all auditory relay nuclei, is maintained in the AC areas AI and AII. Secondary auditory areas include: Wernicke's area (Brodmann's area 22) (Fig. 1), which is important for the interpretation of the spoken word (Siegel and Sapru, 2011) and Broca's area (Brodmann's areas 44 and 45) in the inferior frontal gyrus functionally linked to speech production.

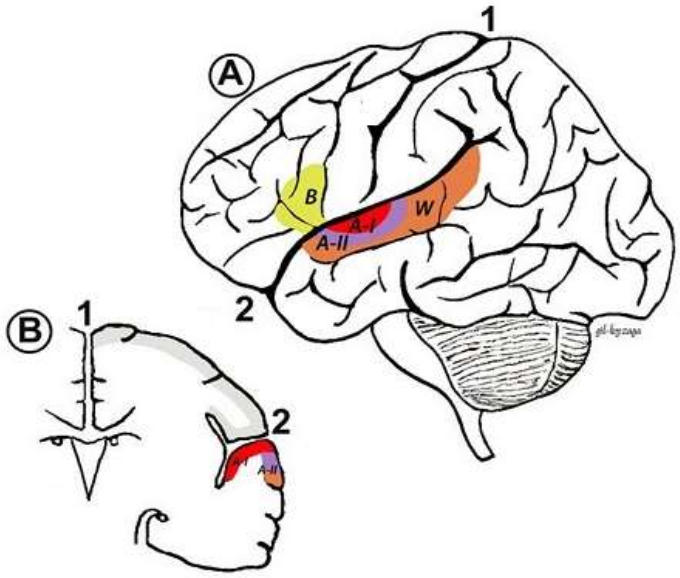

Fig.1 **Anatomical distribution of the auditory cortex**. A - Lateral view showing the distribution of AI and AII, Wernicke's area (W) and Broca's area (B); B - Frontal view showing AI inside the Sylvian fissure and Heschl's gyrus. 1 - Interhemispherical fissure. 2 - Sylvian fissure. Modified from Pujol and Irving (2016).

Wallace et al. (2002) in their complex histochemical study used staining methods for cytochrome oxidase, acetylcholinesterase (AChE) and parvalbumin. They integrated previous works of Hutsler and Gazzaniga (1996) and Rivier and Clarke (1997) and identified within human AC two core regions surrounded by six belt regions (Fig. 2). The core regions are include the primary auditory area (AI) involving the posteriomedial two-thirds of Heschl's gyrus, and a narrow lateroposterior area (LP) adjacent to it and adjoining Heschl's sulcus. Within the belt region were defined 6 subdivisions: ALA, anterolateral area; AA, anterior area; MA, medial area; LA, lateral area (lateral to LP); PA, posterior area; STA, superior temporal area (Fig. 2).

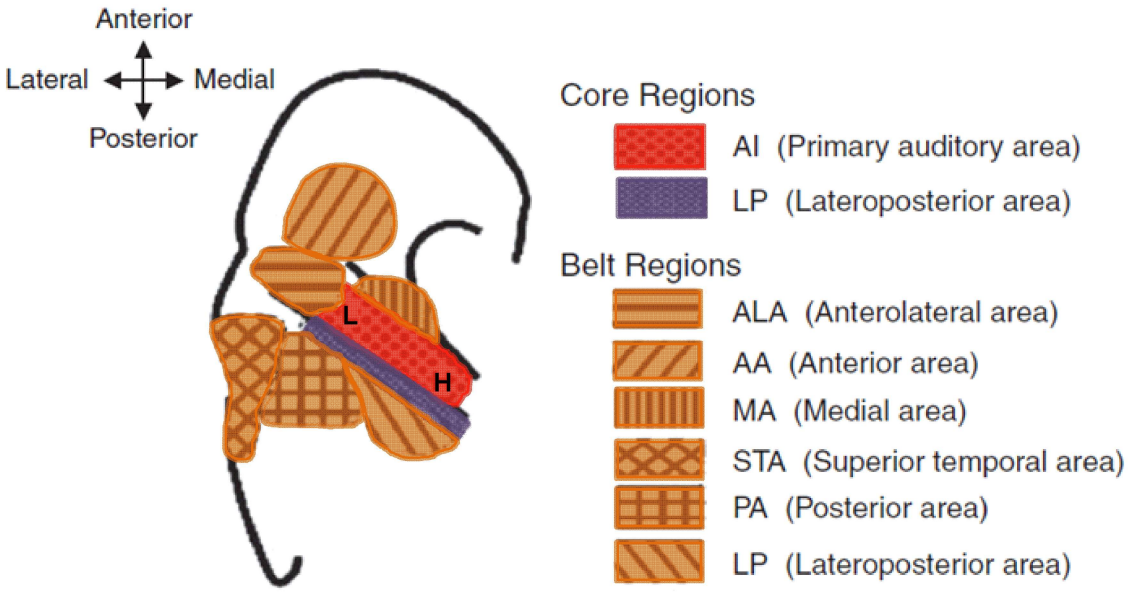

Fig. 2 **Summary diagram of auditory areas on the superior temporal plane**. The core auditory areas: AI, primary auditory area (red) and LP, lateroposterior area (violet). The tonotopic gradient within AI is from low (L) to high (H). The belt areas (orange): ALA, anterolateral area; AA, anterior area; MA, medial area; LA, lateral area (lateral to LP); PA, posterior area; STA, superior temporal area. Modified from Wallace et al. (2002).

The primary auditory area was distinguished by a dense band of cytochrome oxidase activity in layer IV and the base of layer III, as well as a relatively thick, pale layer V and VI. Layers V and VI together made up 40% of the cortical thickness. Acetylcholinesterase (AChE)-containing pyramidal cells were sparsely distributed within the primary auditory area. Lateroposterior area, the part of the auditory core, showed a band of high cytochrome oxidase activity and bands of high parvalbumin immunoreactivity and AChE activity in layer IV. The auditory belt areas did not have a clear band of high cytochrome oxidase activity but contained a moderately high density of AChE-containing pyramidal cells.

1.1.2. Mammalian auditory cortex

Primates are thought to be the closest animal model to the human brain organization. AC in primates has traditionally been divided into three cytoarchitectonic fields: Brodmann areas 41, 42, and 22. Kaas and Hackett (1998) correlated the architectonic features of AC to tone frequency maps and patterns of connections for description of the macaque monkey AC organization. They distinguished three primary-like areas within area 41, each with a discrete

pattern of tonotopic organization and direct inputs from the ventral division of the medial geniculate complex. These three core areas are interconnected and project to a narrow surrounding belt of seven areas which receive thalamic input mostly from the dorsal divisions of the medial geniculate complex. The belt areas connect to a lateral parabelt region that does not have direct connections with the core and the ventral part of the medial geniculate complex. The parabelt fields are linked to more distant cortex in the superior temporal gyrus, superior temporal sulcus, and the prefrontal cortex (Fig. 3).

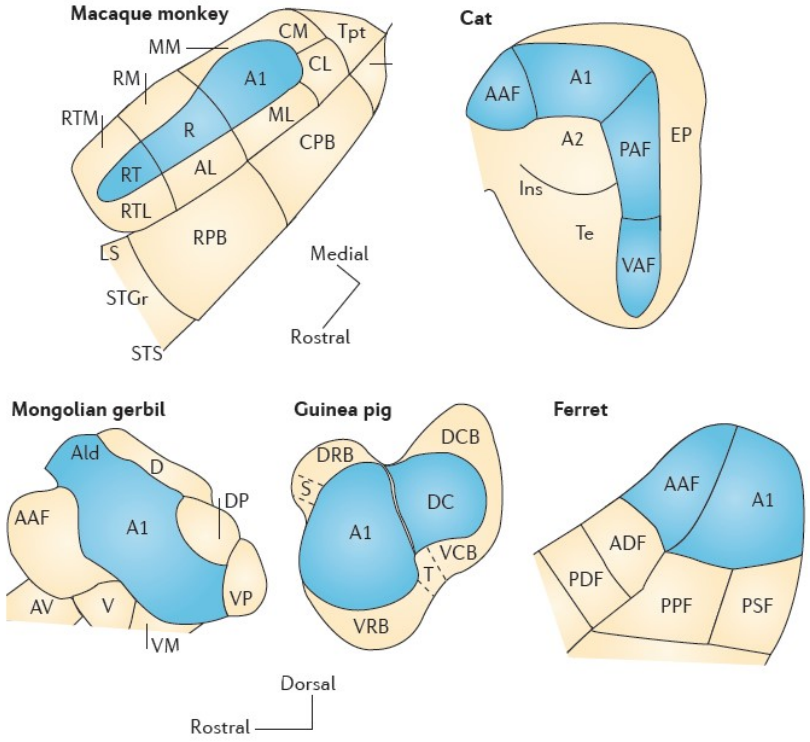

Fig. 3 **A schematic representation of the organization of the AC in different animals.** Core regions of the AC (blue shading), including the primary auditory cortex (A1). (AAF, anterior auditory field; ADF, anterior dorsal field; Ald, dorsal region of the primary auditory field; AV, anteroventral field; CL, caudolateral belt region of the AC; CM, caudomedial area; CPB, caudal parabelt; CS, central sulcus; D, dorsal field; DC, dorsocaudal field; DCB, dorsocaudal belt; DLPFC, dorsolateral prefrontal cortex; DP, dorsoposterior field; DRB, dorsorostral belt; EP, ectosylvian posterior auditory region; IFC, inferior frontal cortex; Ins, insula; IPL, intraparietal lobule; IPS, intraparietal sulcus; LS, lateral sulcus; MM, mediomedial belt; PAF, posterior auditory field; PDF, posterior dorsal field; PMC, premotor cortex; PPF, posterior pseudosylvian field; PSF, posterior suprasylvian field; RM, rostromedial belt; RPB, rostral parabelt; RTL, rostrotemporal lateral belt; RTM,

rostrotemporal medial belt; SRAF, suprarhinal auditory field; STGr, superior temporal gyrus rostral to the parabelt; STS, superior temporal sulcus; T, transitional belt area; Te, temporal; Tpt, temporal lobe association cortex; V, ventral field; VAF, ventral auditory field; VCB, ventrocaudal belt; VLPFC, ventrolateral prefrontal cortex; VM, ventromedial field; VP, ventroposterior field; VRB, ventrorostral belt). Modified from Kaas and Hackett (1998) and Bizley and Cohen (2013).

Similar organizational scheme was found in the other mammal species: cats (Heil et al., 1994), ferrets (Bizley et al., 2005), guinnea pigs (Wallace et al., 2000), mongolian gerbils (Thomas et al., 1993), mouse (Stiebler et al., 1997) and rats (Sally and Kelly, 1988, Profant et al., 2013, Rutkowski et al., 2003); with centrally located tonotopically organized core region, and the secondary areas assigned to belt or parabelt regions, which tend to be located around the core (Fig. 3).

1.1.3. Auditory cortex organization in rat

Despite interspecies differences, the rat AC shares many common anatomical and physiological features with other species, including primary and nonprimary regions (Nieto-Diego and Malmierca, 2016). Based on the differences in the degree of myelination, three subdivisions in the AC of rats were identified: the core region - Te1, with the highest level of myelination (Zilles et al., 1980), and the secondary areas Te2 and Te3 forming a ring-like belt around Te1 (Zilles and Wree, 1985) corresponding to the Brodmann areas in the human AC.

Detailed electrophysiological mapping studies have identified up to five tonotopically organized fields, forming a core region of the rat AC: primary cortex (A1), the anterior auditory field (AAF) (Kalatsky et al., 2005, Profant et al., 2013, Rutkowski et al., 2003, Polley et al., 2007, Sally and Kelly, 1988), the ventral auditory field (VAF) (Polley et al., 2007, Kalatsky et al., 2005), the posterior auditory field (PAF) (Pandya et al., 2008), located in the dorsocaudal border of A1, and the suprarhinal auditory field (SRAF), in the ventral margin of the auditory cortex (Profant et al., 2013, Polley et al., 2007) (Fig. 4).

The core fields are surrounded by a non-tonotopically organized belt area (Fig.4) (Profant et al., 2013, Rutkowski et al., 2003), on some studies divided into three parts: posterodorsal (PDB), dorsal (DB) and anterodorsal (ADB) belt fields (Rutkowki et al., 2003).

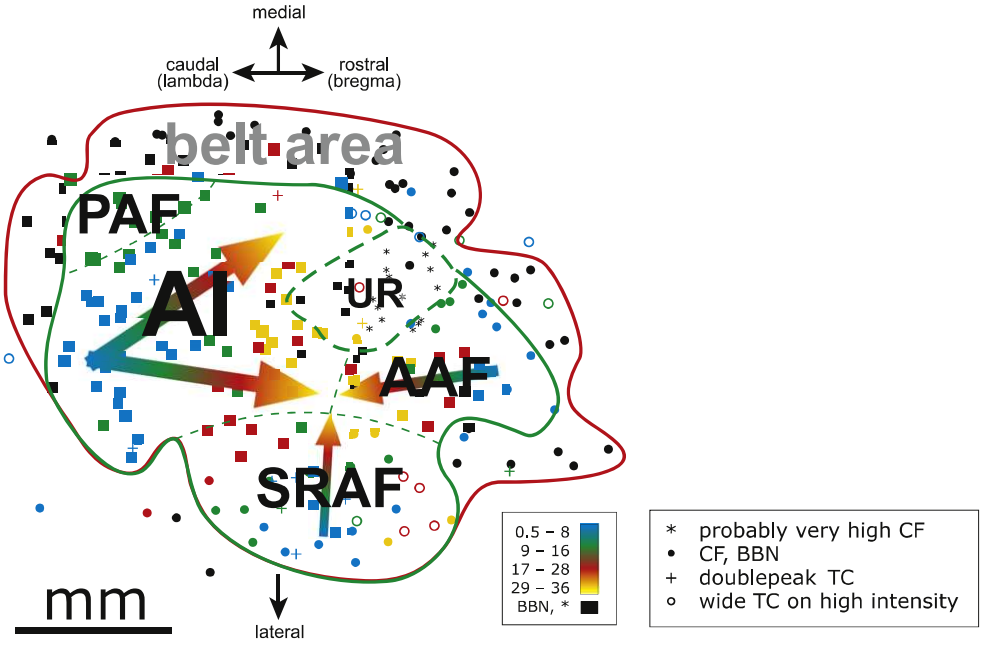

Fig. 4 **Map of the different fields in the right AC based on characteristic frequencies (CF)**. An example of an individual map of a recorded CF from the right AC. The black dots represent recording sites where neurons responded only to broad band noise (BBN) stimulation, and + represents a penetration with no response to BBN or to pure tone stimulation. Modified from Profant et al. (2013).

1.1.4. Response patterns of auditory cortical neurons

Animal models enable functional studies of properties of individual neurons or neuronal networks at various levels of auditory pathway.

Pure tone-evoked excitatory responses of neurons in both A1 and AAF AC areas are characterized by short latencies and sharp tuning (Polley et al., 2007, Recanzone, 2000) with well defined CF. When stimulated by BBN these neurons respond mostly by the pure-onset spiking pattern (Fig. 5) (Profant et al., 2013). Responses of neurons in SRAF and PAF AC areas are characterized by longer latencies, broadly tuned responses (Polley et al., 2007) with the higher concentration of the onset-sustained response pattern then in other AC fields (Profant et al., 2013). Neurons in the belt area show either very poor or no responses to pure tones (Fig. 5), whilst they strongly respond to complex sounds, BBN, frequency modulated sweeps and natural vocalizations (Tian and Rauschecker, 2004, Rutkowski et al., 2003). Their responses are characterized by the longest response latencies and increased representation of the sustained and late-onset response patterns (Profant et al., 2013).

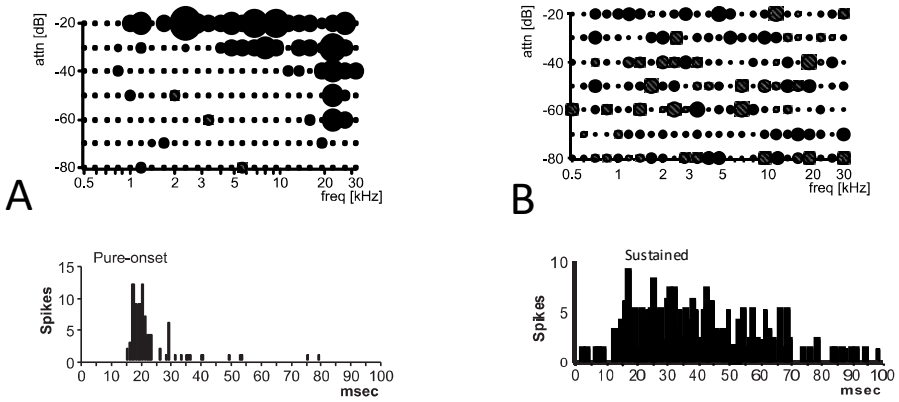

Fig. 5 **Examples of different response patterns of neurons in the rat AC**. The frequency response area – upper panel and poststimulus time histograms constructed from the neuronal responses to BBN bursts– lower panel. In the AI (**A**) neurons show a sharply tuned tuning curve with a clear characteristic frequency and prevalence of the pure-onset response pattern, while a response to pure tones was absent in the belt area (**B**), and neurons showed higher representation of the sustained response patterns. Modified from Profant et al. (2013).

1.1.5. Laminar organization of auditory cortex

Like all receptive cortical areas, AC is a part of the koniocortex, or granular cortex (Kahle et al., 2003) and contain six layers. Superficial layer I is the molecular layer, which contains very few neurons; layer II the external granular layer; layer III the external pyramidal layer; layer IV the internal granular layer; layer V the internal pyramidal layer; and layer VI the multiform, or fusiform layer. Each cortical layer contains various neuronal cell types differing in their shapes, sizes and density, as well as different organizations of nerve fibers (Fig. 6) (Swenson, 2006).

Several cell types have been identified in the mammalian AC (Fig. 6). Pyramidal cells are the main cell type within layers II-III and V. These cells have the conic shaped soma, with an apical dendrite that extends all the way to layer I of the cortex. The thin axon that arises from the base of this pyramidal cell has collaterals and a long process that leaves the cortex. In contrast to other sensory cortexes, stellate or granule cells are not the most prominent in layer IV of the AC, but the small pyramidal cells (Smith and Populin, 2001, Fitzpatrick and Henson, 1994, Winer, 1984). Axons of these cells stay within the cortex. There are several less common cell types including horizontal cells, fusiform cells and the cells of Martinotti occurring in the AC (Swenson, 2006).

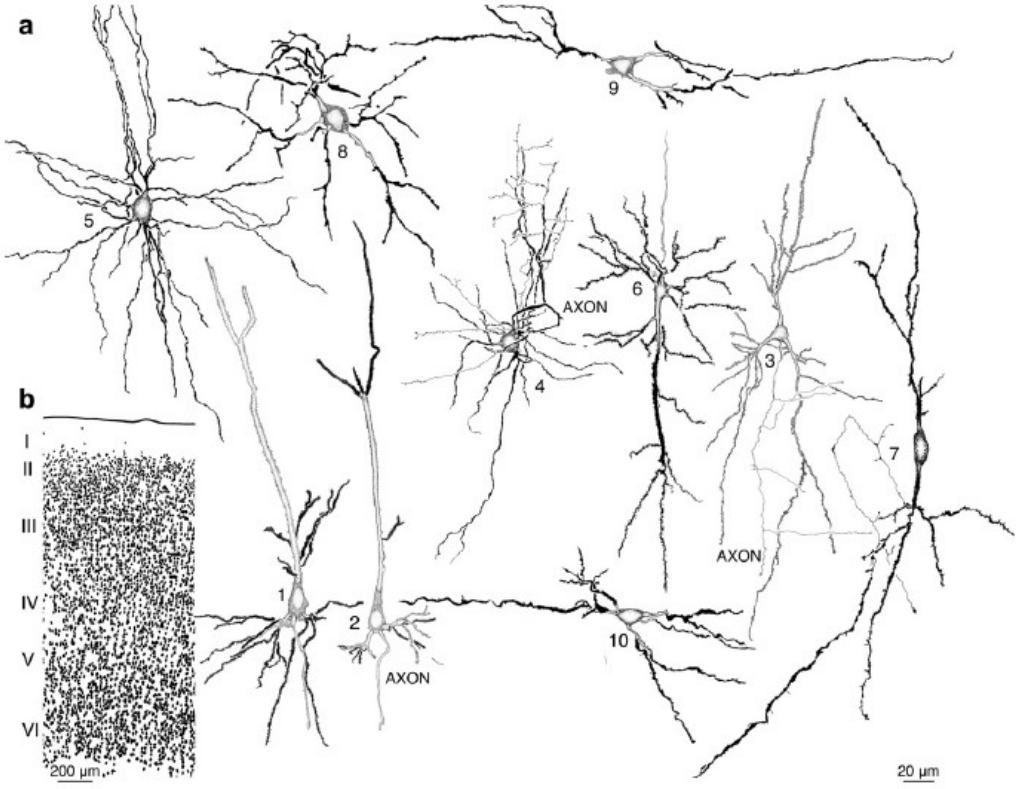

Fig. 6 (**a**) Major cell types of cat primary auditory cortex include glutamatergic pyramidal cells (1–3), GABAergic basket (4) and multipolar (5) neurons, spinous inverted pyramidal cells (6), bipolar cells (7), small multipolar neurons (8), and horizontal cells in layers I (9) and VI (10), Golgi-Cox impregnation; (**b**) AC cytoarchitecture shows a prominent layer I, a dense concentration of layer II cells, smaller layer IV cells, and columnar somatic arrangements in deeper layers, Nissl preparation. Modified from Winer and Lee (2007).

The core and belt areas of AC show some differences in their architectonical patterns (Fig. 7). The belt is characterized by a lower density of myelinated fibers compared to the core AC (Fig. 7). Furthermore, the layer IV of core is more prominent than that from the belt region (Zilles and Wree, 1985).

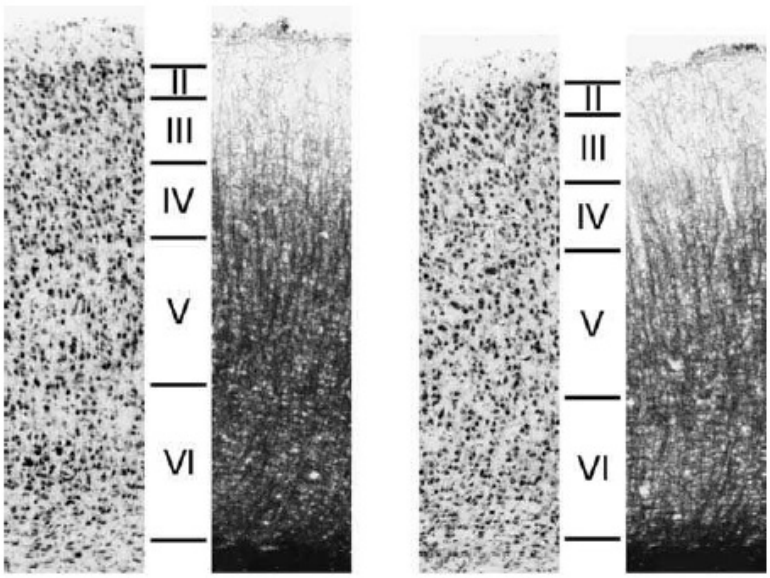

Fig. 7 **Cyto- and myeloarchitectonical structure of the temporal isocortical areas**: primary AC on the **left** and belt AC field on the **right**. Roman numerals indicate cortical layers. Modified from Paxinos (2004).

Functionally, the layers of the cerebral cortex can be divided into three parts. The supragranular layers comprise layers I to III. These layers are the primary origin and termination of intracortical connections, which are either associational (i.e. with other areas of the same hemisphere), or commissural (i.e. connections to the opposite hemisphere, primarily through the corpus callosum). The internal granular layer - comprises the layer IV and receives thalamocortical connections, especially from the specific thalamic nuclei. The infragranular layers, layers V and VI, primarily connect the cerebral cortex with subcortical regions and establishes links to ipsilateral secondary areas of the auditory cortex as well as to contralateral AI, medial geniculate body (MGB) and inferior colliculus (IC) (Fig. 8) (Bannister, 2005, Swenson, 2006, Linden and Schreiner, 2003). Within the core AC area, the supragranular layers show a higher cell density than the infragranular ones. Layers V–VI of the core AC region have a lower packing density than those of the belt (Paxinos, 2004).

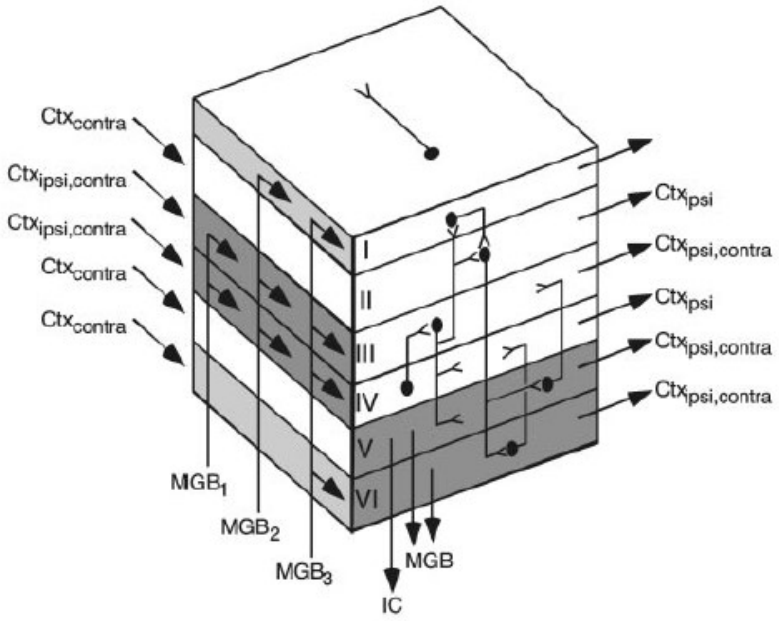

Fig. 8 **Anatomical connections within a column of primary auditory cortex**. Left face of cube shows thalamic and corticocortical inputs; right face displays interlaminar connections as well as thalamic, collicular, and corticocortical outputs. Shading indicates layers that receive thalamocortical input (left) or produce corticothalamic and corticocollicular outputs (right). Lemniscal thalamic inputs (MGB_1) end only in layers III and IV, while nonlemniscal inputs also activate layer I (MGB_2) or layers I and VI (MGB_3). Corticocortical inputs and outputs: ipsilateral - Ctx_{ipsi} or contralateral - Ctx_{contra} or both - $Ctx_{ipsi,contra}$. Modified from Linden and Schreiner (2003).

There is complex intracortical flow of information through the layers of the AC (Fig. 9). Cells in the layer IV, which receive inputs from sub-cortical areas, project upward to the layer III while cells in the layer I send projections to the layer II. Cells in layer III project to layers I, II, IV and V as well as ipsilateral secondary areas and contralateral auditory cortex via the corpus callosum. Cells in layer II receive primary inputs from layers I and III and then synapse onto cells in layers V and VI (Mitani and Shimokouchi, 1985, Mitani et al., 1985).

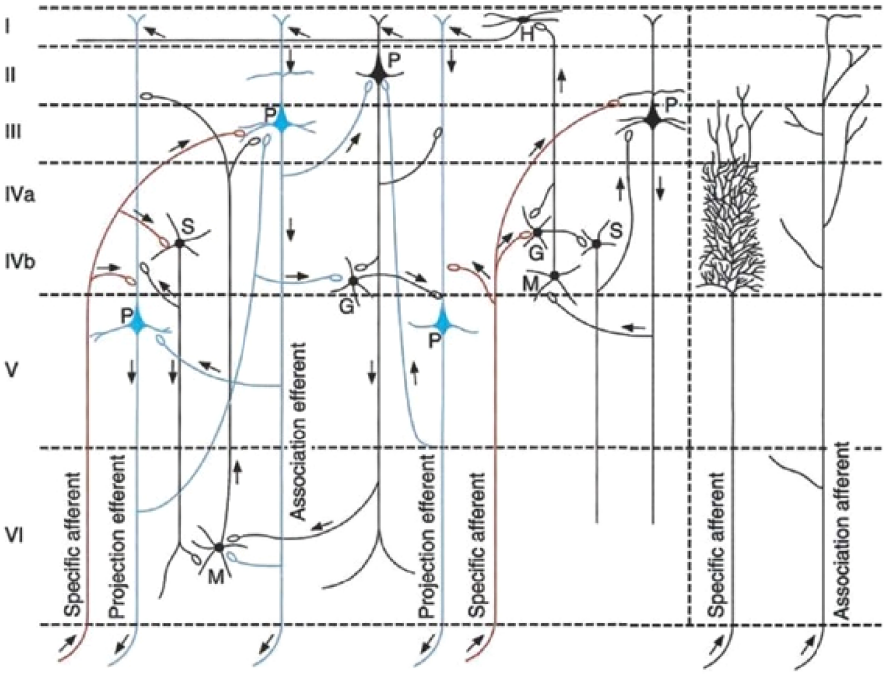

Fig. 9 **Intracortical circuits in the neocortex**. Loops depicted the synaptic connections of afferent fiber projections - origins of the efferent projections, and the origins of intracortical connections within a given column. G = granule cell; H = horizontal cell; M = Martinotti cell; P = pyramidal cell; S = stellate cell. Arrows indicate direction of information flow. Modified from *http://what-when-how.com/neuroscience/the-thalamus-and-cerebral-cortex-integrative-systems-part-1/.*

1.1.6. Distribution of neurotransmitter receptors in the auditory cortex

Zilles et al. in their works (2002a, 2002b) described distribution of the nineteen different receptors in the human brain slices by incubating the sections in solutions of specific tritiated receptor ligands. Glutamate and y-aminobutyric acid (GABA) represents the main mediators of excitatory and inhibitory synaptic transmission in the AC (Aramakis et al., 1997). Synaptically released glutamate induces excitatory postsynaptic currents (EPSCs) in AC neurons, which are mediated by both AMPA (α-amino-3-hydroxy-5-methyl-4-isoxazolepropionic acid)/kainate and NMDA subtypes of glutamatergic ionotropic receptors. GABA acts at ionotropic $GABA_A$ receptors, mediating fast inhibitory postsynaptic currents (IPSCs), and at metabotropic $GABA_B$ receptors mediating slow IPSC (Cox et al., 1992). Glutamate is as a primary neurotransmitter in both thalamocortical and corticocortical communication, whereas GABA is found in a variety of neurons that are activated by glutamate. The interplay between glutamatergic and GABAergic transmission is important for regulating the strength of postsynaptic potentials elicited in pyramidal cortical local circuits

(Aramakis et al., 1997). Several electrophysiological studies in animal models describe significant role of GABAergic inhibition in shaping of the frequency receptive fields of auditory cortex neurons (Kaur et al., 2004, Chang et al., 2005).

Activity of cortical circuits is modulated by a variety of substances; one of these substances is acetylcholine (ACh), which in the AC acts mostly as a neuromodulator. Agonists of both ionotropic and metabotropic cholinergic receptors were found to potentiate NMDA receptor mediated slow excitatory postsynaptic potentials (EPSP) and NMDA-induced membrane depolarization, whilst AMPA/kainate-mediated EPSPs are reduced by cholinergic muscarinic receptor activation (Aramakis et al., 1997, Metherate and Hsieh, 2003).

GABAergic synaptic transmission in the AC was observed to be modulated by serotonine 5-HT (5-hydroxytryptamine) receptors. Modulation effects have the 5-HT receptors on the GABAergic synaptic transmission in the AC; they produce a reduction of GABA release via activation of presynaptic 5-HT_{1A} receptors, and modulation of the $GABA_A$ receptor currents through activation of postsynaptic 5-HT_{2A} receptors (Garcia-Oscos et al., 2015). These actions were suggested that 5-HT receptors play a role in different types of cortical long term plasticity (Dringenberg et al., 2014) and could be involved into processes related to attention, task related processing of auditory information, and the formation of acoustic signal memories relevant for behavior (Jaaskelainen and Ahveninen, 2014, Scheich et al., 2011, Garcia-Oscos et al., 2015).

Presence of the noradrenergic receptors indicates embodying of the AC into the complex circuits with neuromodulary effects, which play role in the formation of the long time plasticity adjusting the gains of cortical synapses in a task-dependent manner (Martins and Froemke, 2015, Manunta and Edeline, 2004) and may facilitate the formation of task-specific behavioral patterns (Aston-Jones and Cohen, 2005).

Different areal distribution of the neurotransmitters was revealed in the AC. Muscarinic M2, nicotinic, $GABA_A$, α_2 adrenoreceptors and 5-HT_2 receptors showed higher densities in the primary than in the secondary AC fields (Mai and Paxinos, 2011, Heil et al., 2005, Zilles et al., 2002a). $GABA_B$ receptors showed uniform distribution in AC areas (Sacco et al., 2009)

1.1.7. Hyperpolarization-activated cyclic nucleotide-gated (HCN) cation channels

Regarding the control of neuronal excitability, hyperpolarization-activated cyclic nucleotide-gated (HCN) cation channels are of special interest. These channels are activated upon hyperpolarization of membrane potential, conduct an inward, excitatory cation currents ($I_{h)}$ and belong to the superfamily of voltage-gated potassium ion channels (Shah, 2014). HCN channels are encoded by HCN1-4 gene family and have four subtypes, with first two subtypes HCN 1 and HCN 2 primarily expressed in the neocortex (He et al., 2014, Moosmang et al., 1999, Santoro et al., 1998). These subtypes were found mostly on the dendrites of the pyramidal cortical cells and to less extent on somata of pyramidal neurons, additionally in some interneurons subtypes and stellate cells (Nolan et al., 2004, Nolan et al., 2007, Shah, 2014, Biel et al., 2009, Wahl-Schott and Biel, 2009, Aponte et al., 2006, Day et al., 2005). HCN channels open at the potentials more negative than -50 mV, so they are active at the normal resting membrane potentials (RMP) and are permeable to Na^+ and K^+ ions (Shah, 2014, Robinson, 2003, Biel et al., 2009). I_h contributes to several basic physiological processes, including resting membrane conductance and stabilization of resting membrane potential (Magee, 1998, Magee, 1999a, Shah, 2014). Therefore, HCN channels are the key modulators of neuronal excitability and synaptic potential integration (Magee, 1999b, Berger et al., 2001, Berger et al., 2003, Shah, 2014). Activity of the HCN channels depends on the their interactions with inwardly rectifying Kir2.2/2.3 K^+ channels and K^+-selective leak (K_{leak}) channels that are constitutively active, hyperpolarizes the membrane potential and thus reduce deactivation of HCN channels (Day et al., 2005).

There are very few works studying the distribution and function of the HCN channels in the auditory pathway and particular in the AC. Huggenberger et al. (2009) in their study provided the evidence for the presence of I_h throughout all layers of the AC. The highest I_h density was found in the layer II/III. Authors suggest a crucial role of the I_h for the temporal summation and improvement of temporal resolution in the AC pyramidal neurons.

1.2. Auditory cortex connectivity

1.2.1. Afferent auditory pathway

Acoustic information transmitted by the auditory system from the organ Corti in the inner ear to the auditory cortex through multiple pathways, especially in the brain stem, where large auditory nuclei form a complicated network of ipsilateral and contralateral projections (Fig.10), so auditory input from each ear flows to both cerebral hemispheres. These nuclei

through integration of multiple projections and local nerve connections do a specific work of decoding and integration of perceived sound time and space parameters (Pujol and Irving, 2016).

Auditory pathway begins with the first order neurons housed in the spiral (cochlear) ganglion, central processes of its neurons collect to form the auditory cochlear nerve (the cochlear division of the vestibulocochlear nerve, CN VIII) (Patestas and Gartner, 2016). The auditory nerve terminates in all of three divisions of the cochlear nuclei (CN): anterioventral (AVCN), posterioventral (PVCN) and dorsal (DCN), and AVCN are the major nucleus of termination of cochlear nerve fibers. From AVCN arising second order fibers ipsilaterally to the medial and lateral superior olivary nuclei, or decussate and with second fibers from other two CN forming three different separate pathways: dorsal (with DCN), intermediate (with PVCN), and ventral acoustic striae. Most of the fibers that leave CN synapse in the superior olivary complex (SOC), either on the same side or on the opposite side. Crossing fibers are forming a structure known as the trapezoid body, a compact bundle of fibers at the midline in the lower pontine region (Hendelman, 2005). The main function of the SOC is to process auditory information from both ears and to determines the of sound source (Patestas and Gartner, 2016). Fibers outgoing from the SOC form the lateral lemniscus (LL) and ascend through the pons to the IC of the midbrain conveying auditory input from both ears. The inferior colliculi are connected to each other via a small commissure (Hendelman, 2005). IC gives rise to a prominent bundle, the brachium of the inferior colliculus, whose fibers end in the ipsilateral medial geniculate nucleus in the thalamus. Medial geniculate nucleus processes auditory input related to sound intensity and frequency, and transmits it to the AC via fibers forming the auditory radiations (Patestas and Gartner, 2016). Information about sound frequency, known as tonotopic organization, is maintained all along the primary auditory pathway, starting in the cochlea. AC is the highest target of afferent auditory information where acoustical signals, already largely decoded during their passage through the previous neurons in the pathway, are recognized, memorized and perhaps integrated into a voluntary response (Pujol and Irving, 2016). A number of anterograde and retrograde tracing studies have shown that core AC region receives its largest input from the ventral division of the medial geniculate nucleus (vMGN) and minor inputs from the medial and dorsal divisions (mMGN, dMGN) (Roger and Arnault, 1989).

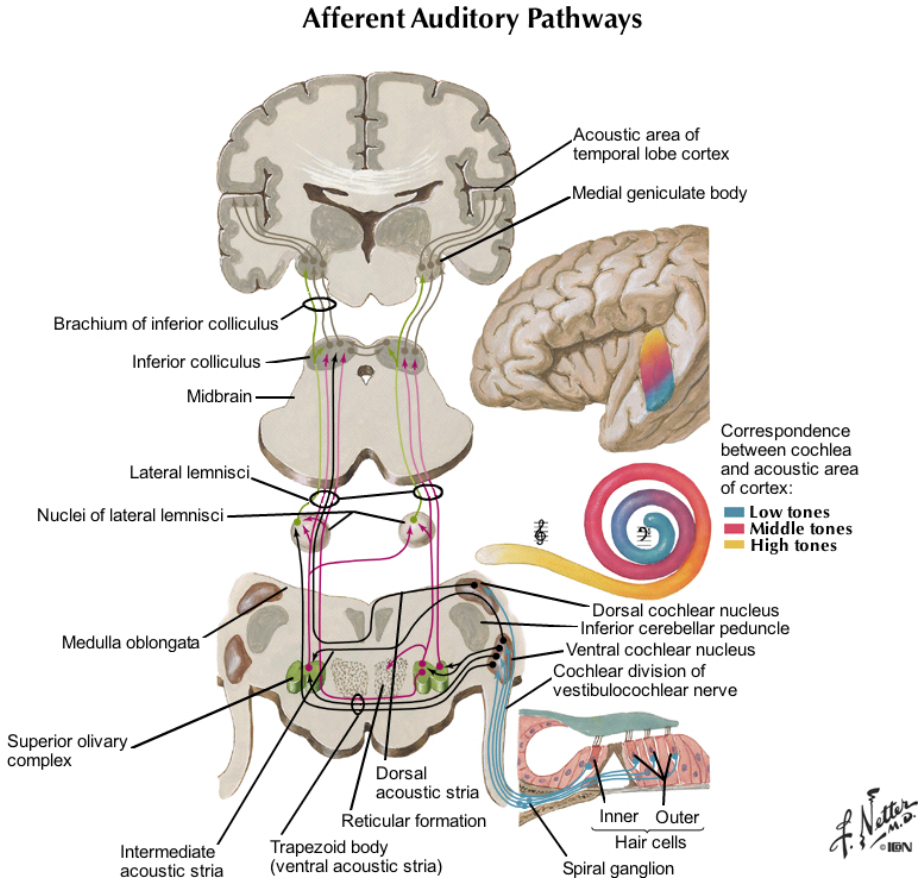

Fig. 10 **Schematic representation of the ascending central auditory pathways**. Modified from Netter (2014).

Non-primary, more diffuse auditory pathways come from the IC through the dorsal division of the MGB (Fig. 12) and multisensory nuclei in the posterior thalamus (de la Mothe et al., 2006, Hackett, 2011) to auditory association cortex - AII, belt area. The polysensory system goes from the IC (including visual and somatosensory inputs) through the medial division of the MGB and project to the anterior auditory field of the cortex, the thalamic reticular nucleus, and the limbic system (Aitkin, 1986, Ehret and Romand, 1997, Møller, 2000).

1.2.2. Descending projections of the AC

The descending pathways (corticofugal system) exist in all sensory systems of the brain. In the auditory system the descending pathway is represented by a very complex, multisynaptic projections originating in the AC, passing through several subcortical and brainstem auditory structures to terminate ultimately on the receptors of the Organ of Corti in the inner ear via the olivocochlear bundle (Warr, 1980, Syka et al., 1988, Ryugo et al., 2010).

The cortical descending projections originate at pyramidal cells in cortical layers V and VI (Fig. 11). AC directly projects to all subcortical levels of the auditory pathway except the cochlea (Fig. 11) (Ryugo et al., 2010). Projections to the MGB and IC are the largest ones so that they have been long time considered as the only projections of AC to lower auditory centers (Ryugo et al., 2010).

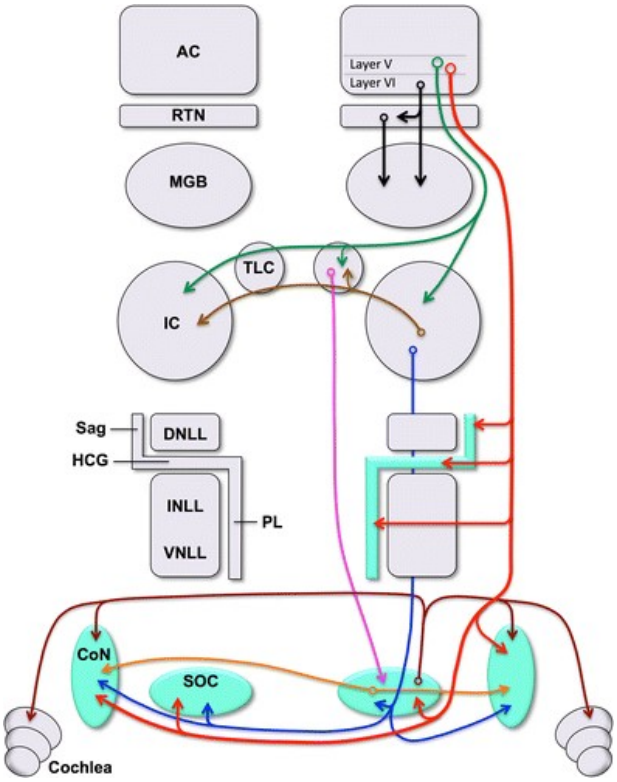

Fig. 11 **Schematic representation of the main descending auditory pathways.** The origin of each projection is represented with an open circle and the targets with arrows. The direct corticosubcollicular projections are depicted in red, and the nuclei innervated by them are highlighted in green. Other descending pathways include: corticothalamic projections (black), corticotectal projections to the IC and the tectal longitudinal column (TLC) (dark green), commissural projections of the IC (brown), descending projections of the IC (blue), projection from the TLC to the superior olivary complex (SOC) (pink), projections from the SOC to the cochlear nuclei (CoN) (orange), and olivocochlear projections (dark crimson). DNLL dorsal nucleus of the lateral lemniscus, HCG horizontal cell group, INLL intermediate nucleus of the lateral lemniscus, PL paralemniscal regions (including the medial paralemniscal nucleus), RTN reticular thalamic nucleus, Sag nucleus sagulum, VNLL ventral nucleus of the lateral lemniscus. Modified from Saldaña (2015).

Development of the tracing methods enabled scientists to reveal a number of new descending projections from AC: to the nucleus sagulum (Sag) and regions surrounding the nuclei of LL (paralemniscal regions) (Saldana, 2015), SOC (Mulders and Robertson, 2000, Doucet et al., 2003), to CN (Weedman and Ryugo, 1996a, Weedman and Ryugo, 1996b, Meltzer and Ryugo, 2006), to pons (Brodal, 1972, Perales et al., 2006) and to basal ganglia (Reale and Imig, 1983) (Fig. 11).

1.2.3. Role of auditory corticofugal systems

Many physiological studies describe modulation roles of descending AC projections in sensory processing. They influence parameters of receptive fields of neurons in subcortical auditory structures: as e.g. threshold, response area, filtering, frequency tuning (Villa et al., 1991, Sun et al., 1996) and response plasticity (Ma and Suga, 2001a, Ma and Suga, 2001b). The corticothalamic system plays a central role in the discharge synchrony modulation (Steriade, 2000).

AC signals directed to premotor structures, basal ganglia and pontine nuclei (Schuller et al., 1991, Beneyto and Prieto, 2001) are integrated into the premotor planning of skeletomotor performance as their output reaches the cerebellum (Winer, 2005). Projections to amygdala (Romanski and Ledoux, 1993) and central grey (Winer, 2005) - targets of the non-primary AC areas, implies a role of the centrifugal projections in control of muscle tone and could therefore influence behavioral reactions such as startle reflexes or milk ejection (Deis and Prilusky, 1984, Yeomans and Frankland, 1995, Yeomans et al., 2002).

1.2.4. Cortico-collicular pathway

Cortico-collicular (CC) projections represent important component of the descending auditory pathway connecting AC with inferior colliculus. The CC system has been previously described as predominantly ipsilateral pathways which mainly target the dorsal (DCIC) and external (ECIC) IC cortices (Diamond et al., 1969, Druga and Syka, 1984a, Druga et al., 1997). Saldana et al. (1996) demonstrated that auditory CC projections also innervate the central nucleus of the IC (CIC) (Fig. 12).

Recent data obtained using sensitive retrograde tracers demonstrate two distinct origins of the CC pathway – a large pathway coming from the cortical layer V and a small pathway (about 10%) coming from the layer VI (Fig. 12) (Schofield, 2009, Slater et al., 2013, Nakamoto et al., 2008). Most of the layer V neurons project ipsilaterally to the IC, smaller

population either contralaterally or bilaterally (Coomes et al., 2005), whereas all layer VI projections terminate ipsilaterally (Schofield, 2009). Quantitative morphometric analyses of showed that layer VI CC projection cells are smaller, have a horizontally oriented very long dendrites that branch profusely both near the soma and distally near the pia; whereas layer V CC projection cells are large pyramidal cells with a long apical dendrite branching mostly near the pial surface (Slater et al., 2013). Within layer V larger pyramidal neurons project to cortical regions of the IC while smaller pyramidal neurons project to the CIC (Malmierca et al., 2015).

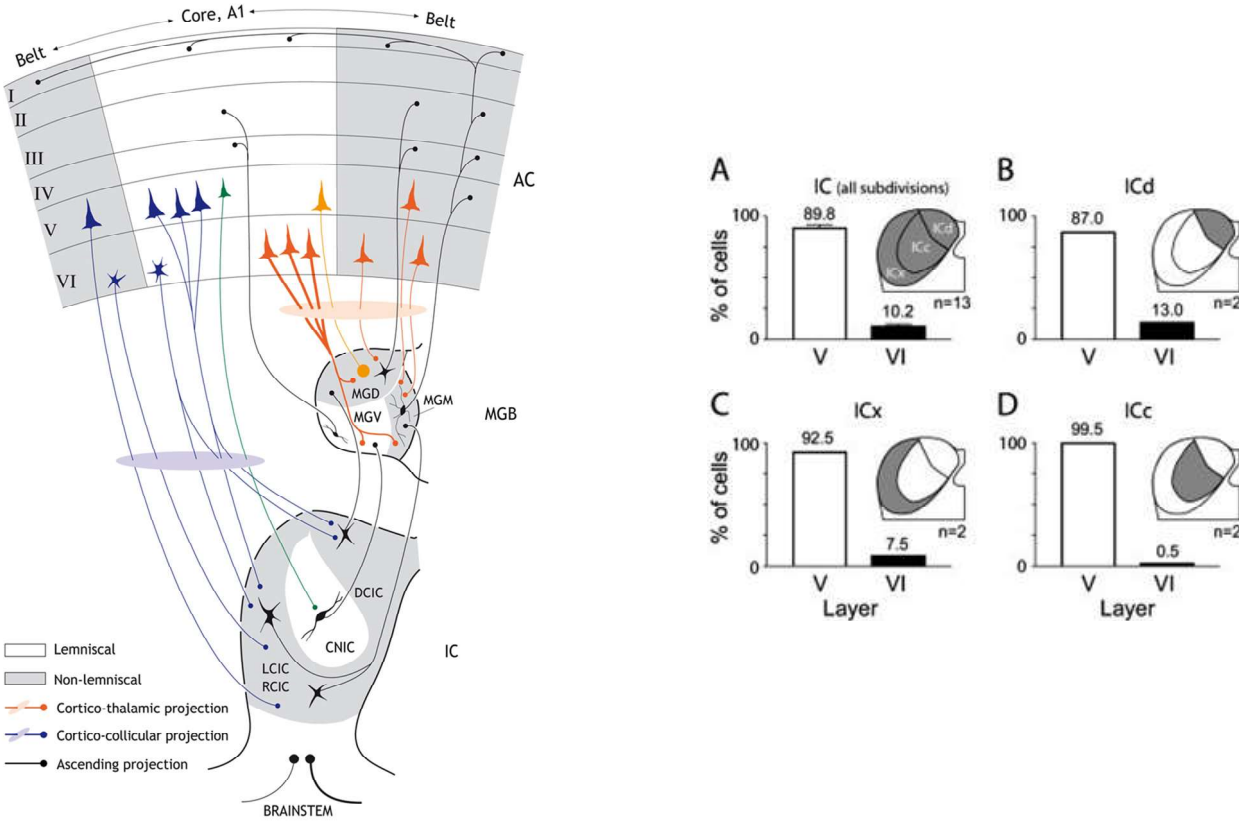

Fig. 12 **Left** – Schematic diagram of major anatomical subdivisions of IC, MGB and AC. It illustrates both ascending and descending pathways from the midbrain up to the cortex and back. Belt divisions are shown as gray areas. Abbreviations: A1, primary AC; CNIC, central nucleus of the IC; DCIC, dorsal cortex of the IC; LCIC, RCIC; lateral and rostral cortex of the IC; MGD; dorsal division of the MGB; MGM; medial division of the MGB; MGV; ventral division of the MGB. Modified from Malmierca et al. (2015).

Right - Bar graphs compare relative number of cells in layer V (white bars) and layer VI (black bars) labeled by retrograde tracer injected into the ipsilateral IC. (A) Overview of

projections to the entire IC (indicated by shading in the IC drawing). Results from small injections restricted to the ICd (dorsal cortex of the IC) (B), ICx (external cortex of the IC) (C) or ICc (central nucleus of the IC) (D). For all panels: numbers above each bar indicate the average percentage, n=number of experiments. Modified from Schofield (2009).

Projections from the core AC region target the collicular cortices bilaterally, with the ipsilateral projections being most dense. Central nucleus of the IC receives weaker but functionally important projections (Fig. 12) (Malmierca et al., 2015). Several studies have shown that projections arising from the primary AC (A1) are tonotopically organized. Low frequency regions of the A1 project to the dorsolateral region of the IC whle the high frequency region of the A1 projects to the ventromedial region of the IC (Straka et al., 2015, Markovitz et al., 2013, Herbert et al., 1991, Bajo et al., 2007). Belt region of AC projects to the lateral and rostral cortices of IC (Malmierca et al., 2015), multisensory intercollicular zone of the IC and has reciprocal connections with cortical areas of different modalities (Herbert et al., 1991). Thus, the belt area may have more associative, multi-modal processing roles compared to core (Rutkowski et al., 2003). Additionally there are also interactions between the core and belt areas of the AC (Fig.12).

Morphological studies have shown that corticofugal fibers are excitatory and glutamatergic (Feliciano and Potashner, 1995). A large proportion of neurons in IC are immunopositive for GABA or its synthesizing enzyme glutamic acid decarboxylase (GAD) (Roberts and Ribak, 1987, Oliver et al., 1994, Merchan et al., 2005). Almost all IC cells have axon collaterals that ramify within the IC, so cortical activation of IC GABAergic cells could be the cause of cortically-driven inhibition of neighboring IC cells (Hernandez et al., 2006, Jen et al., 2001), thus the AC may modulate the processing of sounds in the IC either directly, or through the activation of local inhibitory connections within the IC (Nakamoto et al., 2013). These studies suggest that polysynaptic network mechanisms are necessary to achieve local inhibition in the IC after AC stimulation (Malmierca et al., 2015).

The CC system is strategically placed to influence both descending and ascending pathways arising in the IC (Winer et al., 1998). Therefore, cortico-collicular neurons have the potential to play a key role in shaping auditory information processing. Experimental inhibition or stimulation of the AC proved the modulatory effects of the CC projections on responses of IC neurons. Observed effects included changed in frequency, amplitude and duration tuning (Suga, 2008), rate-level functions (Popelar et al., 2003), pitch sensitivity

(Nakamoto et al., 2010), spatial sensitivity (Nakamoto et al., 2008) and stimulus-specific adaptation (Anderson and Malmierca, 2013).

Since descending fibers from the IC innervate the SOC and CN (Syka et al., 1988, Schofield and Cant, 1999), CC-mediated modulation could influences functions of outer hair cells in the cochlea via the olivocochlear bundle (Liberman and Brown, 1986, Warren and Liberman, 1989).

1.2.5. Methodological approaches used in functional studies of corticofugal projections

Efferent signaling of AC neurons is typically elicited by focal electrical stimulation of the AC areas. This approach was used in bats (Sun et al., 1996, Ma and Suga, 2001a, Ma and Suga, 2001b), cats (Mitani et al., 1983), rats (Syka and Popelar, 1984), mice (Yan and Ehret, 2001) and guinea pigs (Torterolo et al., 1998). To reduce the signaling, various AC inactivation methods were used. The most invasive and irreversible method is AC lesions mechanical, thermal or induced with the use of laser beams or x-rays. Lesions could be made mono- or bilateral. This approach was used in cats, ferrets and squirrel monkeys, and resulted in severe sound localization inability, hearing loss, impairment of frequency discrimination and other hearing deficits. In rats AC ablation had only a little impact on sound localization or temporal resolution indicated by gap detection threshold (Kelly, 1980, Kelly and Kavanagh, 1986, Rybalko et al., 2006, Heffner and Heffner, 1990, Jenkins and Merzenich, 1984).

Widely used is a pharmacological inactivation of the AC. As an inactivation agents for the focal application were proved to be useful a sodium channel blocker tetrodotoxin (TTX) (Nwabueze-Ogbo et al., 2002, Popelar et al., 2003); a $GABA_A$ receptor agonist muscimol (Rybalko et al., 2010, Syka et al., 2005, Jaramillo and Zador, 2011) or local anesthetic lidocaine (Znamenskiy and Zador, 2013).

Another widely used inactivation method relies on a cooling of the AC. This technique was found to be very useful because it provides very effective and reversible inhibition of the AC function without producing any damage, even when cooling the AC repeatedly (Wood et al., 2017, Coomber et al., 2011, Nakamoto et al., 2008, Nakamoto et al., 2010, Anderson and Malmierca, 2013, Antunes and Malmierca, 2011, Malmierca et al., 2015).

Recently, modern optogenetic techniques, which enable fast and precise control over targeted circuit elements within intact tissue and even in freely behaving animals, bring a new very effective and reliable approach to the study of corticofugal projections (Jaramillo and Zador, 2011, Znamenskiy and Zador, 2013, Zalocusky and Deisseroth, 2013).

1.3. Influence of an acoustic environment on the AC development

1.3.1. Development of the AC

For its development the auditory brain needs a proper stimulation from the normally developed and functioning cochlea, especially during the early period of life. Any impairments in cochlear function during this period may result in an abnormalities in the auditory brain development (Pujol and Irving, 2016). In human fetuses, the organ of Corti begins its differentiation within 9 weeks of gestation and has completed its development by birth. In altricious animal species (rats, mice, ferrets, cats), the hearing at birth is immature and undergoes a significant postnatal development (Fig. 13), therefore they are widely used models for the developmental studies of the auditory system (Kral and Pallas, 2010). Whilst the human ear is functionally mature shortly after birth, the brain's auditory pathways and centres develop more slowly and progressively, from the brain stem to the auditory cortex for at least the first decade of life (Pujol and Irving, 2016, Moore, 2002).

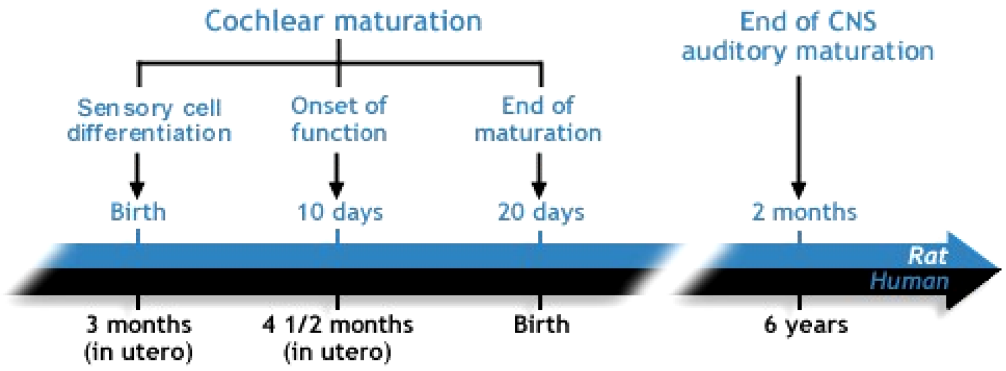

Fig. 13 **Comparative development of the cochlea and the auditory brain in both humans and rats**. Modified from Pujol and Irving (2016).

Cerebral cortex develops from the telencephalic vesicle of the embryonic forebrain. This process involves many different molecular signals that specify the three-dimensional patterning of the cells into columns, layers, and areas (Kral and Pallas, 2010). The cerebral cortex develops in an inside-out pattern, with deep-layer neurons arriving in the cortex first, followed by the upper layers. Neurons migrate during early development, but interneuronal connections become functional much later. At first, developing dendritic and axonal branches establish the background for a first connectivity matrix (Fig. 14), and then this matrix becomes functional after synapses have gained basic functionality. This happens at relatively

late stages of development and it is assumed to be influenced by sensory evoked activity (Kral, 2013).

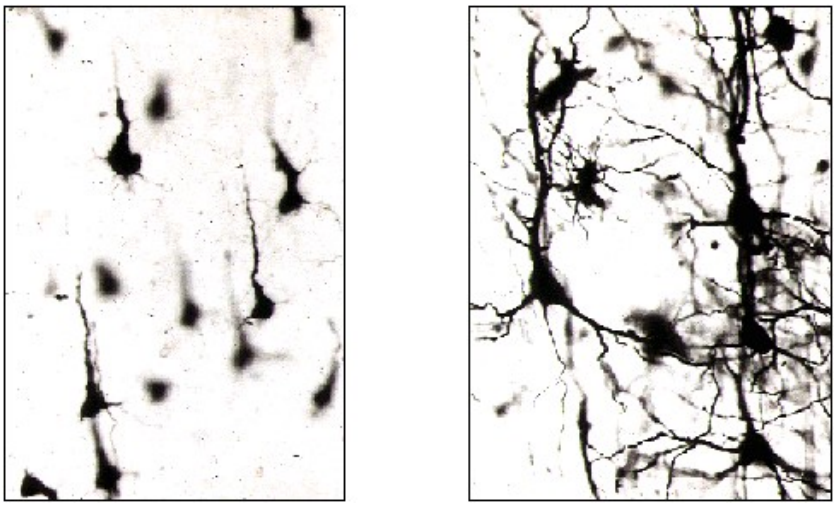

Fig. 14 **Golgi-impregnated neurons in the cat auditory cortex**: from a cat at birth (**left**) and from an adult cat (**right**) with the different level of the arborization. Modified from Pujol and Irving (2016).

1.3.2. Critical period in the brain development

From the moment of birth all sensory systems are influenced by a huge amount of different stimuli. Early in development, the existence of critical period (CP) for the experience-dependent plasticity has been suggested in the auditory, as well as in visual or somatosensory system (Berardi et al., 2000). This period is characterized by heightened sensory receptivity and plasticity. During CP particular environment could have life-lasting effects, so proper sound stimulation is essential for maintaining normal hearing function. In human early auditory surrounding play a crucial role in the language acquisition, in particular, on acquiring the phonological and grammatical patterns of the language and in organizing the neural mechanisms for handling these structures in a proficient way (Newport, 2003, Kuhl, 2010, Friederici, 2012). Links between the congenital hearing loss, severe otitis media during early childhood and occurrence of speech sound disorders is well established. Experimental and clinical evidence suggests that an optimal age for cochlear implants enabling the best auditory performance is during the first 1-3 years of life and impairments during the sensitive period could be hardly fully compensated later in life (Niparko et al., 2010, Geers and Sedey, 2011, Kral and O'Donoghue 2010). Furthermore, musicians who began their training early in life show better task performances and more striking changes in the auditory and motor

regions of brain, which demonstrate the existence of a sensitive period for musical training (Penhune, 2011). Language learning is easiest early in life and even passive listening of a foreign language during early childhood results in the more native-like accent when they learn it as an adults (Au et al., 2002).

Rat pups have an onset of the hearing around P11-P12 (Gealdor et al., 1993) with CP extended over the first month of postnatal life (Zhang et al., 2001, Rybalko and Syka, 2001, de Villers-Sidani et al., 2007). During this period, infant rat AC neurons demonstrate a poor spectral selectivity, weak tonotopic organization and wider tuning curves with spectrally broad and temporally extended sideband inhibitory receptive fields, which makes them better suited for spectral and temporal integration across a very broad range of acoustic inputs (Chang et al., 2005). Overall, rat pups seem to be a proper model for studying the influence of an acoustic environment on the auditory system and particularly auditory cortex during development.

Experimental interventions such as sensory deprivation, monotonous stimulation, or excessive sound exposure during the sensitive period disrupt a proper development of the auditory system and cause permanent alterations of its structure and responsiveness of the auditory brainstem as well as auditory cortex (Chang and Merzenich, 2003, Chang et al., 2005, Zhang et al., 2001, Kral et al., 2001, Bures et al., 2010, Grecova et al., 2009, Zhang et al., 2002). On contrary, a properly organized enrichment of the acoustic environment during early development may improves response the strength, threshold, selectivity, and latency of sound-evoked responses of AC neurons (Engineer et al., 2004, Percaccio et al., 2005) and stimulates the physiological plasticity in the AC (Percaccio et al., 2007) with persist into adulthood.

After the closure of the CP, changes to established sensory maps require higher intensity of stimulation coupled with additional cortical inputs such as attention, arousal or reward expectations.

1.3.3. Factors that control the early development and plasticity of the neocortex

Several factors could act as critical period determinants, including excitatory, inhibitory circuitry or neurotrophins.

Previous studies have shown that early postnatal experience and environment significantly affect NMDA receptor expression in the visual cortex (Chen and Bear, 2007, Berardi et al., 2000, Philpot et al., 2001). Similar effect was observed in the AC, where early

exposure to enriched environment increased NMDA and AMPA receptor subunit expression levels (Cai et al., 2010, Sun et al., 2005, Nichols et al., 2007).

Inhibitory circuitry plays important roles in the control of the experience-dependent plasticity. Rearing in the continuous white noise during early development ("bad" auditory experience) led to the weakened inhibition associated with changes in GABA receptor function, subunit composition, and levels of presynaptic GAD and GABA receptors (Xu et al., 2009). On the other hand beneficial early acoustic experience showed to have an opposite effect (Cai et al., 2010).

Acetylcholine (ACh) has been described to play an important role in many aspects of cortical development and acts as a permissive factor for the early development and plasticity (Yan, 2003, Hohmann and Berger-Sweeney, 1998). As described previously, ACh serves as a neuromodulator and a neurotransmitter in the central nervous system. The source of primary cholinergic afferents to the mammalian cortex is located in the nucleus basalis of the basal forebrain (Mesulam et al., 1983b, Mesulam et al., 1983a). Electrical stimulation of the nucleus basalis increases cortical ACh levels and facilitates cortical responses to sound (Zhang et al., 2006, Yan and Zhang, 2005). There are two major classes of the ACh receptors: nicotinic acetylcholine receptors (nAChRs) and muscarinic receptors (mAChRs). Expression levels of nAChRs are stable during the cortical development whereas those of mAChRs vary, reaching peak level within the first several weeks of postnatal life, corresponding to the time of CP with increased morphogenesis and synaptogenesis (Hohmann et al., 1995), suggesting that exactly mAChRs could play an important role in development and maturation in the auditory cortex (Shideler and Yan, 2010).

Berzaghi et al. (1993) described that activation of M1 subtype of mAChR, regulates the expression of neurotrophins such as brain-derived neurotrophic factor (BDNF) and nerve growth factor (NGF). It is well established that neurotrophins play an important role in the control of the developmental plasticity (Berardi et al., 2000). In the cortex BDNF regulates the maturation of inhibitory system (Huang et al., 1999, Zhou et al., 2011). Additionally infusion of BDNF in early developmental stages amplified the effects of pure tone exposure, probably due the earlier opening of the CP window and therefore amplifying the experience-dependent plasticity induced (Anomal et al., 2013). Higher levels of neurotrophin factors showed an acceleration effect on the development of GABAergic and glutamatergic systems, and promoted a more rapid maturation in the immature cortex (Cai et al., 2010, Zhou et al., 2011).

2. Aims of work and hypotheses

The auditory cortex occupies a pivotal position in the central auditory pathway – provides the final processing of acoustical stimuli and by descending projections controls the function of subcortical auditory nuclei. In the thesis were studied three aspects of the AC function including functional specializations of neurons in the AC subregions, modulatory effects of corticofugal projections on the processing of acoustical stimuli in the IC and relevance of complex acoustical stimulation during maturation for formation of neuronal circuits within the central auditory system.

2.1. Intrinsic electrical properties of pyramidal neurons in the core and belt areas of the auditory cortex in rat

Hypothesis: The centrally located core region and surrounding belt area are morphologically and functionally distinct parts of the AC in their responsiveness to acoustical stimuli and also in their connections to other cortical and subcortical structures. We hypothesize that the differences in sound-evoked responses could be partially explained by different distribution and activity of ion channels and distinctive electrical properties of principal neurons in these two AC areas.

Experimental aims:

- To characterize intrinsic electrical properties of layer V pyramidal neurons recording in acute rat AC slices using the patch-clamp technique.
- To identify ion channels which determine resting excitability of layer V neurons in the core and belt areas of the AC.
- To characterize functional properties of hyperpolarization-activated channels in layer V AC neurons.

2.2. Corticofugal modulation of neuronal responses in the inferior colliculus in rat

Hypothesis: The cortico-collicular projection, an important component of the descending auditory pathway, was suggested to play a role in modulation of both inhibitory circuits in the IC and sound-evoked responses of IC neurons. We hypothesize that AC inactivation by a cooling procedure that silence corticofugal pathways will result in a lower activation of intrinsic inhibitory network within the IC and altered neuronal responses to sound stimuli.

Experimental aims:

- To study the changes in the spontaneous and sound-evoked neuronal activity in the IC after the inactivation of the AC by the cooling procedure.
- The reveal changes in the frequency tuning properties of IC neurons during the cooling period.
- To investigate the effects of the AC inactivation on synchronized responses of IC neurons to a series clicks repeated at high frequency.

2.3. Acoustical enrichment-induced plasticity in rat auditory cortex

Hypothesis: Acoustical environment plays an important role in the maturation of the auditory system. We hypothesize that acoustical enrichment during the developmental period, which is complemented with an active stimulus-reward paradigm, influences the development of the structure of projections, neuronal responsiveness, excitatory-inhibitory balance, or tonotopical arrangement and may enhance the stimulus discrimination ability of the animals by providing more reliable neuronal response patterns.

Experimental aims:

- To study the influence of the acoustically enriched environment (AEE) on excitatory thresholds, frequency selectivity and rate-intensity functions in AC neurons.
- To reveal whether the enrichment changed the AC responsiveness to frequency-modulated and also to amplitude-modulated stimuli.
- To investigate the effects of the AEE on the neurons spike count variance for a repetitive stimulus and a degree of similarity across stimulus repetitions, to assess the influence of the AEE on the reliability, stability and temporal acuity of individual responses of the AC neurons.

3. Material and methods

3.1. Animals

All experiments were performed on rats. Rats were housed under standard conditions on a 12 h/12 h light/dark cycle, with food and water available ad libitum. The specific treatment during acoustical enrichment is described bellow in details. The care and use of animals and all experimental procedures were performed in compliance with the guidelines of the Ethical Committee of the Institute of Experimental Medicine, Czech Academy of Sciences, and followed the European Community Directive 2010/63EU.

The first study of the electrical properties of the layer V pyramidal AC neurons was made on the 30-40 days old Wistar rats. The other two studies, Long Evans rats aged 3-6 months, weighing 328±80 g were used.

3.2. Acoustically enriched environment (AEE)

The *enriched* group of rats (n=27) was exposed to an AEE reinforced with active behavioral feedback between P14 and P28 (Fig. 15).

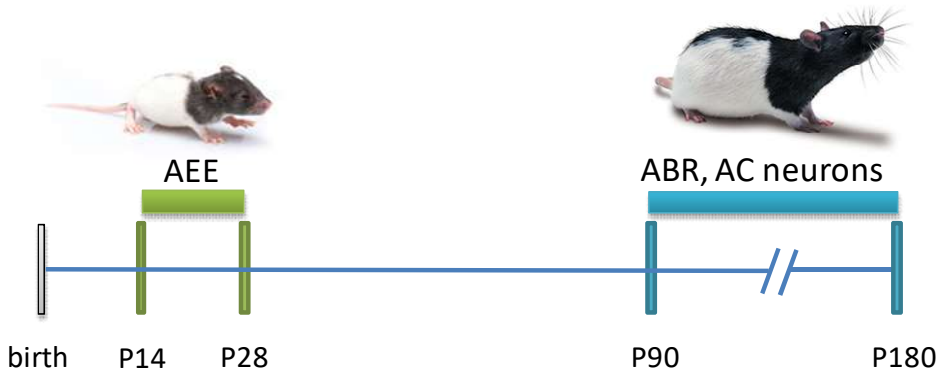

Fig. 15 **Time scheme of the experiment**.

The AEE stimulus represented by a broad-band amplitude-modulated rippled noise with temporally variable sinusoidal spectral envelope (frequency range 983 – 48461 Hz, depth of the spectral ripples 30 dB, amplitude-modulated by a low-pass exponential noise envelope with cut-off frequency 2 Hz). This background noise was presented at 55 dB SPL and it was supplemented with several types of target sounds at 60 dB SPL with 500ms duration. The target signals had a similar fundamental frequency, but increasingly complex spectral content (pure tone at 6 kHz; sawtooth signal at 6 kHz; frequency-modulated tone with carrier frequency 6 kHz, modulation depth 1.5 kHz and modulation frequency 10 Hz; 1/3-octave

noise centred at 6 kHz) (Fig. 16). The target signals appeared randomly in time (average interval 40 s, average interval between rewarded signals 80 s) and the frequency-modulated tone triggered the release of a reward – a drop of sweet syrup. The reward output was delayed relative to the triggering sound by 2 s, giving the animals enough time to attend the delivery spout. The drop was always available for approximately 2 s and then fell out of reach of the animals. The presence and identity of animals at the reward-delivering spout was monitored by a custom-made system based on an infrared gate (Colbourn Instruments), an Arduino RFID reader and a Matlab script. The RFID chips (kindly donated by LUX-IDent, Czech Republic) were subcutaneously implanted on the neck under temporary isoflurane anaesthesia. During the first week of exposure rat pups did not demonstrate an interest in the reward, which was changed during the second week of the exposure. A group of age-matched *control* rats (n=24) were raised in standard housing conditions with no acoustical enrichment. Standard housing utilizes a small local facility shared by approximately 30 rats, the level of the background noise in the facility is 37 dB SPL, the noise is steady with minimal fluctuations.

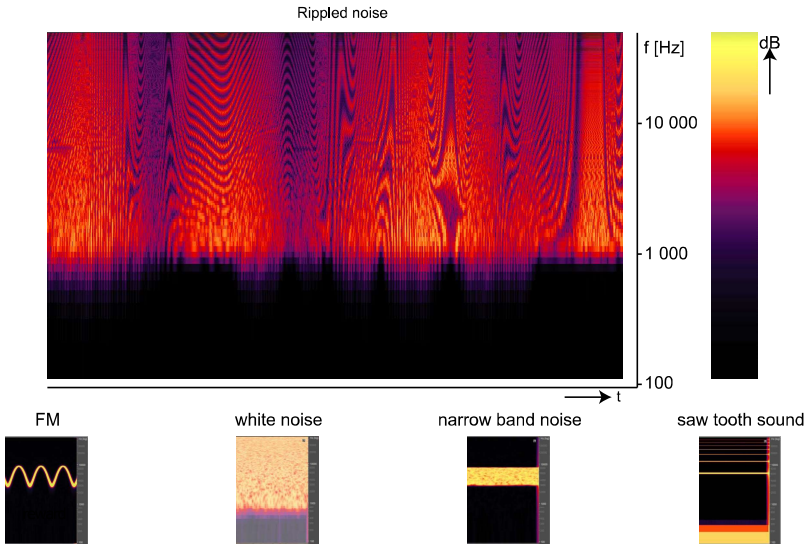

Fig. 16 **Arrangement of the acoustically enriched environment**: a representative spectrogram of the background rippled noise and embedded acoustic signals, FM tone triggered a reward release.

The AEE was presented during the night active period. The activity of AC neurons was recorded in adulthood at the age of 3 to 6 months.

3.3. Anaesthesia

All hearing measurements, surgical procedures and extracellular measurements of the

neuronal activities were performed on anaesthetized animals. The rats were anaesthetized with an intramuscular injection of a mixture of 35 mg/kg ketamine (Narkamon 5%; Spofa, Prague, Czech Rep. or Calypsol 50 mg/ml; Gedeon Richter, Budapest, Hungary) and 6 mg/kg xylazine (Sedazine 2%; Fort Dodge, Animal Health, Fort Dodge, Iowa or Xylapan 20 mg/ml; Vetoquinol SA., Lure Cedex, France). Additional subcutaneous injections of one half of the original dose of the anaesthetics were made in 1hr intervals during an experiment to maintain a sufficient level of the anaesthesia. Basal reflexes (pedal reflex or eye blink reflex), respiratory rate, and heart rate, were routinely checked during the experiment. The body temperature was maintained at 37–38 °C using an electronically controlled heating pad.

3.4. Recording of auditory brainstem responses (ABR)

ABRs were recorded to assess the hearing thresholds of rats. Measurements were performed in anaesthetized rats in the sound-proof anechoic room. ABRs were measured using three subcutaneous electrodes: an active electrode on the vertex, ground and reference electrode placed on both sides of the neck.

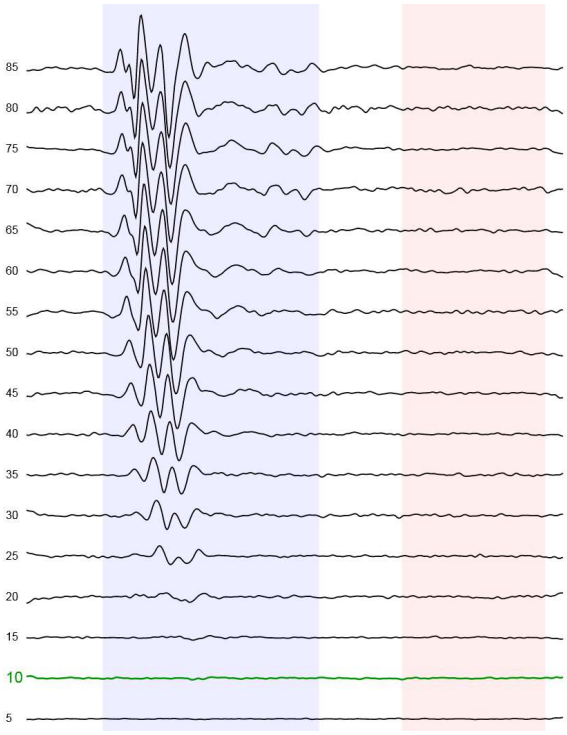

Fig. 17 **Typical ABR responses evoked by short tone bursts with decreasing stimulus intensity**. Threshold response is accentuated with green color.

ABRs were evoked using short tone bursts (3 ms duration, 1 ms rise/fall times, frequencies of 2, 4, 8, 16, 32 and 40 kHz) delivered with decreasing stimulus level (from 100

to 0 dB SPL) with 5dB step. Electric signals from recording electrodes were amplified and band-pass filtered over the range of 300 Hz to 3 kHz, processed with a TDT System III Pentusa Base Station and analyzed using BioSigTM (TX, USA) software. ABR thresholds at each frequency were defined as the lowest tone intensity which still evoked an appropriate detectable response (Fig. 17).

3.5. Surgery

The skin and underlying muscles on the skull were removed to expose the dorsal cranium (for the access to the IC) and right temporal region of the skull (for the access to the AC), S-shaped holder was fixed by two stainless steel screws to the skull above the frontal part of the right hemisphere. Using a electrical drill, a craniotomy with diameter about 5 mm was made into the skull above the dorsal part of the right IC and another hole was made above the right AC (about 3mm at the age 30-40 days). The animal's head was then fixed in a stereotaxic apparatus using a holder, leaving the pinnae and outer ear canal intact. The dura mater was removed from the AC surface for the extracellular recording of the neuronal activity and remained intact during the cooling inactivation. For the extracellular recording from the IC, the dura mater above the cerebellum was extracted and the cerebellum was slightly pushed aside to visualize the IC.

3.6. Inactivation of the AC using a cooling probe

The cooling device was based on a combination of a Peltier element, supplied by the regulated DC voltage, and a cold water cooling system (Fig.18). Such cooling device operates based on the thermoelectric effect of the Peltier element: when the DC current flows through the device, it transmits heat from one side to the other, so one side gets cooler while the other gets hotter. The cooling part of the Peltier element was attached to a round-shaped probe, 4 mm in diameter, which covered the whole extent of the AC; the heated part of the Peltier element was connected to a cooler part by circulating cold water. The temperature of the cooling probe was continuously monitored with a micro thermocouple T1. Another micro thermocouple (T2) monitored the temperature within the brain. The Peltier element enabled a fast decrease in the temperature of the brain tissue and fast recovery of the brain temperature by reversing the polarity of the DC voltage. Within one minute after starting the cooling procedure the temperature on the surface of the AC reached 3-5ºC.

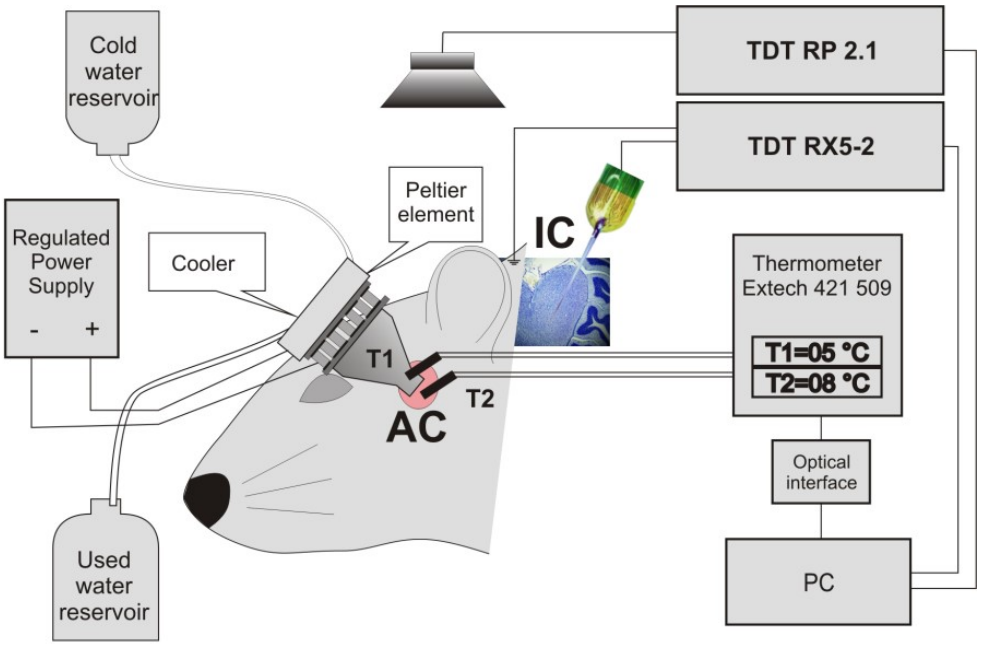

Fig. 18 **Schema of the experiment arrangement of the reversible inactivation of the AC using a cooling probe**. The cooling device is based on a combination of a Peltier element, supplied by regulated DC voltage, and cold water cooling. The probe temperature was continuously monitored with an EXTECH thermometer using a micro thermocouple (T1). Another micro thermocouple (T2) monitored the temperature at specific locations in the brain.

Measurement of the temperature profile within the AC by the micro thermocouple demonstrated that the temperature in the sixth layer of the AC (where the cortical descending projections originate) ranged between 15-20ºC, low enough to eliminate any neuronal activity in this location. Additionally, our measurements demonstrated that in subcortical auditory structures (auditory thalamus, IC) the temperature did not drop below 28°C during the whole period of AC cooling (Fig. 19).

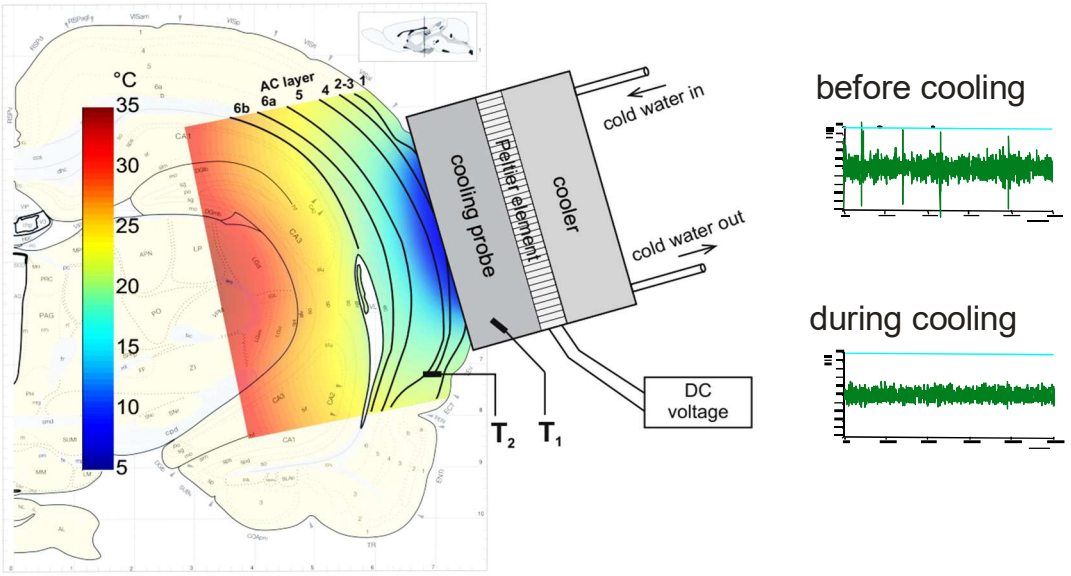

Fig. 19 **Left** - Schematic drawing of the cooling device with a temperature gradient in the brain below the cooling device; **Right** - Simultaneous recording of neuronal activity in the layer VI of the AC with the microelectrode showed the elimination of neuronal spiking at a temperature below 20 °C.

3.7. Extracellular recording of the neuronal activity

Single or multiple extracellular unit activity was recorded in a sound-proof anechoic room with the walls and ceiling covered by cones made of a sound-absorbent material. The signal from the individual electrodes was amplified 10 000 times, band-pass filtered over the range of 300 Hz to 10 kHz, and processed by a TDT (Tucker Davis Technologies, Alachua, FL, USA) System III using an RX5-2 Pentusa Base Station. The signal was processed with BrainWare software (Jan Schnupp, Tucker-Davis Technologies, Alachua, FL, USA) and analyzed by custom made Matlab scripts.

3.7.1. Recording of the neuronal activity in the IC

The 16-channel multielectrode probe produced by NeuroNexus Technologies (single shank probe, 100 μm distance between electrode spots) was introduced into the IC in dorso-ventral direction passing through the DCIC into the CIC using a three-axis electronic micromanipulator (0.1 mm step; MCL, Märzhäuser Wetzlar) under visual inspection through an operating microscope (Fig. 21).

Electrode probe was inserted into the IC gradually with continuous control of responses to broad-band noise stimulation, which appeared gradually on individual electrodes. When the

response occurred on the last, most upper electrode (i.e. electrode No. 1) the insertion of the electrode probe was stopped (Fig. 21). Each individual electrode on the probe detects small voltage deflections originating from the current fields generated by adjacent neurons action potentials in response to acoustic stimulations.

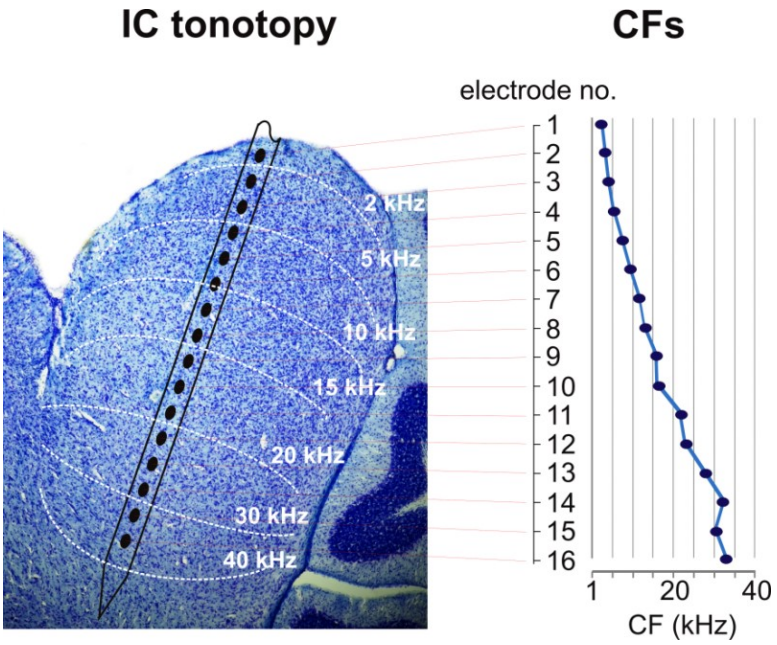

Fig. 21 **Left** - Sagittal section of the IC showing a principle of the electrode probe insertion into the IC with frequency contours and IC subnuclei delineation. **Right** - The characteristic frequency (CF) profile of individual electrode probe track.

3.7.2. Acoustic stimulation and data evaluation

The stimulation signals were generated using the TDT System III with the RP 2.1 Enhanced Real-Time Processor (Tucker Davis Technologies, Alachua, FL, USA). Acoustic stimuli were delivered in a sound-proof anechoic room in free-field conditions via a two-driver loudspeaker system (Jamo woofer and SEAS T25CF 002 tweeter in experiments with AC inactivation and AC mapping; Selenium 6W4P woofer and RAAL70-20 tweeter in the experiments with AEE effect) placed 70 cm in front of the animal's head.

3.7.3. Frequency-intensity mapping

To determine the neuronal receptive fields, pure tones (frequency 0.5 – 40 kHz with 1/4 octave step for the AC and 1/8 octave increments for the IC, 60 ms duration, 5 ms rise/fall times, intensity between -20 and 80 dB SPL with 5dB step were presented in a random order, each stimulus appearing five times. A discrete matrix, corresponding to the response

magnitude evoked by each of the frequency-intensity combinations, was thereby obtained. This was smoothed using cubic spline interpolation, and used for extraction of the basic parameters: the excitatory response threshold (the lowest stimulus intensity that excited the neuron, measured in dB SPL), the characteristic frequency (CF) – the frequency with the minimal response threshold, measured in Hz, and the bandwidth of the excitatory area 30 dB above the excitatory threshold, expressed by quality factor Q30 (Q30= CF/bandwidth). The quality factor Q, is a measure of the frequency selectivity of a neuron – the higher the Q, the sharper the tuning (Fig. 22).

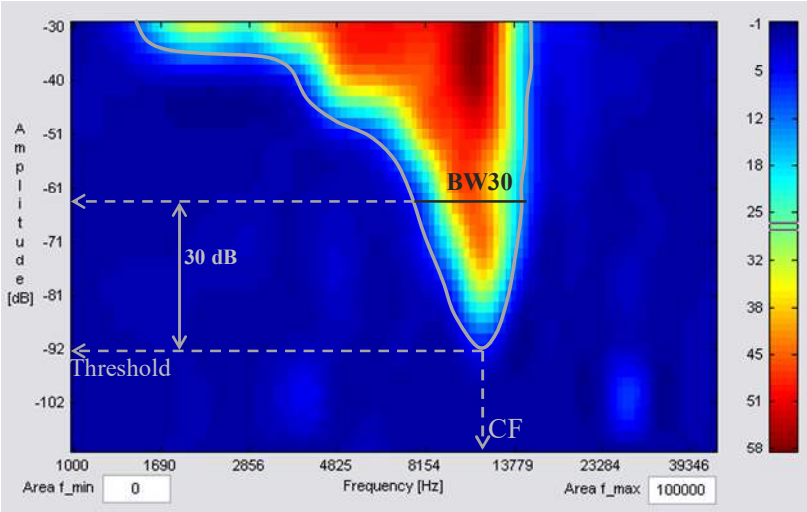

Fig. 22 **Example of the excitatory response area and frequency tuning curve** (gray line) of recorded neuron with marked evaluated parameters: characteristic frequency (CF), threshold, and bandwidth of the excitatory area 30dB above the threshold (BW30). The bandwidth of the excitatory area expressed by the quality factor is a measure of the frequency selectivity of neurons. The response magnitude is represented by the colour pallet; red and blue correspond to maximal and minimal activity, respectively.

3.7.4. Neuronal intensity coding

To quantify the level-dependent responses to a wide-band stimulus – the noise-evoked rate-intensity functions (RIF), white noise bursts (60 ms in duration, 5-ms rise / fall times) with a variable intensity (10-dB step) from 0 to 100 dB SPL were repeatedly (50 times) presented in a random order. Neuronal responses to BBN of variable intensity were used to RIF's construction. A 100% scale was assigned to the neuron's total range of response amplitudes, 0% corresponding to spontaneous activity and 100% corresponding to its

maximum response magnitude. RIFs were further used for evaluating the following parameters: the percentage of non-monotonic, and strictly monotonic RIFs. An RIF was qualified as non-monotonic if the response magnitude at the highest stimulus intensity was smaller than the maximum response magnitude by more than 20%. The remaining RIFs were qualified as strictly monotonic (Fig. 23).

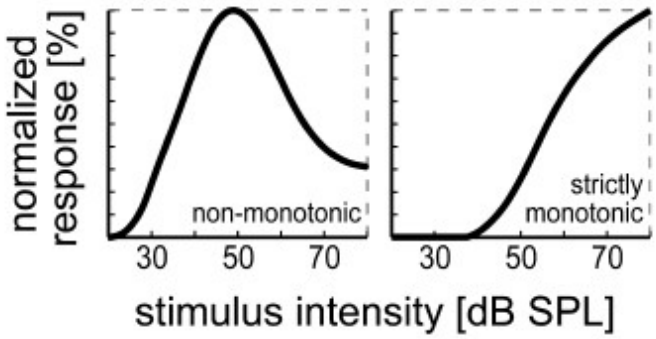

Fig. 23 **Typical examples of two types of RIFs, representing the spline-smoothed responses of two different neurons**. Modified from Bures et al., (2010).

Spontaneous activity of the IC neurons was determined at the 0dB SPL BBN stimulation.

3.7.5. Testing the adaptation ability of the IC neurons

For testing the adaptation ability of individual IC neurons the animals were stimulated with the 600-ms series of 100-μs clicks with linearly decreasing and increasing inter-stimulus intervals from 25 to 6.6 ms and back to 25 ms (Fig. 24).

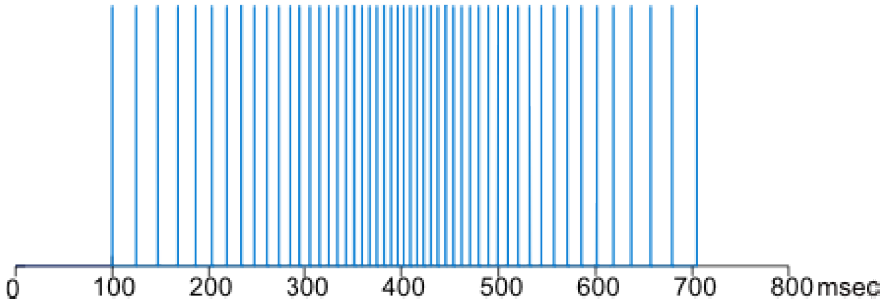

Fig. 24 **Scheme of the train of clicks with the rate continuously changing spike frequency.**

3.7.6. Recording of the neuronal activity in the AC

In order to determine A1 location the custom-made low-impedance 15-channel electrode array was used. After the dura mater removal, the transparent sham array with printed marks of with in place of electrodes was placed in several locations to cover entire surface of the craniotomy and photographed (Fig. 20A). The real array of electrodes was inserted in the same positions as the sham array and middle latency responses (MLRs) were recorded in each location. MLR was elicited in a free field condition by a series of pure tones of 60 ms duration in the frequency range of 1 to 45 kHz with 0.5 octave step. The sound intensity was set at 50 dB SPL and a stimulation rate 1.3 Hz and the responses were calculated as an average of at least 15 repetitions. In the obtained MLR wave forms the first positive (P1) and the first negative (N1) peak was detected and the calculated P1-N1 amplitude difference was defined as the amplitude of MLR (Fig. 20B). The frequency of stimulus that evoked the highest MLR amplitude in a given position was taken as the local best frequency (BF). Results were plotted into photography of the AC and the distribution of BF of MLR on the cortical surface was reconstructed (Fig. 20C). The position of the primary AC (AI) was determined according to reconstructed tonotopic map with low frequency-tuned MLR predominated in ventro-caudal regions, higher BFs gradually rostro-dorsally (Fig. 20).

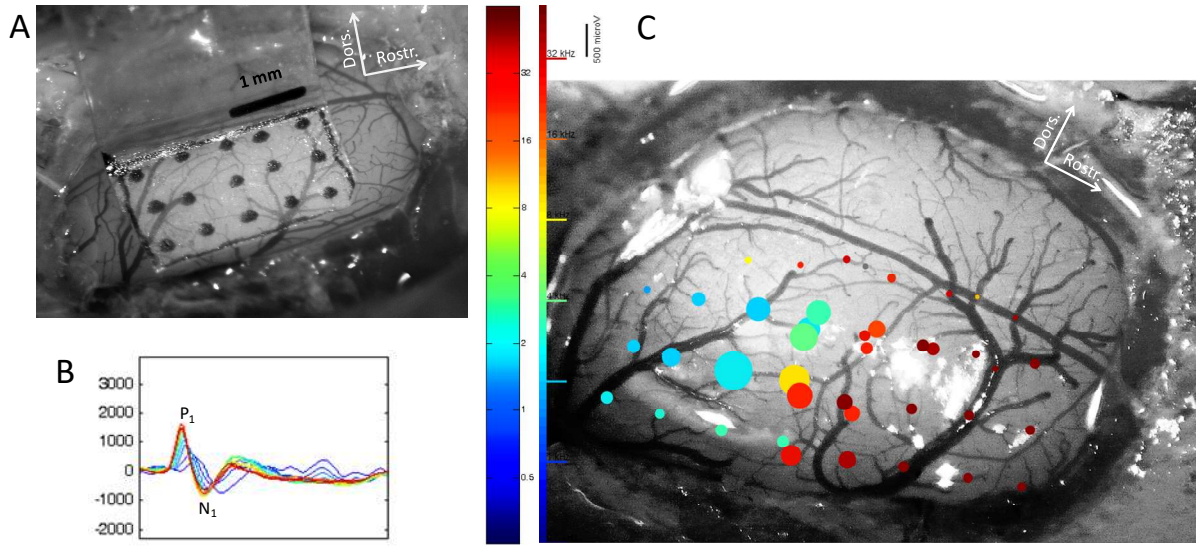

Fig. 20 **Middle latency responses and neuronal properties in example animal**. A - A micrograph of the rat cortex with placed transparent sham array with printed marks of individual electrodes positions. B - Examples of MLR evoked by tones of constant intensity (50 dB SPL) and variable frequency (1 - 45 kHz, see panel C for color-coding; C - A

micrograph of the rat cortex with electrode positions (dots). The color of dots represents the frequency of stimulation which evoked the highest amplitude of MLR (best frequency, BF), the value of that amplitude is represented by the dot diameter. Locations where MLR amplitudes did not reach 100 μV were not analyzed because of too low signal-to-noise ratio.

Afterwards, the 16-channel electrode array (NeuroNexus Technologies, single shank probe, 50 μm or 100 μm distance between electrode spots) was introduced into the AC using a three-axis electronic driver for recording the extracellular unit activity. Individual spikes in the recorded signal were isolated online based on amplitude discrimination. The recorded responses mostly represented the activity of a several adjacent neurons – multiunit activity.

3.7.7. Responses of the AC neurons to modulated sounds

Two types of stimuli were used. Firstly, white noise bursts of 500ms duration were sinusoidally modulated using a 100% modulation depth, the equivalent SPL being 60 dB. The modulation frequencies varied between 4 and 24 Hz with a 2Hz step. Secondly, pure tone bursts of 1sec duration were sinusoidally modulated with an average frequency shift set to 0.23 octaves and the equivalent SPL set to 60 dB. The carrier frequency matched the best frequency of the measured neuron. The modulation frequencies were logarithmically spaced and varied approximately between 2 and 100 Hz. The response strength was expressed as relative spike rate, obtained by dividing the spike rate evoked during the first modulation period by the spike rate elicited by the remainder of the response (Chang et al., 2005). The modulation-transfer functions (MTF) for the AM and FM sounds were plotted as the dependences of the relative spike rate on the modulation frequency. In the cases of the FM tones, the low-frequency cut-offs of the MTFs were measured as that modulation frequency where the high-frequency tail of the MTF crosses the level of 50 % of the MTF's total dynamic range. In the responses to the FM tones, the strength of the onset (first 20 ms of the response) and sustained parts were also analyzed separately. In the case of click trains, short rectangular pulses (0.1 ms pulse duration, 2000 ms click train duration) were presented with a variable repetition rate. The repetition rate varied logarithmically from 2 Hz to 100 Hz. Additionally, all three temporally structured stimuli (i.e., the AM noise, the FM tones, and the click trains) were used to determine the amount of synchronization of neuronal responses with the stimulus. Vector strength values along with the Rayleigh statistics were computed for each sound-evoked spike pattern; only responses having Rayleigh statistics of at least 5.991 were considered as significantly phase-locking (Zhou and Merzenich, 2008). In addition, the FM

tones and click trains were used to determine the similarity of spike trains evoked by the same stimulus. Van Rossum distance (Cheng et al., 2017) was computed for each pair of responses of the same neuron to the same stimulus.

3.8. Identification of the boundary line between the core and belt AC areas

The core and the belt areas of the AC were identified in each animal using extracellular recording of their characteristic neuronal responses to sound stimuli. Two types of acoustical stimuli were presented: BBN bursts (60 ms duration, 5 ms rise/fall times, 80 dB SPL) and pure tones (as for frequency-intensity mapping), presented in random order of changing frequency (1/4 octave steps) and intensity (5 dB steps). Neuronal responses were recorded using silver wire electrodes inserted into glass capillaries filled with 3M KCl. The delineation between core and belt AC areas was based on the fact that neurons in the belt area characterized by weak or no responses to pure tones while produce stronger responses to BBN. In contrast, responses of neurons in the core AC to pure tones had sharp neuronal receptive fields with low thresholds and well defined CF.

After the recording, position of dorsal belt and core fields were identifies, dorsal borderlines separating of the core and belt areas and ventral borders of the core area were marked by the injection of the Evans Blue dye with recording glass capillary.

3.9. Patch clamp recordings from neurons in acute brain slices

3.9.1. Preparation of brain slices

After decapitation the brain was exposed and cuts in the coronal plane were made at the rostral margin of the cerebellum and one-third of the way through the rostrocaudal extent of the cerebral cortex (Fig. 25). The block of tissue between these two cuts was removed and glued rostral side down. Coronal brain slices (350-400 μm thick) of the AC were prepared with a vibratome Leica VT 1000S (Leica Microsystems) from a right hemisphere. After cutting the tissue in oxygenated (95% O_2-5% CO_2) ice-cold (0-4 ^oC) dissecting Ringer solution (130 mM NaCl, 3.5 mM KCl, 24 mM $NaHCO_3$, 1.25 mM NaH_2PO_4, 0.5 mM $CaCl_2$, 3.0 mM $MgCl_2$ and 10 mM glucose), the slices were equilibrated for 1 hour at 32-33 ^oC and then stored at room temperature (RT) in the same solution until recording. At the recording time a single slice was placed in a recording chamber and constantly superfused at a rate 2-2.5 ml/min with oxygenated recording Ringer solution in which [Ca^{2+}] and [Mg^{2+}] were adjusted to 1.5 mM and maintained at a temperature of 33-34 ^oC.

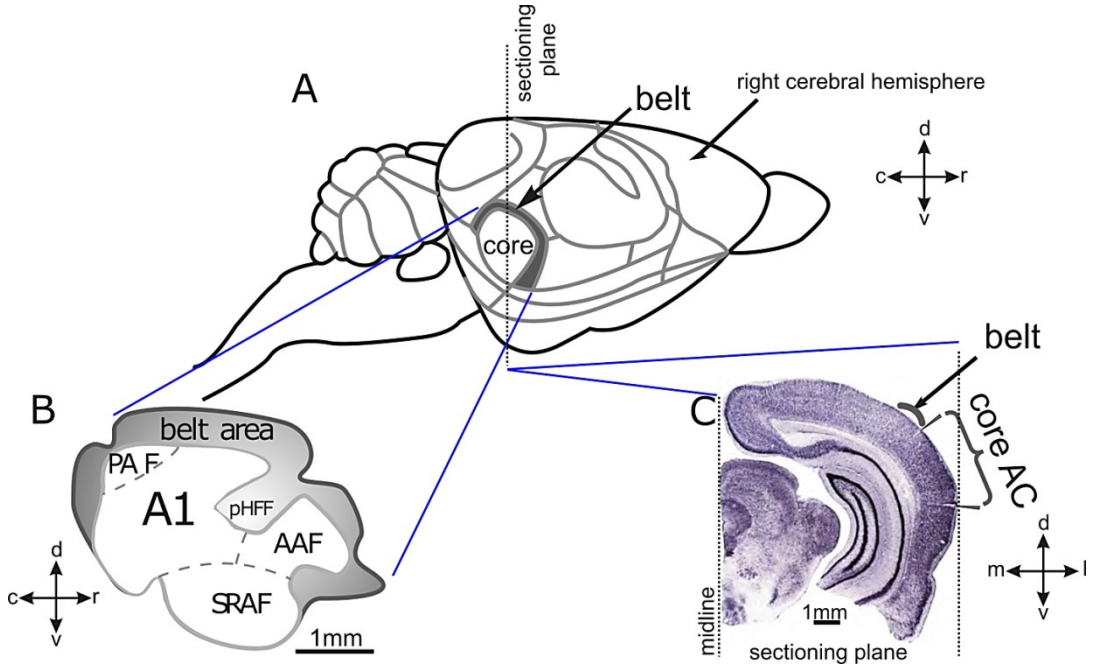

Fig. 25 **Schematic illustration of the AC located on right side of the rat brain** (**A**). **B** - shows the map of AC areas consisting of the core (white) and the belt (grey) (adapted from (Profant et al., 2013); **C** – micrograph of brain slice containing the AC (Nissl staining).

3.9.2. Patch-clamp technique

Whole-cell patch-clamp recordings were made from somata of pyramidal neurons located in the layer V of the core or belt AC areas. Neurons were visually identified by their typical morphology using an Olympus BX51WI microscope with ×10 and ×60 water-immersion objectives. Patch-clamp pipettes were pulled from borosilicate glass capillaries (outer diameter 1.5 mm and inner diameter 0.75 mm, Sutter instrument, Novato, USA) using a P 80 micropipette puller (Sutter instrument, Novato, USA). The pipettes (3-6 MΩ) were filled with an internal solution containing (in mM): 102 K-gluconate, 32.5 KCl, 10 HEPES, 0.1 EGTA, 4 Mg_2ATP, 0.6 NaGTP, 10 TrisPCr, pH was adjusted to 7.2-7.3 with KOH and the osmolarity was 275-285 mOsm. The Axopatch 200B patch clamp amplifier, Digidata 1322A interface and pClamp 9.2 software (Axon Instruments, Foster City, California) were used for data acquisition. Only cells that had resting membrane potential more negative than -60 mV were included into analyses. Membrane voltages and currents were recorded from the whole

neurons in the current-clamp or voltage-clamp mode (Fig. 26). Glass pipettes for whole-cell recording had resistances of 2–3MΩ. Series resistances during recordings were <10MΩ and were compensated electronically by 80%.

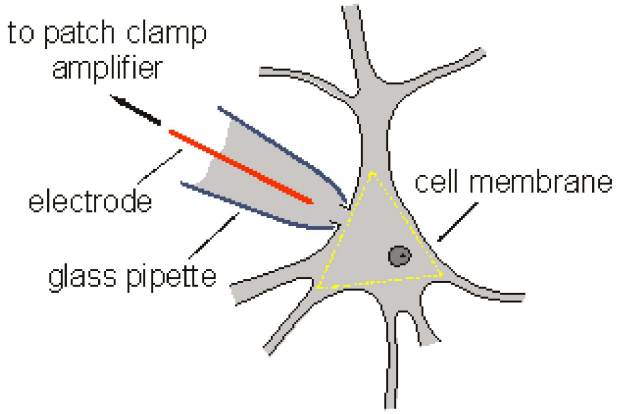

Fig. 26 **Scheme of the whole-cell modes of the patch-clamp technique.**

Resting membrane potential was determined as the membrane voltage in the absence of current stimuli. Cell capacitance was calculated using membrane time-constant (**τ**) and cell resistance (IR) values obtained from voltage responses of cells upon applying hyperpolarizing -10 pA steps at the resting potential. Stimulus threshold (rheobase) was defined as amplitude of minimal depolarizing current that induces one action potential (AP). To obtain the action potential threshold, first-order derivates (denoted d*V*/d*t*) of the somatic membrane potentials were calculated (Kress et al., 2008) and plotted against the somatic membrane potential. The threshold of AP was then the membrane potential at which d*V*/d*t* reached 10 mV ms^{-1} (Naundorf et al., 2006). Steady state firing rate and the latency of the first AP were measured during 1s-long 0.4 nA current injections Single APs were evoked by brief current steps (1.2 nA/2 ms).

Recordings were stored using PC-based data acquisition software (Clampex 9.2, Axon Instruments). Errors caused by liquid-junction potential were corrected.

3.9.3. Drugs used

To block I_h, the specific antagonist ZD7288 (BIOZOL Diagnostica Vertrieb GmbH) was prepared as a 40 mM stock solution in H_2O, divided into aliquots and stored at -20 °C. The final concentration was 10-40 µM in the recording Ringer solution. Glutamate, GABA-A, glycine and voltage-gated Ca2+ channels were blocked by bath application of 10 µM DNQX, 5 µM R-CPP (BIOZOL Diagnostica Vertrieb GmbH), 50 µM picrotoxinin, 10 µM SR95531 and 200 µM $CdSO_4$. In some experiments action potentials were prevented by bath application of 0.5

μM TTX and K+ currents were blocked by bath application of 1 mM $BaCl_2$. All drugs were purchased from Sigma-Aldrich unless otherwise noted.

3.10. Histology and morphometric analysis

3.10.1. Verification of the recording electrode position in the IC

At the end of the AC inactivation experiment the electrode probe was moved several times up and down in the IC in order to make a larger lesion and enable some cerebrospinal fluid and blood to enter into the electrode track. The animal was given an overdose of thiopental (100 mg/kg) and was intracardially perfused with a 4% paraformaldehyde. The brain was removed and sectioned into 40 μm sections with a freezing microtome. The electrode track was reconstructed from the sections and stained with cresyl violet under a light microscope.

3.10.2. Intracellular labelling of the layer V pyramidal AC neurons

Biocytin hydrochloride was dissolved in the pipette solution to final concentration 0.5% and cells were filled during recording for at least 45 min. Afterwards, the slices were fixed in 4% paraformaldehyde in 0.1 mM phosphate buffer (PB) at 4 ^{o}C for 12-24 hrs. For staining, slices were rinsed in PB (3×10 min) and then placed in 0.4 % triton x-100/PB for 90 min. Then slices were incubated with streptavidine conjugated with Alexa fluor 488 (KRD, Invitrogen) for 100 min at RT. Then slices were rinsed again in PB (3×10 min) and mounted on the coated glass slides. The immunofluorescence was analyzed using a confocal laser scanning microscope (Olympus BX61) (Fig. 27). A subset of neurons was reconstructed three-dimensionally with Neurolucida computerized reconstruction system (MicroBrightField, Willistone, VT).

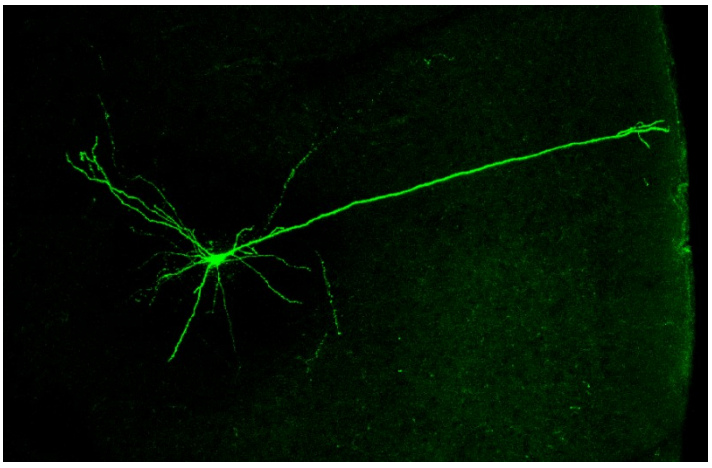

Fig. 27 **Micrograph of layer V pyramidal neuron labeled with biocytin**.

3.10.3. Analysis of expression levels of HCN channels in the AC neurons

(performed by collaborators: Mgr. Ján Kriška, Institute of Experimental Medicine AS CR, Department of Cellular Neurophysiology; Ing. Lukáš Valihrach, Ph.D., Institute of Biotechnology AS CR, Laboratory of Gene Expression)

Cytoplasmic samples of layer V pyramidal neurons from the core and belt AC areas were collected with glass capillaries from the acute brain slices. cDNA synthesis was performed as described in Benešová et al. (2012). Preamplified cDNA was diluted fourfold and used in qPCR to determine Hcn1–4 expression. Primer design as well as qPCR was performed according to the protocol described in (Benesova et al., 2012). All qPCR reactions were run in technical duplicates. Data were pre-processed and analyzed in GenEx software (MultiD) as described in (Honsa et al., 2014).

3.10.4. Immunohistochemistry

(performed by collaborators: Helena Pavlíková Institute of Experimental Medicine AS CR, Department of Cellular Neurophysiology; MUDR. Tetyana Chumak, Ph.D., Department of Auditory Neuroscience)

The procedure was similar to one described in (Honsa et al., 2014). Briefly, animals were deeply anesthetized with ketamine-xylazine mixture and perfused transcardially with 100 mL of saline followed by 200 mL of cooled 4% paraformaldehyde (PFA) in 0.1 M phosphate buffer (PB). Brains were removed, post-fixed overnight with PFA and treated with a sucrose gradient (10–20–30%) for cryoprotection. Coronal 30 µm thick slices were prepared using a cryostat (Leica CM1850, Leica Microsystems, Wetzlar, Germany). Slices were washed in PBS followed by blocking of the nonspecific binding sites with 5% Chemiblocker (Millipore, Billerica, MA) and 0.2% Triton in PBS. The blocking solution was also used to dilute the antisera. The slices were incubated with the primary antibodies at 4–8 ^{o}C overnight and the secondary antibodies were applied for 2 h. Following primary antibodies were used: rabbit anti-HCN1 (1:200; Abcam, Cambridge, UK), rabbit anti-HCN2 (1:200; Alomone Labs, Jerusalem, Israel), rabbit anti-HCN3 (1:200; Pierce, Rockford, IL, USA), rabbit anti-HCN4 (1:200, Alomone Labs), rabbit anti-Map2 (microtubule-associated protein was used for dendrite visualization) (Sigma-Aldrich, St. Louis, MO). The secondary antibodies were goat anti-rabbit IgG conjugated with AlexaFluor 488 or 594 (Life Technologies). To visualize the cell nuclei, the slices were incubated with 300 nM 4, 6-diamidino-2-phenylindole (DAPI) in PBS for 5 min at room temperature and mounted using Aqua Poly/Mount (Polysciences,

Eppelheim, Germany). The labeling was analyzed using Zeiss 510DUO LSM confocal microscope, equipped with Ar/HeNe lasers and 40x or 63x oil objectives.

3.11. Statistical analysis

Statistical analyses were performed using Clampfit 9.2 (Axon Instruments), Excel 2007 (Microsoft office), GraphPad Prism version 6.00 for Windows (GraphPad Software, San Diego, California, USA) and Matlab R2007b (MathWork, Inc.).

In order to evaluate the changes of the relative response magnitudes of the IC neurons to BBN stimulation, which were recorded at individual electrode spots during the cooling procedure with respect to the pre-cooling magnitude, 100% of the one-sample t-test was used. For comparison of the average percentage of responses to individual clicks in the series during the cooling procedure with respect to the pre-cooling magnitude the two-way repeated measures ANOVA with Bonferroni post-hoc test was used.

For comparison of the means of two data sets, Student's t-test was computed; the case that the variances of the data sets were not comparable (tested using an F-test), Welch's correction was used. To compare two dependences of some parameter on a given variable (for example, the dependencies of excitatory thresholds on frequency in the enriched and control groups, the dependences of the vector strength on modulation frequency in the enriched and control groups), two-way ANOVA with Bonferroni post-hoc test was used. A Chi-square test was employed to compare the percentage of phase-locking neurons. To evaluate relationships between two trends, a linear regression with a subsequent F-test was used. In all cases, the alpha level was set to 0.05.

4. Results

4.1. Intrinsic electrical properties of the pyramidal neurons in the core and belt areas of the rat auditory cortex

The aim of this experiment was to reveal passive and active electrical properties of layer V AC neurons. These neurons exhibit non-uniform patterns of sound-evoked responses in vivo. We wanted to test whether variability in the intrinsic electric properties contributes to the variability of neuronal responses recorded in vivo. We therefore compared properties of neurons of two AC areas that strikingly differ in their sound-evoked responses, the core and the belt. These AC areas were preidentified in each animal using extracellular recording of their characteristic neuronal responses to sound stimuli (see Methods). Electrical properties of layer V pyramidal neurons were studied by the patch-clamp technique.

The neurons were identified based on their morphological properties and typical spiking patterns induced by long depolarizing stimuli (Fig. 28). In these experiments, synaptic conductances mediated by excitatory ionotropic glutamate or inhibitory GABA-A/glycine receptors were blocked by specific antagonists (see Methods).

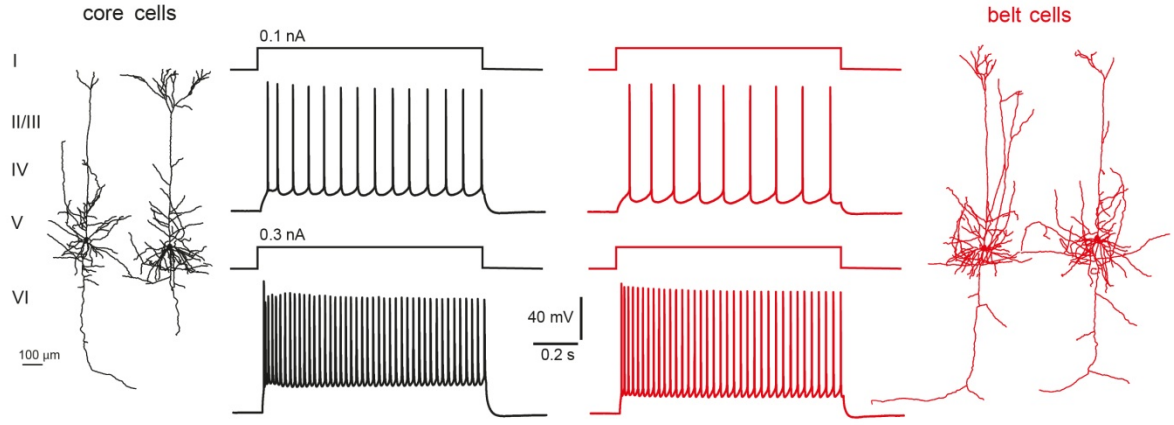

Fig. 28 **Identification of layer V pyramidal AC neurons.** Examples of morphological properties of core (black) and belt neurons (red) (biocytin staining). Neurons from both areas had long apical dendrites with tufted terminal arborizations mostly reaching the layer I. Traces in the middle show typical spiking patterns of those neurons. Most of neurons were classified as the regularly spiking type and the adaptive or non-adaptive subtype.

4.1.1. Differential excitability of layer V neurons from core and belt

We found that the resting membrane potential of core and belt neurons slightly differed (Table 1). The membrane time constant (τ_m) and input resistance (R_{in}) of core neurons were significantly increased compared to those found at neurons from belt. Such observations suggested differences in basal excitability of core and belt neurons. This hypothesis was further tested by measuring the rheobase of action potentials evoked by 1 s–long voltage steps of increasing amplitude (Fig. 29A). The rheobase was defined as minimal amplitude of depolarizing current stimulus that needed to be applied to induce at least one action potential. We found significantly lower values of rheobase for core neurons than for neurons from the belt (Table 1). The threshold of action potentials evoked by 0.2nA current steps was not significantly different between these two groups (Table 1). On the other hand, the latency of action potentials induced by weakly depolarizing current injections (0.1 nA) was significantly shorter in core neurons than in neurons from belt (Fig. 29A) (core: 28.5 ± 18.5 ms, n = 27; belt: 56.3 ± 28.8 ms, n = 23, $p < 0.001$, unpaired t-test). Latency of action potentials induced by stronger stimuli (>0.1 nA) was not significantly different between neurons of core and belt ($p = 0.882$ for 0.2 nA and $p = 0.199$ for 0.3 nA stimuli). The data therefore indicate a higher basal excitability of core neurons.

Parameter	Core (mean ± SD)	Belt (mean ± SD)	P (t-test)
V_{rest}(mV)	-76.9 ± 3.2	-75.7 ± 3.3	0.028
τ_m (ms)	27.4 ± 10.4	18.0 ± 5.7	< 0.001
R_{in} (MΩ)	191.0 ± 64.2	122.2 ± 41.2	< 0.001
$AP_{threshold}$ (mV)	-53.3 ± 2.4	-53.1 ± 1.9	0.717
Rheobase (pA)	64.6 ± 35.9	94.1 ± 46.2	< 0.001

Table 1 **Passive and active intrinsic electrical properties of core and belt neurons** with statistic significance of differences between the areas. The data is collected from 76 neurons of core and from 78 neurons of belt.

In both areas, values of rheobase negatively correlated with values of R_{in} and resting membrane potential (V_{rest}) (Fig 29B, C). This indicated the presence of shunting and depolarizing membrane conductance that regulated the basal excitability of AC neurons. The

correlation coefficients obtained from scatter plots of rheobase vs R_{in} were significantly higher than those from scatter plots of rheobase vs V_{rest} ($p = 0.0111$ for core and $p = 0.008$ for belt). Thus, rheobase appeared to be more tightly related to R_{in} than to V_{rest} in both core and belt. The correlation coefficients of relationships between rheobase and R_{in} or between rheobase and V_{rest} were not significantly different in core and belt neurons (Fig. 29). This suggested similar ionic mechanisms underlying the conductance in both areas. On the other hand, the slope of linear regression of relationship between rheobase and R_{in} (but not between rheobase and V_{rest}) was significantly steeper for belt neurons than for those from core (Fig. 29). This indicated that the shunting conductance and its effect on basal excitability were significantly stronger in neurons from the belt.

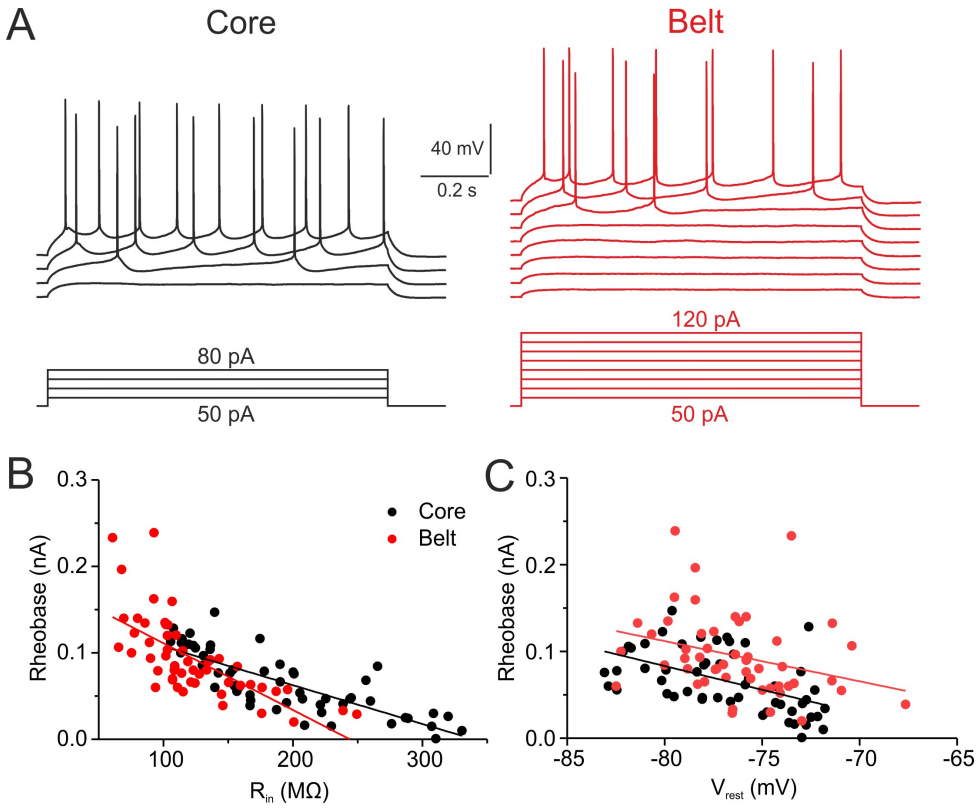

Fig. 29 **Differential excitability of core and belt neurons. A** - examples of the responses of the core and belt neurons to current steps of gradually increasing amplitude; **B** and **C** - the scatter plots show relationship between rheobase and input resistance (R_{in}) or between rheobase and the resting membrane potential (V_{rest}) in 53 neurons from the core and 53 neurons from the belt. Coefficient of correlation (Pearson r) calculated for data in B is r = -0.798 (core) or r = -0.690 (belt) and for data in C is r = -0.526 (core) or r= -0.302 (belt). The difference between each pair of correlation coefficients was not significant ($p = 0.2187$ for

plot in B; p = 0.177 for plot in C). Solid lines indicate linear regression fitted to data in each plot. The regression slope of relationship between rheobase and R_{in} was significantly steeper for belt neurons than for those from core (core: -0.449; belt: -0.773, p = 0.0054). The slopes in plot C were similar (core: -5.467, belt: -4.637, p = 0.726).

4.1.2. Identification of the shunting conductance in layer V neurons from core and belt

Basal excitability of layer V cortical neurons was previously shown to be controlled by constitutively active low voltage activated K+ channels (LVAK), inwardly rectifying Kir2.2/2.3 K+ channels (KIR), K+-selective leak (K_{leak}) channels and hyperpolarization/cyclic nucleotide gated (HCN) cation channels (Day et al., 2005, Huggenberger et al., 2009, Bekkers and Delaney, 2001). In our next experiments, we investigated whether core and belt neurons exhibit differences in activity of these channels. We first tested effects of 4-aminopyridine (4-AP), an inhibitor of LVAK (Bekkers and Delaney, 2001), on excitability of core and belt neurons. Application of 100µM 4-AP in the presence of inhibitors of GABAA, glycine, NMDA and AMPA/kainate receptors (10mM SR95531, 0.3µM strychnine, 5µM CPP and 10µM DNQX) increased R_{in} or τ min both core (by 8.9 ± 8.8% or 13.5 ± 13.5%, n = 14, p<0.001 or p=0.004, paired t-test) and belt neurons (by 8.9 ± 6.7% or 14.7 ± 17.3%, n = 14, p=0.005 and p=0.012, paired t-test). The effects of 4-AP were not significantly different in core and belt neurons (p=0.980 or p = 0.838) suggesting similar densities of LVAK in neurons of core and belt. Consistent with this, 4-AP in both auditory areas significantly decreased rheobase (core: by 22.2 ± 23.5%, n = 10, p = 0.036 paired t-test; belt: by 19.9 ± 25.1%, n = 13, p = 0.023) and shortened latency of spikes evoked by weakly depolarizing current injections (100 pA) as in Fig. 29A (core: by 34.4 ± 26.4%, n = 10, p = 0.009, paired t-test; belt: by 34.0 ± 21.8%, n = 12, p = 0.005, paired t-test). Differences in effects of 4-AP on rheobase or spike latency between core and belt neurons were not significant (p = 0.827 or 0.969).

Next, we tested differences in amplitudes of currents mediated by K_{leak} and KIR channels expressed by core and belt neurons. These channels were found to be sensitive to extracellular Ba^{2+} (Day et al., 2005). We induced current responses of these channels by voltage ramps (-140 to +50 mV) injected into layer V neurons and isolated them by subtracting a membrane leak recorded in the presence of 1 mM BaCl (Fig. 30A). In both areas, those currents reverted at membrane potential that was close to Nernst equilibrium

potential for K^+ (-94.8 mV) (Fig. 30B). Average density of conductance triggered by these Ba^{2+}-sensitive channels was similar in core and belt neurons (Fig. 30B). This indicated that differences in activities of K_{leak} or KIR could not explain different excitability of neurons from core and belt.

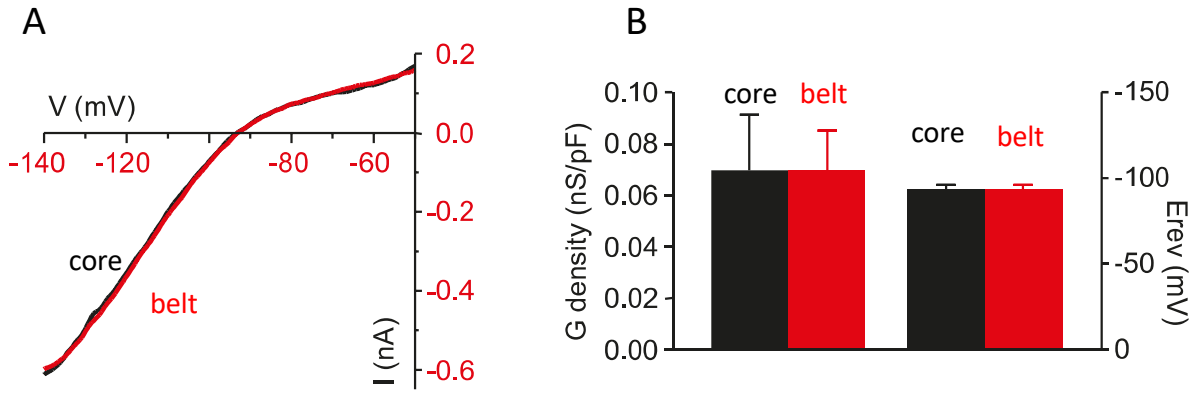

Fig. 30 **Similar density of K_{leak} and KIR channels in core and belt neurons. A -** current to voltage (I/V) relationship of Ba^+-sensitive currents induced by voltage ramps (-140 to +50 mV) injected into neurons of core (black) and belt (red) Membrane conductance induced by activity of Ba^+-sensitive channels was deducted from the slope of linear function fitted to the negative part of I/V plot. **B -** bar graph shows average conductance density (conductance normalized to cell size) and reversal potential (E_{rev}) of Ba^+-sensitive currents in core and belt neurons.12 neurons from each area were analyzed; differences in G density or E_{rev} were not significant; p = 0.974or 0.939, unpaired t-test.

4.1.3. Differential density of I_h in layer V neurons from core and belt

Activity of HCN channels was induced by hyperpolarizing voltage commands from a holding potential at -60 mV, injected into neurons of core and belt. The hyperpolarizations triggered a slowly activating inward current (Fig. 31A) that was identified as the hyperpolarization-activated current (I_h) on the basis of its insensitivity to 4-AP and Ba^{2+}, and sensitivity to ZD 7288. The current had an apparent reversal potential (E_{rev}) of -35.7 ± 7.4 mV in core neurons (n = 15) or -36.5 ± 5.8 mV in neurons from the belt (n = 9). A half-maximal activation voltage ($V_{1/2}$) of the I_h was -86.5±9.0 mV in core neurons (n = 29) and -87.2± 6.3mV in neurons from the belt (n = 23) (Fig. 31B, C). The slope of the activation curve of Ih was 12.1± 6.2mV in core neurons and 13.3± 4.9mV in neurons from the belt. The values of E_{rev}, $V_{1/2}$ or slope were not significantly different in both neuronal groups.

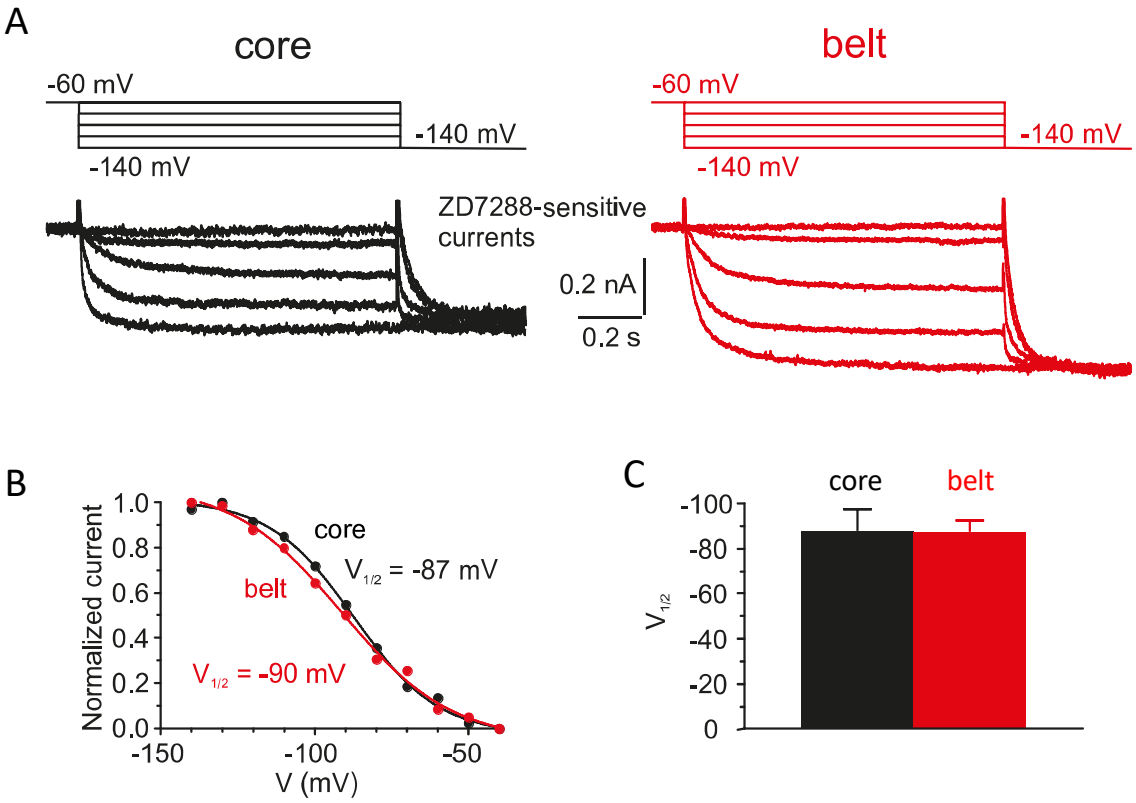

Fig. 31 **Hyperpolarization-activated current (I_h) in neurons of core and belt. A** - traces show inward currents activated by hyperpolarizing voltage commands (from -60 mV to -140 mV with -20 mV decrement; top) injected into neurons of core (black) or belt (red). The leak current, insensitive to ZD7288 (10 μM) was digitally subtracted. **B** - the amplitude of tail-current traces (recorded from neurons in A) measured immediately after the voltage step to -140mV was plotted as function of the preceding membrane potential. The data were fitted by the Boltzmann equation to obtain the half-maximal activation voltage ($V_{1/2}$) of the I_h. **C** - values of $V_{1/2}$ were similar in neurons of core and belt ($p = 0.7649$, unpaired t-test).

We next determined membrane conductance induced by activity of HCN channels in neurons form core and belt. A prepulse to −140 mV was applied from a holding potential of −40 mV to maximally activate the channels, followed by a test pulse to potentials between −140 and −40 mV to determine the I/V relationship (Fig. 32A). The current at the beginning of the test pulse was plotted against test-pulse voltage, and analysed by linear regression (Fig. 32B). The regression slope was significantly steeper in neurons from belt (3.4 ± 1.5 nS, n = 27) than in neurons from core (2.4 ± 1.6 nS, n = 43, p = 0.012). After normalizing the slope to cell capacitance we obtained the conductance density of HCN channels, which was

significantly increased in neurons of belt (Fig. 32B, C). This suggested that I_h was not uniformly distributed among AC areas and could thus contribute to differences in excitability of neurons from core and belt.

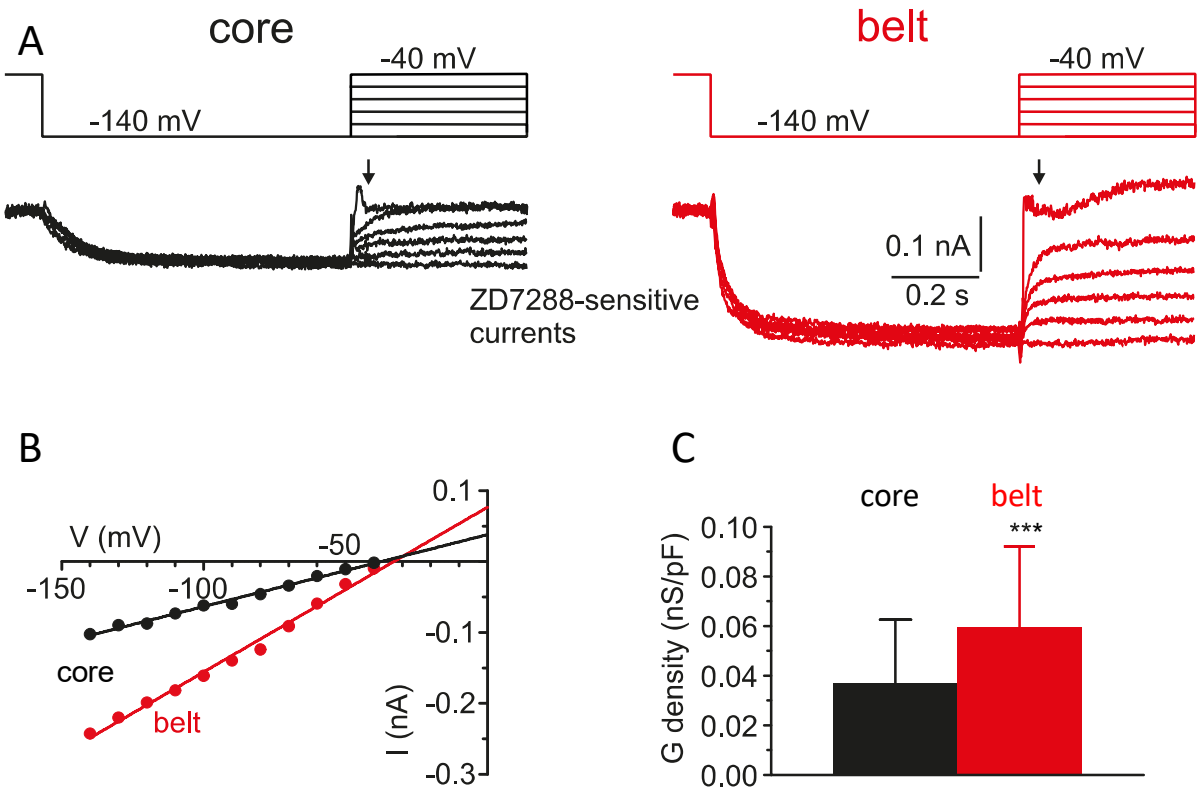

Fig. 32 **Higher density of Ih in neurons from belt. A** - traces show inward currents triggered by hyperpolarizing voltage commands (from -40 mV to -140 mV) preceded by a prepulse to −140 mV and injected into neurons of core (black) or belt (red). I_h was isolated pharmacologically by subtracting currents in the presence of 10 μm ZD 7288 from those under control conditions. **B** - I/V relationship for fully activated channels obtained by subtracting the tail-current amplitudes of two sets of tail currents. The tail current amplitudes were measured immediately after the voltage clamp to the indicated test voltages was settled (indicated by arrows in panel A). **C** - conductance density of HCN channels expressed by core neurons was significantly lower compared to one found in neurons of belt ($p < 0.001$, unpaired t-test).

To investigate effects of I_h on basal excitability of core and belt neurons, we compared electrical properties of these neurons in the absence and presence of ZD7288 (Fig. 33). We found that ZD7288 significantly hyperpolarized neurons and increased R_{in} and τ_m, which confirmed that I_h was already activated at the resting membrane potential of AC neurons.

Also, ZD7288 lowered rheobase and shortened latency of action potentials induced by weak depolarizing stimuli (Fig. 33 and 34A), which was consistent with the shunting effects of I_h. Importantly, all ZD7288-induced effects on the electrical properties appeared to be stronger in belt neurons than in neurons of core (Fig. 33).

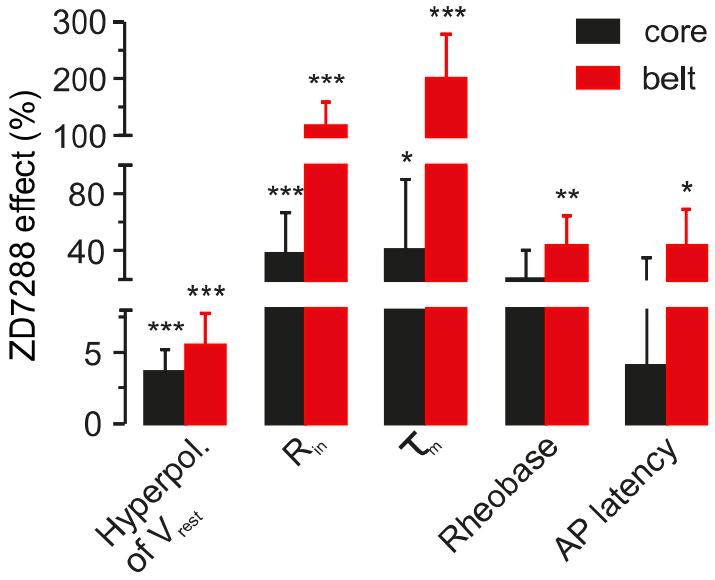

Fig. 33 **I_h-mediated control of basal excitability is more strong in belt neurons than in neurons from the core.** Bar graph summarizes changes in electric properties of core and belt neurons in the presence of I_h blocker, ZD 7288. Each column represents an average effect of the blocker on a quantity, calculated as (1-(value obtained in the presence of ZD 7288/value obtained in the absence of ZD 7288) × 100%). Except for rheobase and spike latency in core neurons, ZD 7288-induced changes were significant in both neuronal groups (paired t-test). Effects of ZD 7288 on R_{in}, τ_m and latency of action potentials significantly differed in core and belt neurons ($p < 0.001$, 0.001 and 0.05, two-way ANOVA with Bonferroni post-hoc test). Data collected from 17 core and 12 belt neurons.

The effect of ZD 7288 on spike latency became insignificant when action potentials were induced by stronger depolarizing stimuli (0.2 nA; $p = 0.125$ for 10 core neurons and $p = 0.079$ for 7 neurons from belt, paired t-test). This indicated that I_h operates and exerts its influence mainly around the resting membrane potential, by shunting the spike triggering depolarizations. Consistent with this, the amplitude and the half width of already triggered action potentials were not different in core and belt neurons (Fig. 34B). We found however, that in addition to spike latency, I_h also affected the shape of action potentials induced in layer V AC neurons. The first derivative of an action potential triggered by 0.2 nA current step

showed two clear peaks that correspond tothe axonal and somatic action potentials (Kress et al., 2008, Colbert and Johnston, 1996) (Fig. 34C). We found that ZD 7288 both increased the peaks and shifted them to less depolarized potentials (Fig. 34C) suggesting that I_h by decreasing excitability of layer V AC neurons could affect their spiking properties.

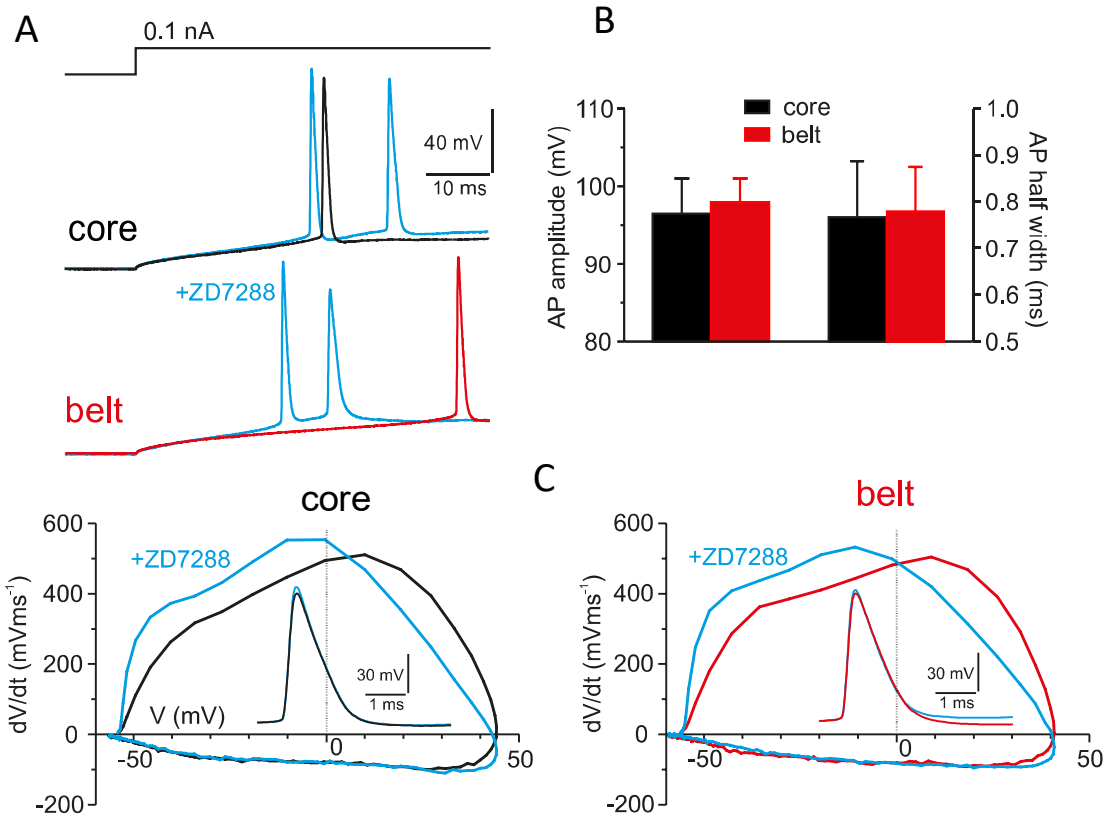

Fig. 34 **Effects of I_h on the shape of action potentials in layer V AC neurons. A** - traces show action potentials induced in core (black trace) or belt (red trace) neurons by 0.1 nA current steps (top) in the absence or presence (blue traces) of 10μM ZD 7288. Note that the I_h blocker dramatically shortened the latency of action potentials induced in neurons of belt but not in neurons of core. **B** - bar graph compares average amplitudes and half-width of action potentials as in A, induced in 41 core and 37 belt neurons ($p > 0.05$ for both quantities, two-way ANOVA with Bonferroni post-hoc test). **C** - plots show relationship between the slope (dV/dt) of an action potential (displayed as an inset in each phase plot) and the membrane voltage recorded from core or belt neurons in the absence (black and red traces) or presence (blue traces) of ZD 7288.

4.1.4. I_h-mediated modulation of spiking of layer V AC neurons

To assess the modulatory role of I_h in mechanisms of spike generation by AC neurons, we compared the firing rates of core and belt neurons that differ in density of I_h. We sought an experimental protocol that would include both the shunting effects of constitutively active and the depolarizing effects of phasically activated I_h. To ensure this, we stimulated action potentials by trains of 100 brief current steps injected into core and belt neurons at high frequency. The frequency of steps was chosen based on kinetics of depolarization sag observed in voltage responses of AC neurons to hyperpolarizing current injections (Fig. 35). The presence of such sag is thought to be the hallmark of neurons expressing I_h (Robinson, 2003). We found that the sag in voltage responses of AC neurons was sensitive to ZD 7288, which confirmed that it was linked to I_h (Fig 35). The sag induced by hyperpolarization step (-0.5 nA/1 s) had similar amplitude in neurons of core and belt (4.7 ± 2.5 mV in 66 core neurons and 4.7 ± 2.4 mV in 71 belt neurons) but activated with different time course (mean time constants: 108.1 ± 46.9 ms and 144.5 ± 53.3 ms in 63 core and 68 belt neurons; $p < 0.001$, unpaired t-test).

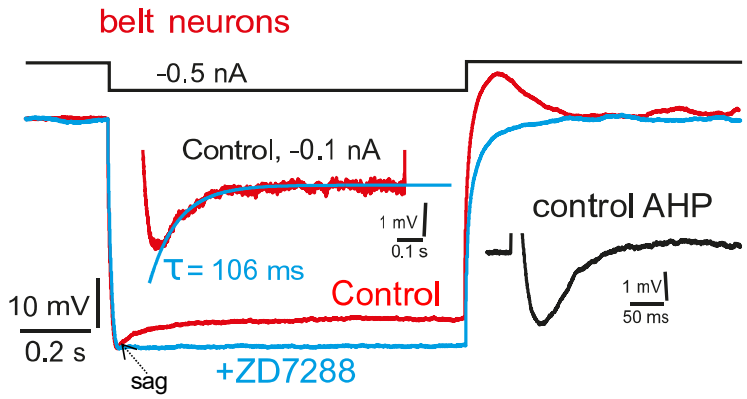

Fig. 35 **Depolarization sag in hyperpolarizing responses of layer V AC neurons.** The traces show examples of voltage responses of belt neurons upon hyperpolarizing current injections (0.5 nA/1 s) made in the absence (red) or presence (blue) of ZD 7288. Note the voltage-dependent activation of a time-dependent sag (arrow) in the hyperpolarizing response. This sag was virtually eliminated by ZD 7288. The sag amplitude was determined as repolarization from peak hyperpolarization (core: -106.9 ± 10.5 mV; belt: -103.0 ± 11.2 mV) to a steady-state value during the 1 sec current injection. The time course of sag was analyzed by its fitting to sum of two exponential functions and the mean amplitude-weighted time

constant was calculated. Inset in the middle shows the time course (τ) of the depolarizing sag during the hyperpolarization step -0.1 nA, which is close to the time course of decay of the afterhyperpolarization (AHP) of action potentials (inset on the left).

Our hypothesis was that depolarizing sag would accelerate the decay of spike afterhyperpolarization (AHP, as shown in Fig. 35) and therefore increase the probability of action potentials repeatedly stimulated at intervals that match the sag kinetics. Action potentials induced in AC neurons by single current steps (1.2 nA/2 ms) exhibited AHP that peaked at -2.5 ± 0.9 mV or at -2.2 ± 0.8 mV in 35 core or in 35 belt neurons ($p = 0.167$, unpaired t-test) within ~50 ms after the step. After the peak, the AHP decayed to resting potential level within another 161.4 ± 48.9 (core) or 108.5 ± 33.5 (belt) ms ($p < 0.001$, unpaired t-test), i.e. ~150 – 200 ms after the spike. Assuming that AHP at its decaying phase would be more sensitive to weak depolarizations induced by I_h, we set the interval of current steps in a train to either 100 or 150 ms (Fig. 36A). In each cell, amplitudes of steps were preadjusted to produce about half maximal initial probability of spike generation. These amplitudes were required to be higher in belt neurons, consistent with their lower excitability (Fig. 36B). After the adjustment, neurons of belt responded to trains of 100 current steps by steady state firing rates that were actually significantly increased compared to those produced by neurons of core (Fig. 36A, C).The increase was observed for action potentials stimulated at 150 but not at 100 ms intervals, finding which was consistent with the slow activation kinetics of I_h. Thus the data suggest that at certain stimulation frequencies layer V AC neurons could generate either the onset type or the sustained type of response (Fig. 36A), mostly depending on their I_h density. Taken together, we observed a complex role of I_h in mechanisms that determine spiking properties of layer V AC neurons. We conclude that differential distribution of I_h could contribute to variability of sound-evoked responses of layer V AC neurons observed in vivo.

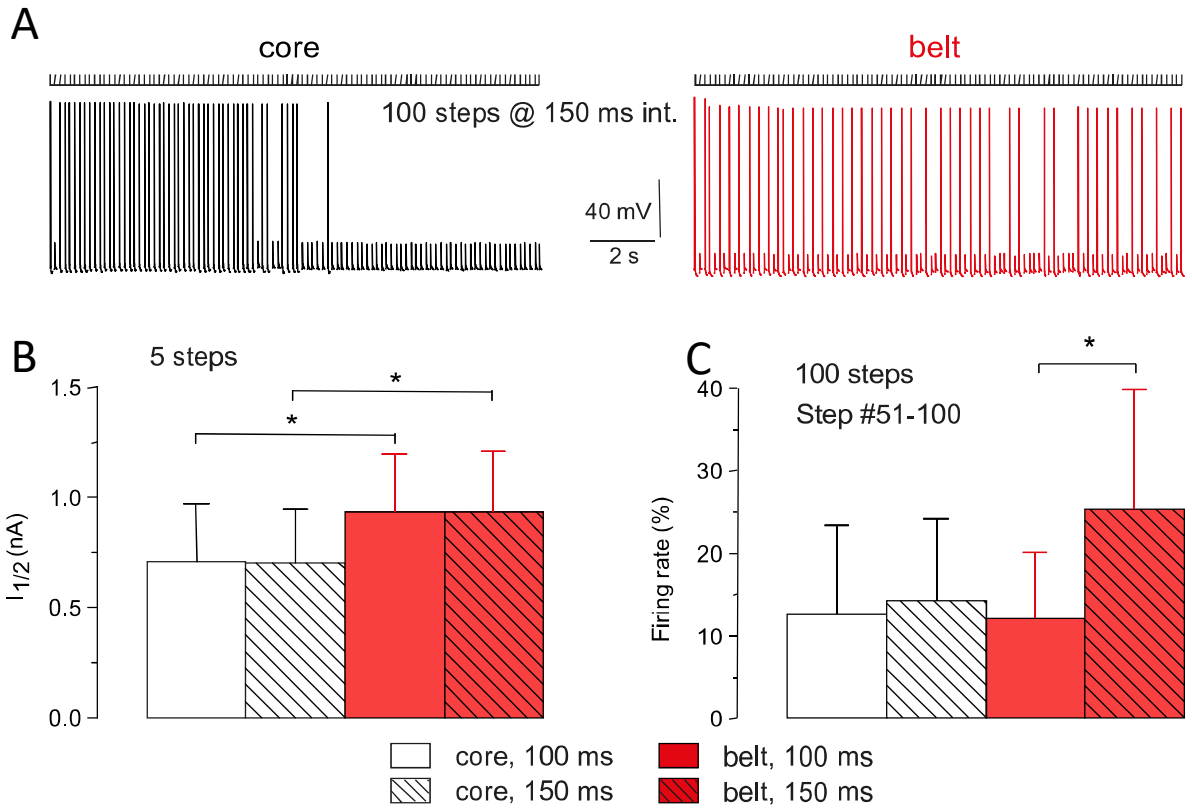

Fig. 36 **Higher steady state firing rates in belt neurons than in neurons of core. A** - traces show examples of voltage responses of core and belt neurons to trains of 100 depolarizing current steps delivered at 150 ms interstimulus intervals. Note that both types of neurons responded by a mixture of action potentials and their failures. The amplitude of current steps was set to induce about half maximal firing rate during initial phases of a train. **B** - bar graph shows average amplitudes of current steps ($I_{1/2}$) inducing half maximal firing rate when injected as a train of 5 at 100 or 150 ms intervals into 23 core or 18 belt neurons. $I_{1/2}$ was significantly increased in neurons of belt (two-way ANOVA with Bonferroni post-hoc test). **C** - steady state firing rates in voltage responses of 7 core and 7 belt neurons to trains of 100 current steps as shown in A. The firing rate was calculated as probability of an action potential during last 50 stimulations in a train. Belt neurons showed significantly increased firing rates when stimulated at 150 ms intervals ($p < 0.05$, paired t-test).

4.1.5. Identification and localization of HCN channel subtypes in layer V AC neurons

Last set of experiments was aimed to address whether belt neurons that show higher amplitudes of I_h actually express higher levels of HCN channels. In mammals, four homologous HCN channel subunits (HCN1-4) have been cloned (Robinson, 2003). They

provide individual HCN currents that quantitatively differ from each other with respect to their functional properties (Biel et al., 2009). A shallow activation curve and intermediate $V_{1/2}$ suggested more HCN subtypes to be expressed in core and belt neurons. We analyzed the expression of *Hcn1–4* genes encoding HCN channels in layer V AC neurons using single-cell RT-qPCR (see Methods). We found that most of core and belt neurons express high levels of *Hcn1-3* transcripts and low levels of *Hcn4* (Fig. 37A). Expression levels of all mRNAs were not significantly different in core and belt neurons (Fig. 37B). Thus, differences in I_h density in core and belt neurons do not seem to be explained by unequal expression of HCN channels in these neuronal groups.

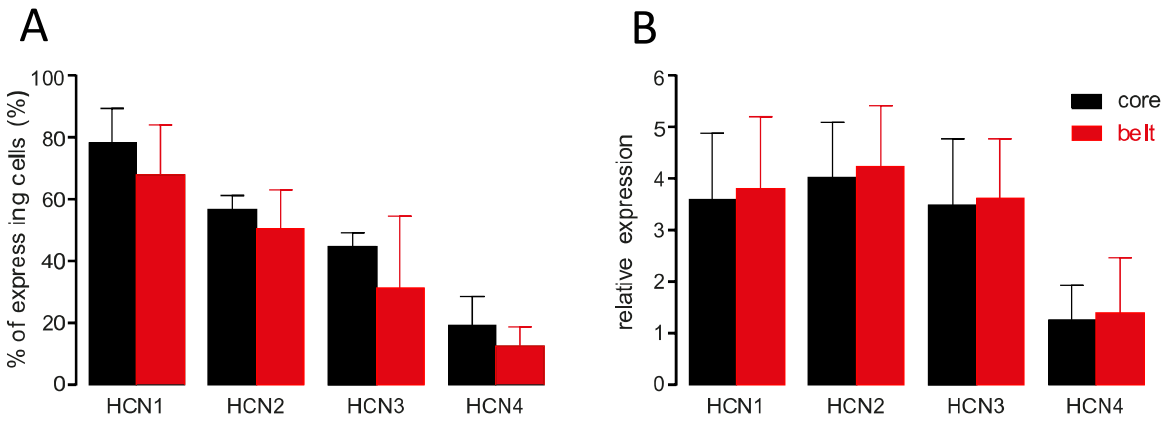

Fig. 37 **Expression of *Hcn1-4* genes in core and belt neurons. A** - percentage of neurons expressing *Hcn1-4* transcripts. **B** - relative expression of *Hcn1–4* genes was not significantly different in core and belt neurons. The values are presented as mean ± SEM. Significance was evaluated using one-way ANOVA.

We next asked if HCN channels could localize to different cellular compartments in core and belt neurons. The subcellular distribution of HCN channels was studied using immunohistochemistry methods by Tetyana Chumak. Sections of AC were labelled with specific antibodies raised against HCN1 and HCN2 subunits (that exhibit prevalent expression levels) and the staining was observed in confocal microscope. We found that both types of subunits localized to somatic and dendritic compartments in layer V AC neurons and the staining did not shows any obvious differences between core and belt neurons. Thus, differences in I_h density in core and belt neurons cannot be explained by differential distribution of HCN subunits in these neurons.

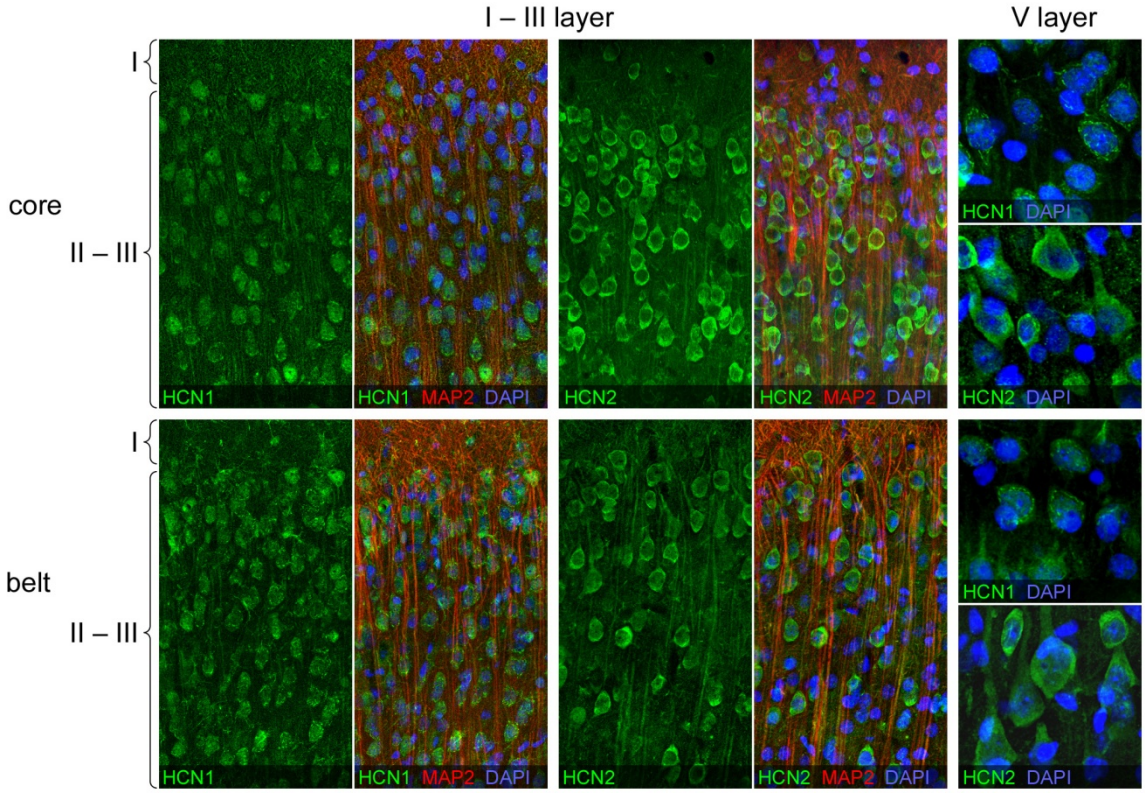

Fig. 36 **Localization of the HCN1 and HCN2 channel subtypes in AC neurons.** Confocal micrographs show triple staining of coronal AC slices with antibodies against microtubule-associated protein 2 (MAP2, red), nuclear dye DAPI and HCN1 or HCN2 (green). The labeling revealed the HCN1 or HCN2 immunopositive somata and MAP2-positive apical dendrites in both core and belt neurons.

4.2. Corticofugal modulation of the neuronal responses in the inferior colliculus of rat

In adult rat (Long Evans strain), the ipsilateral AC was inactivated using a cooling probe and single- or multiple-unit activity in the IC in response to acoustical stimulation was recorded before, during and after the AC cooling. In total, 13 electrode probe insertions representing 208 electrode spots were analyzed.

4.2.1. The CF profile of individual electrode probe tracks

The electrode probe was inserted into the IC in a dorso-ventral direction. The distance between individual electrode spots was 100 μm; therefore 16 spots of the multielectrode probe

covered almost the whole extent of the frequencies represented in the IC (Fig. 21). The CF profiles of individual electrode probe insertions (Fig. 37) were very similar; small CF variability reflected slight differences in ventro-medial or rostro-caudal directions of electrode probe insertion.

On the basis of the histological control and neuronal response parameters the first three uppermost electrode spots at a depth of 100-300 µm were classified to be localized in the DCIC. DCIC neurons responded well to broad-band noise and low-frequency tones (up to 10-15 kHz) of higher intensity. However, stimulation with low-frequency tones of lower intensity resulted in weak responses with relatively high thresholds (about 50 dB SPL) and the CF was usually difficult to identify from their excitatory response areas (an example in Fig. 37, insert a).

Neurons recorded at electrode spots 6-16, localized at the depth of 600-1600 µm in the IC, responded well to pure tone stimuli and had sharp frequency tuning curves with low thresholds at the CF (examples in Fig. 37, inserts b and c). These neurons were classified to be localized in the CIC.

The area in the IC at a depth of 400-500µm (electrode spots 4 and 5) was identified as a transition zone between the DCIC and CIC (gray band in Fig. 37), neurons localized within this zone showed minimal changes during AC inactivation.

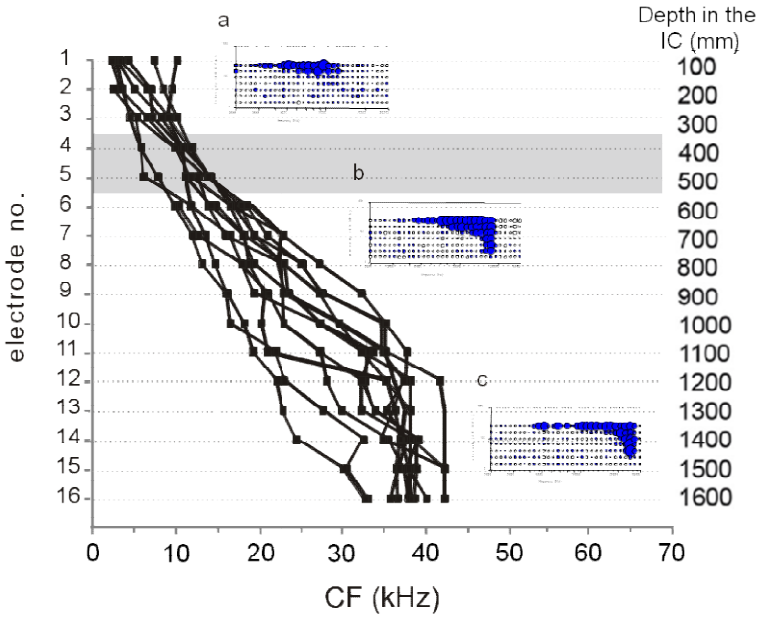

Fig. 37 **The CF profile of individual electrode probe tracks** with inserted examples of excitatory response areas of IC neurons recorded from electrodes at different depths in the IC (insert **a** represents electrode No. 2, insert **b** represents electrode No. 7 and insert **c** represents electrode No. 14). The gray band represents the transition zone between DCIC and CIC.

4.2.2. Effect of AC inactivation on frequency tuning of IC neurons

Mapping of the neuronal excitatory response areas in individual IC neurons was performed under pre-cooling conditions, during the AC cooling and after the cooling. AC cooling did not change significantly any parameters of the frequency tuning curves (neuronal CF, CF threshold, shape of the response area) in any of the recorded IC neuron (Fig. 38).

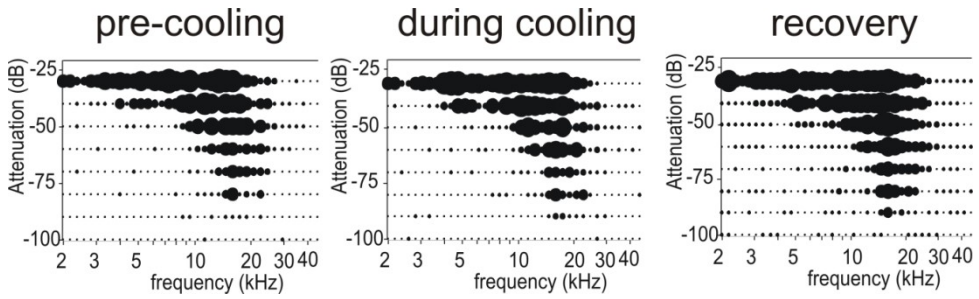

Fig. 38 **Frequency-intensity response areas of an IC neuron measured before, during cooling and after AC cooling**.

4.2.3. Effect of AC inactivation on response magnitude to sound stimulation

At first, the response magnitude to BBN stimulation, expressed as a number of spikes in response to 60-ms BBN stimulus presentation, was studied. During AC cooling the spike rate significantly increased in comparison with the pre-cooling state in 47% of neurons ($p < 0.05$) located through the whole IC. In the remaining neurons, the spike rate either did not change (in 39% of units, $p > 0.05$) or decreased (in 14% of units, $p < 0.05$).

The response magnitudes of the IC neurons to BBN stimulation recorded at individual electrode spots during the cooling procedure were averaged across all the animals and expressed as a relative response with respect to the pre-cooling magnitude that was taken as 100% (CTR, straight gray lines in Figs. 39A, B). The solid blue line in Fig. 39A demonstrates an average relative response at individual electrode spots during AC cooling. The maximal increase of responses to BBN stimulation during AC cooling was detected in the DCIC at a depth of 100 and 200 μm (electrodes 1 and 2), reaching average values of 177.1±25.2% and 216.5±40.2%, respectively (mean ± SEM, $p<0.05$%, one-sample t-test). At deeper spots (electrodes 4 and 5, depths of 400 and 500 μm in the IC) the AC cooling produced only minimal and non-significant changes in the response magnitude (119.9±10.7%, and 117.2±9.0%, respectively). This area can be considered as a transition zone between the DCIC and CIC, neurons recorded in this area show minimal changes not only in evoked responses, but also in spontaneous activity (Fig. 39B).

In the central part of the IC (electrodes 6-14, depth 600-1400 µm in the IC) the response magnitude again increased, ranging between 119% and 159% (SEM=10-20%) of the pre-cooling values at individual electrodes positions ($p<0.05$% on electrodes 6-11, one-sample t-test).

Individual time segments of the response to BBN stimulation were influenced by AC cooling in a different extent. The dotted line in Fig. 39A demonstrates the effect of AC cooling on the initial 10 ms part of the response (onset part of the response spanning the first 10-20 ms after stimulus onset), the dashed line shows the effect on the last 10 ms of the response (end part spanning the 60-70 ms of the response after the stimulus onset). The shapes of all three curves are almost identical, i.e., the maximal increase of the relative response occurred in the DCIC, followed by a drop in the depth 300-500 µm in the IC and relative amplitude again increased in the CIC. However, changes in the onset part of the responses were generally much smaller than the changes in the end segments of the responses (Fig. 39A).

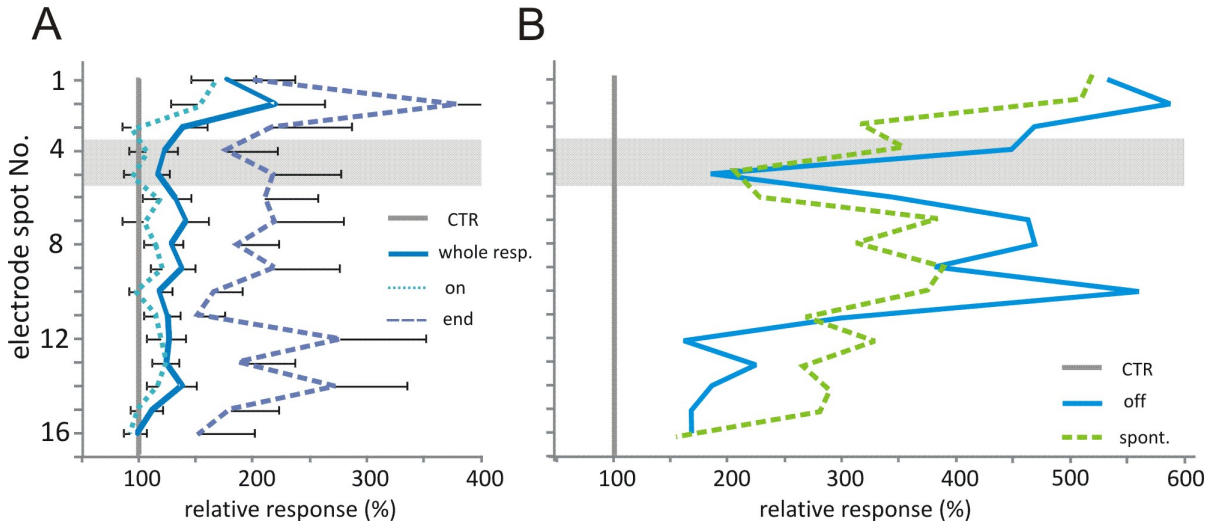

Fig. 39 **IC depth profile of the average relative response changes to BBN stimulation** with respect to the pre-cooling magnitude that was taken as 100% (CTR, straight gray lines in the panels A and B). **A**- whole average relative response is depicted with a blue solid line, the initial 10 ms onset part of the response (the onset part) with a dotted line, and the last 10 ms end part of the response (the end part) with an dashed line. **B** - IC depth profile of the average relative off response (solid blue line) and spontaneous firing rate (dashed green line). The gray bands represent a transition zone between DCIC and CIC. Bars in A represent +/- SEM.

A pronounced effect of the AC cooling was observed on excitatory off-responses, which usually followed 0-10 ms after the end of the normal response (i.e. 10-20 ms after the stimulus offset). In most neurons the off response was not present at all or it was very small in the control

recordings (a red ellipse in a pre-cooling example, shown in Fig. 40). During the cooling procedure, the off response in many neurons increased enormously and recovered 60 min after the end of the cooling procedure (Fig. 40, 41). The solid blue line in Fig. 39B represents the average relative magnitudes of off responses in individual electrodes, recorded during the AC cooling procedure. The shape of the curve is similar to that of the whole-responses (solid blue line in Fig. 39A), i.e., the maximum effect was present in the DCIC, followed by the drop in the depth 300-500 μm and then again increased in the central part of the IC, with the average relative values of the off responses ranging between 200% to 500% of the pre-cooling magnitudes (significant for electrodes 1-9, $p<0.05\%$, one-sample t-test).

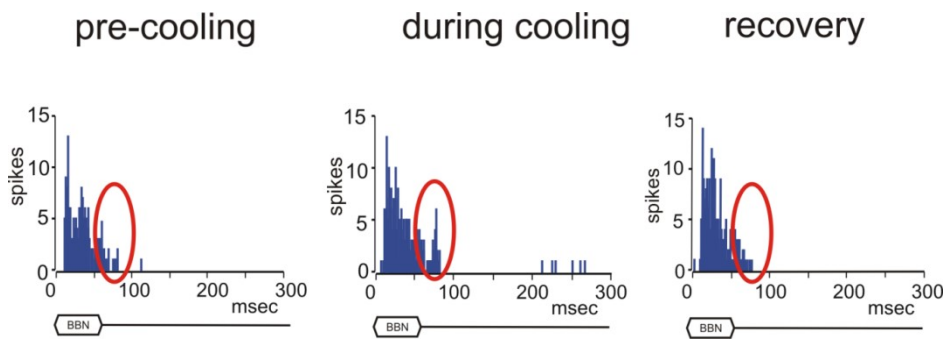

Fig. 40 **Peri-stimulus time histograms (PSTHs) of the one IC neuron** to demonstrate changes in the off response during AC cooling and recovery.

4.2.4. Changes in spontaneous activity

The changes in the evoked activity were also accompanied by changes in the spontaneous firing rate. Spontaneous firing rate was extracted from the last 100 ms of the recorded activity to stimulation using low-level BBN stimuli. The dashed line in Fig. 39B demonstrates the average spontaneous firing rate at individual electrode spots during AC cooling. Relative changes in the spontaneous firing rate at individual electrodes were very large, much larger than changes in the evoked responses, reaching sometimes more than 500% of pre-cooling values. However, due to the low level of spontaneous activity in many IC neurons under normal conditions, any increase in the spontaneous firing rate by only a few spikes resulted in a large relative change of firing rate. Thus, the variability of spontaneous firing rate changes was very large and the increase in spontaneous activity was statistically significant only at some isolated electrode spots ($p<0.05\%$ for electrode spots 3, 7-8, 10, 13, Wilcoxon Signed Rank Test).

4.2.5. Post-excitatory inhibition

In many IC neurons the response to sound stimuli under control conditions was followed by a period of post-excitatory suppression of spontaneous activity lasting 50-200 ms (red rings in examples in Fig. 41A, B). Of the 80 IC neurons expressing a sufficient level of spontaneous activity, 30 neurons demonstrated significantly reduced post-excitatory inhibition during AC cooling: spontaneous activity appeared immediately after the end of the evoked response (Fig. 41A, B). In most of these neurons, the weak suppression of spontaneous activity in the period of post-excitatory inhibition was associated with an increase in the off response (Fig. 41B). The post-excitatory suppression as well as off responses recovered to the pre-cooling state within approximately 30-60 min after the cooling was finished.

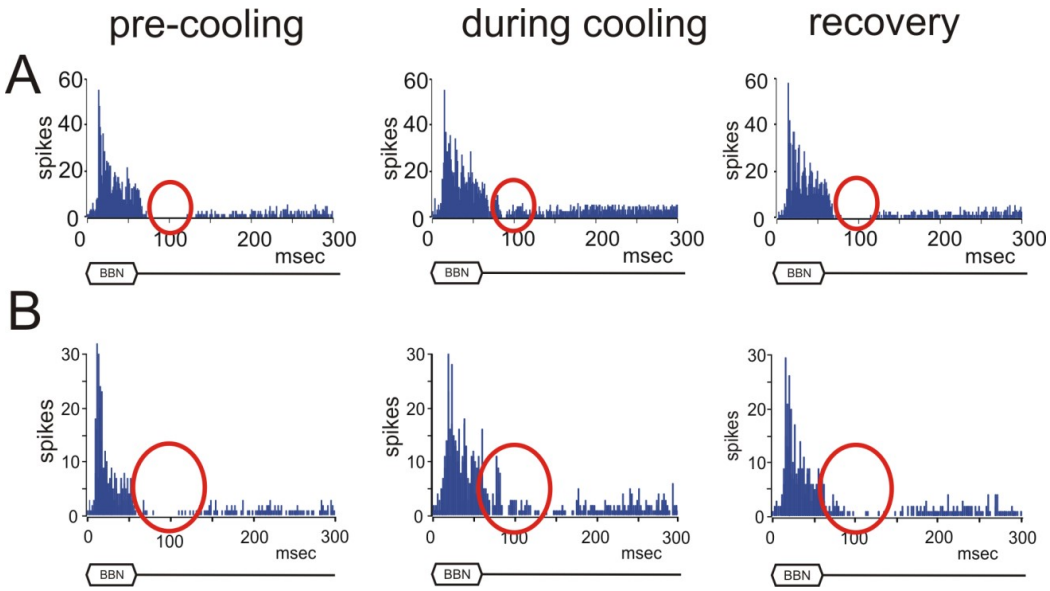

Fig. 41 **Peri-stimulus time histograms (PSTHs) of the two IC neurons** to demonstrate changes in the post-excitatory inhibition during AC cooling and recovery.

4.2.6. Responses to a series of clicks – neuronal adaptation

To test the adaptability of individual IC neurons, five animals from the whole group of tested rats were stimulated with a train of clicks with linearly decreasing and then increasing interstimulus intervals: decreasing from 25 ms to 6.6 ms and then increasing back to 25 ms, at the intensity of 60 dB SPL. Fig. 42 demonstrates representative examples of the responses to click train stimulation in neurons recorded in different depths of the IC in two animals. Under pre-cooling conditions, the IC neurons localized in the superficial layer of the DCIC (examples in Fig. 42 in the IC depth of 100 μm in both animals) quickly adapted to repeated clicks; they

usually responded to only a few initial clicks and their response to further clicks was very weak and not synchronized with the click occurrence. Neurons located in the central part of the IC (Fig. 42, examples in the IC depth of 900-1600 μm) were able to follow higher stimulus repetition rates with a synchronous response, but the response to the second part of the click train (with increasing inter-stimulus intervals) was much weaker.

During AC cooling, the responses of IC neurons to the click trains were different. Most of the IC neurons, including neurons localized in the DCIC, changed their response patterns: they responded with spikes synchronized to click train even at a high click repetition rate and also responded well to the later part of the click train with increasing click inter-stimulus intervals.

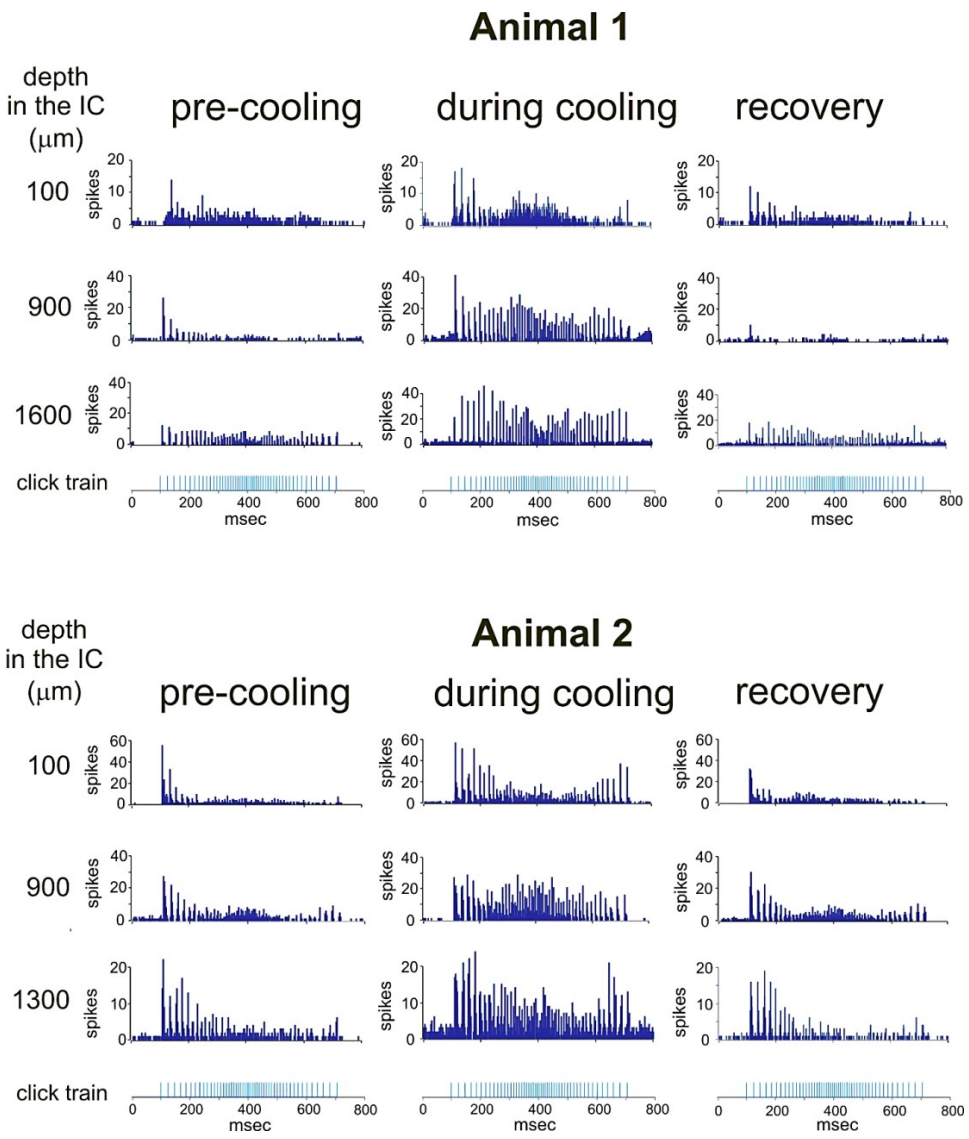

Fig. 42 **Representative examples of PSTHs of the responses to click train stimulation of IC neurons in two animals**, recorded in different depth in the IC before AC cooling, during cooling and 30-60 min after the end of cooling.

A significant increase in the number of spikes synchronously responding to individual clicks in the train during AC cooling was present in 71 neurons (out of 80, $p<0.05$). The remaining nine neurons, located in the marginal electrode positions (most dorsally or ventrally) in two animals did not change or even slightly decrease their responses to the click train. The average relative response magnitudes during AC cooling ranged between 120% and 260% of pre-cooling values.

However, the increase in the number of spikes in a response was not a dominant effect; the main effect of AC cooling was the improved synchronization of spikes with individual clicks up to high repetition rates. Fig. 43 demonstrates the average percentage of responses to individual clicks in the series. The maximal response percentage 100% means that each click in a series evoked at least one spike as a response. The green line with green circles in Fig. 43 demonstrates that during the control conditions, the average response percentage was very low in the DCIC (electrodes 1-3) and reached maximal values in the CIC. The variability between individual CIC neurons was very large, ranging between 20% to almost 100%; due to this large inter-individual variability the standard deviations are not shown. During AC cooling (blue solid line with blue rings), the response percentage almost in all IC neurons enormously increased and recovered to pre-cooling level 30-60 min after the AC cooling (dashed turquoise line with triangles). The curves representing the response percentage before and during AC cooling are significantly different ($p<0.0001$, two-way repeated measures ANOVA, $F=60.64$).

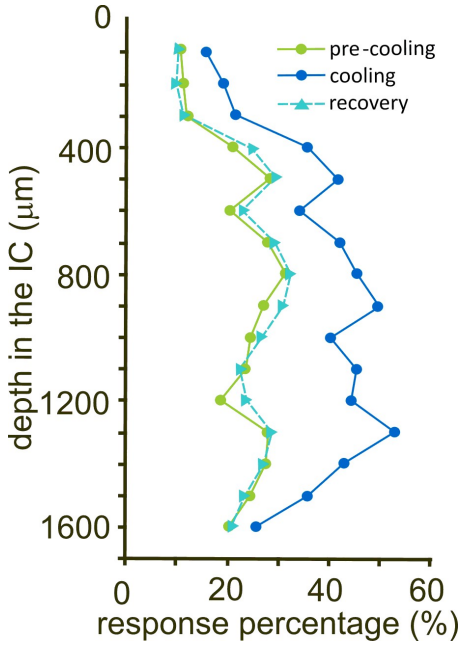

Fig. 43 **The average probability (%) of response to individual clicks in the series** before AC cooling, during cooling and 30-60 min after the cooling.

4.2.7. Recovery of neuronal activity after the end of AC cooling

Recovery of neuronal activity after cessation of the AC cooling was very individual and depended on the duration of AC cooling and the change of the response magnitude. In experiments in which the cooling lasted only 15-30 min, the responsiveness returned to pre-cooling values almost completely within 60 min. However, in experiments in which AC cooling lasted 40-60 min, the neuronal activity measured 60 min after the cooling offset still showed only partial recovery.

4.3. Acoustical enrichment-induced plasticity in rat auditory cortex

Long Evans rat pups (n=27) with mother spent two weeks in an AEE consisting of amplitude-modulated rippled noise with temporally variable sinusoidal spectral envelope (frequency range 983 – 48,461 Hz) presented at 55 dB SPL. To attract the animals' attention, the noise background was supplemented with four types of embedded target sounds presented randomly in time at 60 dB SPL (frequency-modulated tone, pure tone, 1/3-octave noise, sawtooth signal); the FM tone triggered release of sweep syrup. The AEE was applied only during active night periods. Controls (n=24) were raised in standard housing conditions. The hearing of animals was tested 3-4 months after the enrichment with recording of the auditory brainstem responses and multiunit neuronal activity in the AI area of the AC.

4.3.1. Auditory brainstem responses

Recording the responses from the auditory brain stem, evoked by the tones bursts of different frequencies, showed lower auditory thresholds in the enriched animals compared to the controls ($F=12.35$, $p=0.0006$), see Fig. 44, therefore confirming an improved sound detection ability already in the peripheral part of the auditory pathway. The threshold improvement was mostly expressed at lowest sound frequencies.

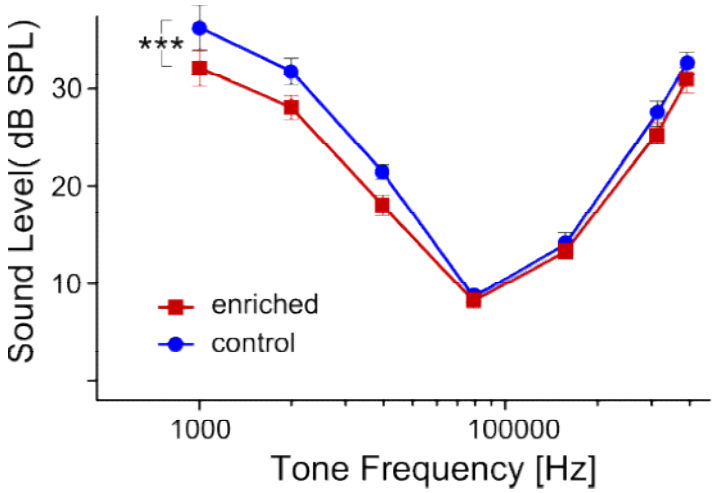

Fig. 44 **Auditory thresholds measured by means of auditory brainstem responses** (mean ± SEM, p=0.0006, two-way ANOVA).

4.3.2. Excitatory thresholds and frequency tuning

The receptive fields were analyzed in 975 units from the control animals and 966 units from the enriched animals.

Neuronal excitatory thresholds correspond to the lowest sound intensity that the neurons can detect. The enriched animals show significantly lower values of the excitatory thresholds compared to the controls (enriched: 7.980±0.254 dB SPL; controls: 11.62±0.261 dB SPL; $p<0.0001$, unpaired t-test), see Fig. 45A. This indicates a higher sensitivity of the enriched cortical neurons to very faint sounds. When the excitatory thresholds are averaged in ½-octave bins, it is possible to plot the dependence of the mean threshold on neuronal characteristic frequency. Fig. 45B shows that the averaged frequency-dependent excitatory thresholds differ between the experimental groups ($F=72.79$, $p<0.0001$), they also differ significantly in most of the individual frequency bins (two-way ANOVA with Bonferroni post-hoc test).

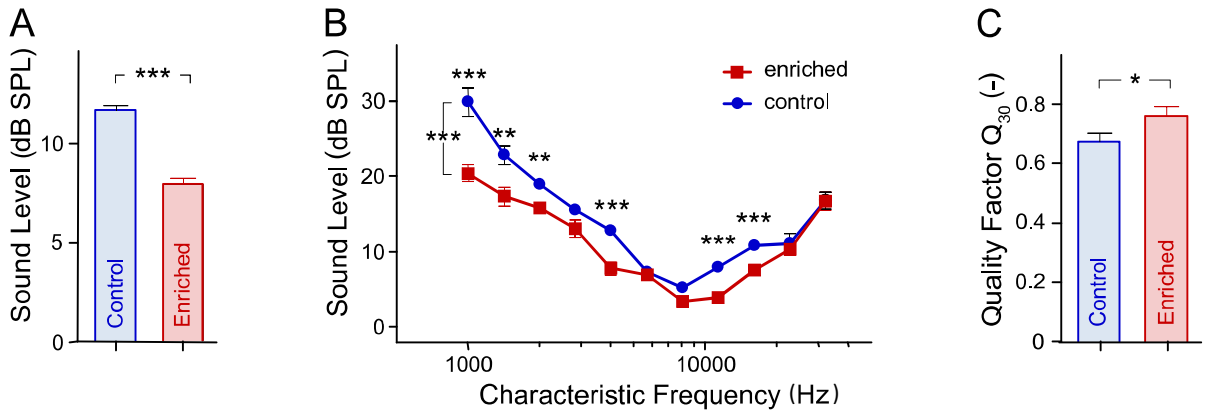

Fig. 45 **Basic parameters of neuronal receptive fields of the control and enriched animals**. **A** - mean neuronal excitatory thresholds (mean±SEM, $p<0.0001$, unpaired t-test). **B** - neuronal excitatory thresholds averaged in ½-octave bins (mean±SEM); the curves are significantly different ($p<0.001$, two-way ANOVA), significant differences of individual data pairs marked with asterisks (two-way ANOVA with Bonferroni post-hoc test). **C** - sharpness of neuronal tuning expressed with quality factor Q_{30} (mean ± SEM, $p<0.05$, unpaired t-test).

The sharpness of the frequency tuning was analyzed using the quality factor Q_{30}, which "normalizes" the bandwidth of the neuronal receptive field according to the characteristic frequency. The higher the Q_{30}, the sharper the tuning is. Only the units with a V-shaped receptive field were taken into account in this analysis; in total, these were 127 in the control animals and 129 in the enriched animals, respectively. The enriched animals have a significantly higher quality factor than the control animals (enriched: 0.7621±0.0303; controls: 0.674±0.0320; $p<0.05$, unpaired t-test), indicating that the V-shaped units have a higher frequency selectivity in the enriched rats, see Fig. 45C.

4.3.3. Level-dependent responses

The responses to white noise bursts of varying intensity were analyzed in 1714 units from the control animals and 2051 units from the enriched animals. Firstly, the magnitudes of responses to the stimulus at 70 dB SPL were compared. The enriched animals have slightly, but significantly lower evoked magnitudes (enriched: 74.51±1.14 spikes/sec; controls: 79.83±1.4 spikes/sec; $p<0.01$, unpaired t-test with Welch's correction), see Fig. 46A. A similar finding holds when only the first 20 ms of the responses were analyzed, focusing on the response onsets (enriched: 136.2±1.98 spikes/sec; controls: 144.7±2.38 spikes/sec; $p<0.01$, unpaired t-test with Welch's correction), see Fig. 46B.

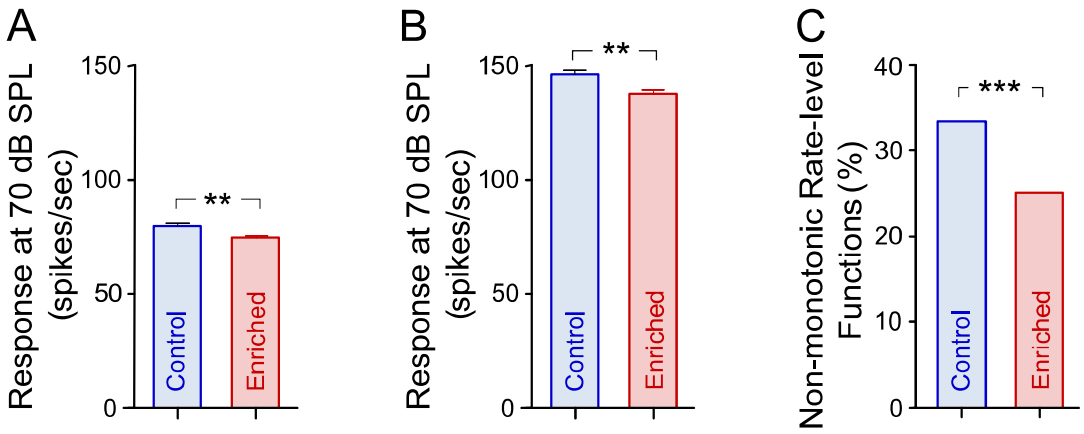

Fig. 46 **Level-dependent responses of neurons of the control and enriched animals**. **A** - responses evoked by broad-band noise bursts at 70 dB SPL (mean±SEM, $p<0.01$, unpaired t-test with Welch's correction). **B** - responses evoked by broad-band noise bursts at 70 dB SPL evaluated during the first 20 ms of the response (mean±SEM, $p<0.01$, unpaired t-test with Welch's correction). **C** - proportion of non-monotonic rate-intensity functions (percents, $p<0.0001$, Chi-square test).

Subsequently, the shapes of the rate-intensity functions were classified. The enriched animals exhibit a lower proportion of non-monotonic rate-intensity functions (enriched: 25.1%; controls: 33.4%; $p<0.0001$, Chi-square test), see Fig. 46C. This indicates that the developmental enrichment has also impacted on the processing of stimulus intensity.

4.3.4. Rate code stability

The stability of the rate code, in which information is carried by the number of discharges during a time window, was measured in 2051 units of enriched animals and 1714 units of control animals, by computing the variances of spike counts for responses evoked by broad-band noise pulses. To test the possible level-dependent behavior, the noise stimuli ranged in level from 30 to 70 dB SPL. Fig. 47 shows the spike count variances for the two experimental groups. The enriched animals exhibit significantly lower variances, indicating a higher stability of responses (two-way ANOVA, $p<0.001$, $F=55.87$). When the spike count variances are compared at individual stimulus levels, significant differences occur at 50, 60, and 70 dB SPL (two-way ANOVA with Bonferroni post-test, $p<0.001$ in all three cases). Furthermore, the reliability of responses improves with the increasing sound level in the enriched animals: the slope of a linear fit is significantly non-zero in the enriched group (slope = -0.075 ± 0.018, linear regression with F-test, deviation from zero: $p=0.0261$) while in the

control group, the linear fit is nearly constant (slope = 0.0078±0.0104, linear regression with F-test, deviation from zero: p=0.51).

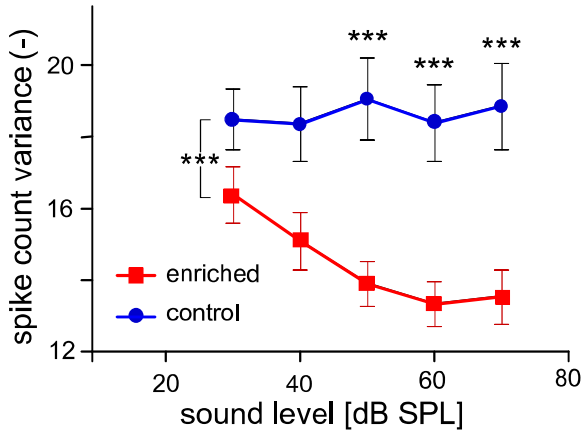

Fig. 47 **Spike count variances computed for noise-evoked responses** (mean ± SEM). The curves are significantly different (two-way ANOVA, $p<0.001$). Significant differences of individual data pairs are marked with asterisks (two-way ANOVA with Bonferroni post-hoc test, $p<0.001$).

4.3.5. Responses to modulated stimuli

To see whether the exposure to an acoustic environment containing modulated sounds affected the responses to amplitude-modulated (AM) and frequency-modulated (FM) stimuli, for AM-noises measurements were made in 593 units of enriched animals and 640 units of control animals; in 288 units of enriched animals and 259 units of control animals for FM tones.

4.3.6. Amplitude-modulated noises

The shapes of the AM-noise modulation-transfer functions (MTFs) in the enriched and control animals have a nearly identical shape; only slightly lower relative response magnitudes in the enriched rats were observed. When the functions are compared using ANOVA, they are significantly different ($F=49.33$, $p<0.0001$), see also Fig. 48A. This difference, however, is due to the nearly constant displacement of the two curves; when one of the functions is shifted by their average difference, the statistical difference disappears ($F<0.0001$, $p>0.99$).

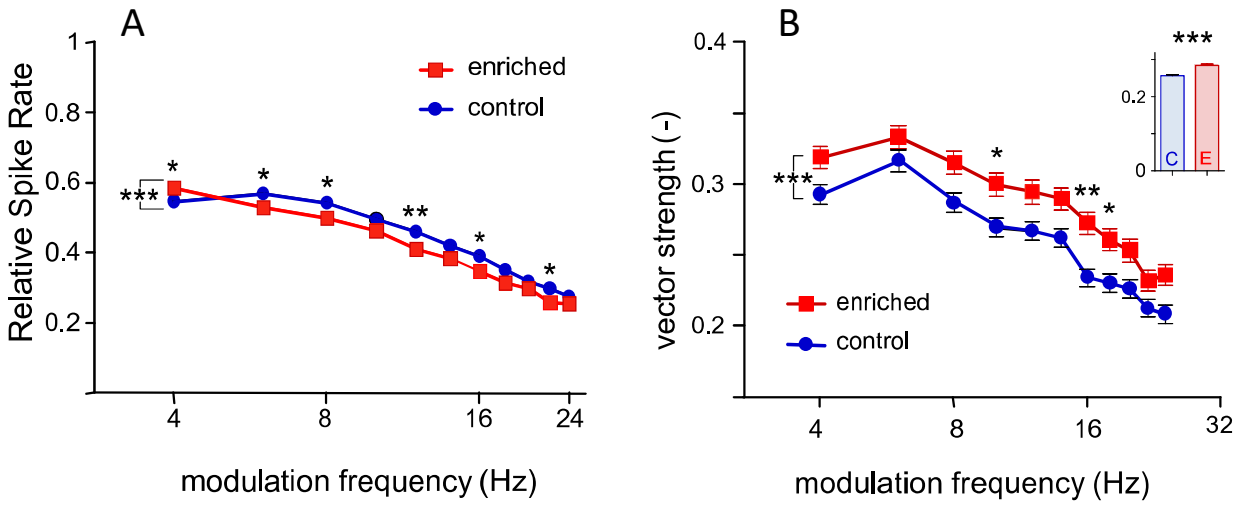

Fig. 48 **A** - modulation transfer functions (MTFs) measured for amplitude-modulated noise (mean±SEM); the curves are significantly different (two-way ANOVA, $p<0.0001$), significant differences of individual data pairs marked with asterisks (two-way ANOVA with Bonferroni post-hoc test). **B** - vector strength computed for responses to amplitude modulated noise (mean±SEM). The curves are significantly different (two-way ANOVA, $p<0.001$). Significant differences of individual data pairs are marked with asterisks (two-way ANOVA with Bonferroni post-hoc test). **Inset** - mean vector strength pooled over all modulation frequencies, the E and C symbols denote enriched and control groups, respectively (t-test, $p<0.0001$).

Synchronization of the responses with temporally varying stimuli was quantified by the vector strength and the dependence of vector strength (VS) values on the modulation frequency was plotted (Fig. 48B).

The vector strength quantifies how well the individual spikes are synchronized (phase-locked) with a periodic signal. The enriched animals show a significantly higher degree of synchronization both when analyzed in a frequency-dependent manner (two-way ANOVA, $p<0.001$, $F=75.23$), and when analyzing the pooled data (enriched: 0.28±0.0024, control: 0.26 ± 0.0021, t-test, $p<0.0001$). Looking at individual modulation frequencies, significantly different values occur at 10, 16, and 18 Hz (two-way ANOVA with Bonferroni post-test, $p<0.01$ at 16 Hz, $p<0.05$ otherwise). The percentage of phase-locking neurons given by the Rayleigh statistics is not different in the two experimental groups (enriched: 76.4%, control: 75.3%, Chi2 test, $p>0.05$) (Fig. 48B).

4.3.7. Frequency-modulated tones

In the case of the FM tones, the enriched and control groups show slightly different results. The MTFs differ again significantly (F=28.72, p<0.0001), see Fig. 49A. This time, however, the cumulative MTF of the enriched animals appears less steep in comparison with the control one, suggesting that the enriched animals are less selective to different modulation frequencies than the control animals. Hence, when the passband is computed, the low-pass cut-off frequency is shifted to higher values in the enriched animals see (Fig. 49B) (enriched: 9.365 ±0.6567 Hz; controls: 7.633±0.4213 Hz; p<0.05, unpaired t-test with Welch's correction).

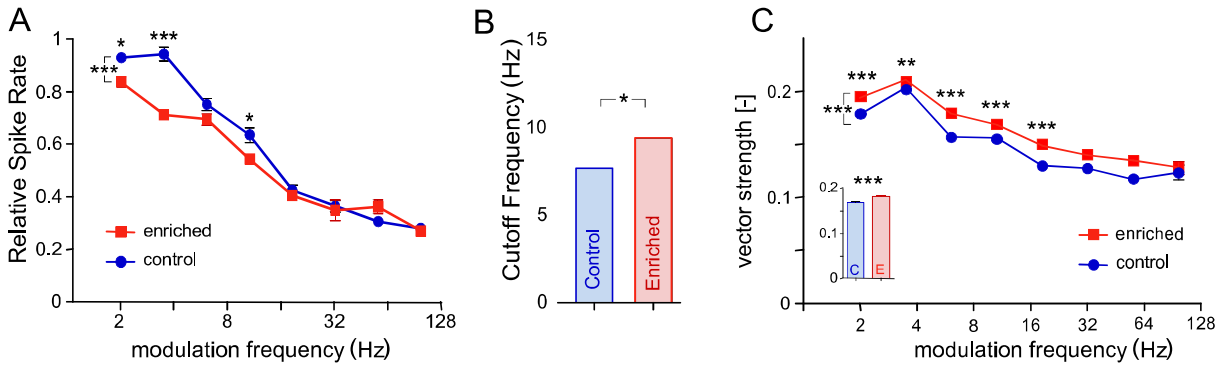

Fig. 49 **A** - MTFs measured for frequency-modulated tones (mean±SEM); the curves are significantly different (two-way ANOVA, p<0.0001), significant differences of individual data pairs marked with asterisks (two-way ANOVA with Bonferroni post-hoc test). **B** - Low-pass cut-off frequency of the MTFs of the FM tones (mean±SEM, p<0.01, unpaired t-test with Welch's correction). **C** - VS computed for responses to frequency modulated tones (mean±SEM). The curves are significantly different (two-way ANOVA, p<0.001). Significant differences of individual data pairs are marked with asterisks (two-way ANOVA with Bonferroni post-hoc test). **Inset** - mean vector strength pooled over all modulation frequencies, the E and C symbols denote enriched and control groups, respectively (t-test, p<0.0001).

Next, synchronization with a deterministic and stationary stimulus was measured for responses to frequency-modulated tones. The dependence of VS values of significantly phase-locking responses on the modulation frequency is shown in Fig. 49C. As in the case of the amplitude-modulated noise, the enriched animals exhibit significantly higher VS values (two-way ANOVA, p<0.001, F=40.13; pooled data enriched: 0.19 ± 0.0009, control: 0.17±0.0007,

t-test, p<0.0001). The difference is most significant at modulation frequencies below 32 Hz (two-way ANOVA with Bonferroni post-test, p<0.01 at 3.5 Hz, p<0.001 otherwise). The percentage of phase-locking neurons is not different in the two experimental groups (enriched: 42.5%, control: 42.1%, Chi2 test, p>0.05).

4.3.8. Series of clicks

Phase-locking ability to a series of clicks with different repetition rates was tested in 290 units of enriched animals and 255 units of controls. In this case, the repetition-rate dependent curves are not significantly different as a whole (two-way ANOVA, p=0.06, F=3.5), nevertheless, the post-hoc tests show higher VS values at low repetition rates (two-way ANOVA with Bonferroni post-test, p<0.001 at 2 Hz, p<0.01 at 3.5 Hz), see Fig. 50. In addition, the pooled values also indicate an improved synchronization in the enriched group (enriched: 0.19±0.004, control: 0.17±0.003, t-test, p=0.0014). The percentage of phase-locking neurons is again not different (enriched: 66.6%, control: 67.8%, Chi2 test, p>0.05).

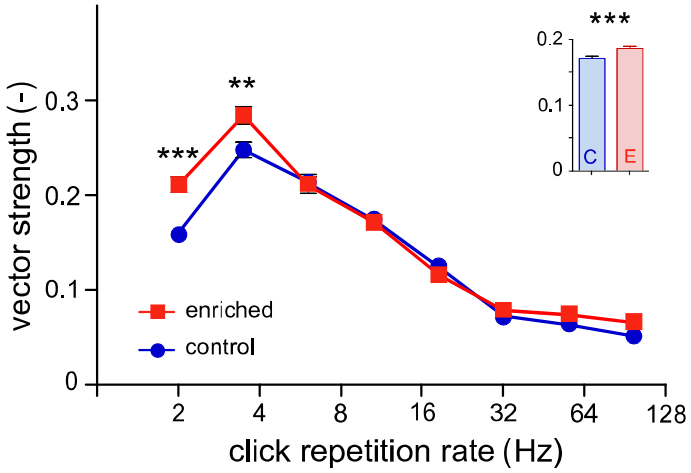

Fig. 50 **VS computed for responses to click trains** (mean±SEM). The curves are not significantly different (two-way ANOVA, p=0.06). Significant differences of individual data pairs marked with asterisks (two-way ANOVA with Bonferroni post-hoc test). Inset: mean vector strength pooled over all repetition rates, the E and C symbols denote enriched and control groups, respectively (t-test, p<0.0001).

4.3.9. Degree of responses similarity

The VS measure evaluates the position of each spike within the period of the signal. Simply put, to achieve high VS, most spikes have to lie near a specific phase of the periodic

signal. The VS thus indicates the ability of the neuron to capture the periodicity of the signal. However, it means neither that a spike has to appear in every signal period, nor that the response patterns as a whole have to be similar. In order to see whether the individual neurons give response patterns that are similar to each other, we computed van Rossum distances of different responses to the same stimulus. For both FM tones and series of clicks the van Rossum distances were not dependent on the modulation frequency (two-way ANOVA, p=0.33, F=1.15) or repetition rate (two-way ANOVA, p=0.06, F=1.96), respectively, thus we present only the pooled data. Fig. 51 shows the van Rossum distances for the FM tones and click trains. Clearly, the enriched animals express a higher degree of similarity of responses across multiple stimulus repetitions both for the FM tones (enriched: 10.5±0.029, control: 11.66 ± 0.034, t-test, p<0.0001) and for the series of clicks (enriched: 13.7±0.15, control: 15.47±0.17, t-test, p<0.0001).

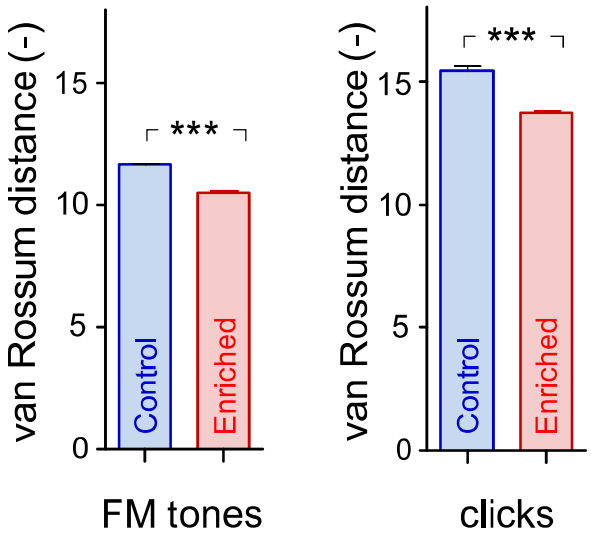

Fig. 51 **Van Rossum distances of responses to a repetitive stimulus** computed for responses to frequency modulated tones and click trains; the E and C symbols denote enriched and control groups, respectively (mean±SEM). Significant differences are marked with asterisks(t-test,p<0.0001).

5. Discussion

5.1. Intrinsic electrical properties of the pyramidal neurons in the core and belt areas of the rat auditory cortex

5.1.1. Differential excitability of layer V neurons from core and belt

We have identified I_h as a strong regulator of excitability of layer V AC neurons. The distribution of I_h density in neurons which belong to distinct AC areas appeared to be non-uniform, reaching the highest levels in those of the auditory belt. Accordingly, the belt neurons exhibited strikingly low excitability when compared with neurons of the core area. Inhibition of I_h by ZD7288, HCN channel blocker (Harris and Constanti, 1995), hyperpolarized layer V AC neurons, increased their τ_m and R_{in}, decreased their rheobase and shortened latency of action potentials induced by weak depolarizing stimuli. The effects of ZD7288 were significantly stronger in neurons of belt, consistent with I_h as main determinant of the differential excitability of core and belt neurons. This interpretation though relies on specificity of the drug for HCN channels. ZD7288 is the most widely used experimental blocker of I_h (Biel et al., 2009). Previously reported evidence has indicated, however, that ZD7288 at higher concentrations may also interact with other ion channels such as low voltage activated Ca^{2+} channels or Na^+ channels (Sanchez-Alonso et al., 2008, Wu et al., 2012). In our experiments, voltage-gated K^+ or Na^+ channels are unlikely target of ZD7288 because the drug did not block amplitudes of action potentials and hyperpolarized layer V AC neurons, and other K^+ channel blocker, 4-AP, similarly reduced excitability in core and belt neurons. Furthermore, T-type Ca^{2+} channels were not found in layer V pyramidal neurons (Almog and Korngreen, 2009). We therefore suggest that ZD7288 exerted its effects in layer V AC neurons via specific inhibition of I_h.

5.1.2. I_h-mediated modulation of spiking of layer V AC neurons

Our results indicated a complex role of I_h in mechanisms that determine spiking properties of layer V AC neurons. We found that I_h 1) shunts small depolarizing stimuli and thus increases rheobase and the spike latency, 2) stabilizes the steady state firing rates, and 3) changes the time course of action potentials. The shortening of spike latency in the presence of ZD7288 suggests that weak depolarizing stimuli can effectively inactivate HCN channels in layer V AC neurons. The channels, in turn, cease their shunting action and allow the membrane potential to reach the spike threshold. It also suggests that the tonic excitatory function of I_h, to depolarize the membrane potential near the resting membrane potential (Kase et al., 2012), is not affecting spiking properties of layer V AC neurons significantly. In

agreement with this, belt neurons that exhibit higher density of I_h also show significantly tighter correlation between rheobase and R_{in} than between rheobase and V_{rest}.

The depolarizing effect of I_h seems to play a role in mechanisms that elevate probability of action potentials repeatedly triggered with high frequency. We found that layer V AC neurons responded to hyperpolarizing stimuli by a ZD7288-sensitive depolarization sag (Robinson, 2003) that accelerated the decay of spike AHP. The shortening of the AHP led to faster recovery of the membrane potential, which increased the probability of a subsequent spike in the train and facilitated sustained activities of the belt neurons. Our results are consistent with previously published observations of relationship between I_h, AHP and neuronal excitability (Nolan et al., 2007, Shah, 2014, Aponte et al., 2006, Momin et al., 2008). It is well established that properly timed neuronal firing improves the representation of the stimulus by a sensory spike train (Billimoria et al., 2006, Bialek et al., 1991). In neurons integrating multiple inputs, e.g. in the belt AC neurons, the modulation of spike timing is very important for temporal integration of information and could significantly affect the reliability of the neuronal response for sensory neurons (Billimoria et al., 2006).

Interestingly, amplitudes of depolarization sag appeared to be similar in core and belt neurons. It suggests that the amplitude of the sag component recorded in current-clamp is not necessarily indicator of the I_h amplitude but might, for instance, also be affected by other conductances in the subthreshold range (Huggenberger et al., 2009). Also, the relatively shallow voltage dependence of the activation curve implies relatively small changes in open probability of I_h during hyperpolarizing current pulses. Thus, our results indicate that the correlation between sag and HCN channels expression is not absolute.

The effect of I_h on the shape of action potentials would be consistent with the view that HCN channels create a shunt that partially prevents the charging of the membrane in response to depolarizing inputs and affects activities of Na^+ channels in layer V AC neurons. The first derivative of the action potential in these neurons shows two components that correspond to the axonal and somatic action potentials (Kress et al., 2008, Colbert and Johnston, 1996). The delay in the second component originates as the action potential needs to back-propagate from the axonal initial segment to the soma. ZD7288 facilitated both components indicating that somatodendritic I_h indeed controlled both the generation and spreading of spikes in these neuronal compartments. We identified HCN1 and HCN2 as prevalent subtypes expressed by layer V AC neurons. We did not find any obvious difference in expression levels or localization of both subtypes in core and belt neurons. It is therefore possible that higher density of I_h in belt neurons reflected increased activity of HCN channels

opening with higher probabilities due to e.g. elevated intracellular concentration of cAMP in these neurons (Zong et al., 2012).

Overall, our results suggested that differential distribution of I_h in layer V neurons of distinct AC areas could contribute to variability of sound-evoked responses of these neurons observed in vivo. Besides the AC (Huggenberger et al., 2009), the role of I_h in the modulation of neuronal excitability was already established in hippocampus (Magee, 1998, Aponte et al., 2006), subiculum (van Welie et al., 2006), inferior colliculus (Koch and Grothe, 2003), sensorimotor cortex (Strauss et al., 2004), frontal cortex (Day et al., 2005) or entorhinal cortex (Nolan et al., 2007). In neocortical layer V pyramidal neurons, the density of I_h linearly increases with the distance from the cell body along the apical dendrites (Williams and Stuart, 2000). The highest density of I_h in the apical dendrite enables decreasing the likelihood of summation of dendritic synaptic inputs and increasing integration of the excitatory postsynaptic potentials at the cell soma and axon (Williams and Stuart, 2000, Desjardins et al., 2003, Pavlov et al., 2011).

5.1.3. Functional organization of the auditory cortex

The two distinct AC fields - the core and the belt area located around the core (Hackett, 2011, Schreiner and Winer, 2007) – significantly differ in terms of their responsiveness to acoustical stimulation. This was reported in many studies in several species: rats (Rutkowski et al., 2003, Profant et al., 2013), gerbils (Thomas et al., 1993), guinea pigs (Wallace et al., 2000), cats (He et al., 1997) or monkeys (de la Mothe et al., 2006, Romanski et al., 1999). In contrast with core AC neurons, which readily respond to relatively simple acoustic elements such as pure tones and have also well defined characteristic frequencies (CF), neurons in the belt cortex area prefer complex stimuli, including broad-band noise and vocalizations (Rauschecker et al., 1997). Other differences between the core and belt cortical fields were reported in the latencies of neuronal responses, which were shorter in the core AC neurons and longer in the belt neurons and in the response patterns – prevalence of the onset pattern in the core AC field, while in the belt area is frequent sustained type of the response pattern (Profant et al., 2013, Rutkowski et al., 2003).

There are many factors that may contribute to the diversity among cortical fields in neuronal responses, in particular neuronal connectivity, incoming signals and intrinsic properties. A number of anterograde andretrograde tracing studies have shown that the primaryauditory cortexreceives its largest input from the ventral division of themedial geniculate nucleus (vMGN), with minor inputsfrom the medial and dorsal divisions (mMGN,

dMGN), while the major inputs to the fields of the belt regions are from the dorsal nucleus (Roger and Arnault, 1989) and multisensory nuclei in the posterior thalamus (de la Mothe et al., 2006). Descending outputs from the core area project to the vMGN, dMGN and inferior colliculus (IC) (Paxinos, 2004), while those from the belt project into the multisensory intercollicular zone of the IC and have reciprocal connections with cortical areas of different modalities (Herbert et al., 1991). Thus, the belt area may have more associative, multi-modal processing roles (Rutkowski et al., 2003).

Our results clearly demonstrate that intrinsic neuronal parameters significantly differ between core and belt regions what support hypothesis that incoming signals are processed differently by neurons of the core and the belt area (Bai et al., 2004, Herbert et al., 1991, de la Mothe et al., 2006).

5.2. Corticofugal modulation of the neuronal responses in the inferior colliculus of rat

For the revealing of the corticofugal influences on the responsiveness of rat inferior colliculus we used the reversible inactivation of the AC by cooling. Recording configuration, used in current study, enables to record neuronal activity simultaneously from the large region of the IC from the surface of the DCIC to the deep layers of CIC. Maximal effect of AC inactivation were observed in the DCIC and in the central part of the CIC, whereas neurons located in the transition zone between the DCIC and CIC showed only weak or no changes.

Inactivation of the AC affected neuronal activity in the IC; however, the effect was not uniform among IC neurons. In approximately one half of neurons (47%), increased response strength to BBN stimulation and increased spontaneous activity was observed after cortical inactivation. An apparent decrease in the response strength and spontaneous activity was observed less frequently, in about 14% of neurons. In remaining 39% of neurons, the response strength and spontaneous activity were not significantly affected by AC cooling. Other observed effects of AC inactivation included the emphasized off-responses, suppressed post-excitatory inhibition and much stronger responses to click train with a more precise synchronization to individual clicks. On the contrary, the frequency tuning properties of the IC neurons (such as the excitatory threshold, characteristic frequency, or tuning bandwidth) were not altered by AC inactivation.

5.2.1. Inactivation of the AC by cooling procedure

In our experiments we used a modified cooling probe of Lomber et al. (1999) based on Peltier elements and cold water cooling system. The cooling probe was attached to the brain surface and the probe temperature ranged between 2 to 5°C that produced the temperature drop to 15-20°C observed in layer VI of the AC bellow the cooling probe, but did not cause any cooling of other surrounding brain structures. Lomber et al. (1999) demonstrated in cat cerebral cortex and superior colliculus that 20°C is the critical temperature below which neurons fail to be activated by afferent signals, but temperatures above 24°C showed little diminution in neuronal evoked activity. Our experiments confirmed that in subcortical auditory structures (auditory thalamus, IC) the temperature did not drop bellow 28°C during the whole period of AC cooling. Similar results were obtained by Coomber et al.(2011).

Most of the previous experiments investigating the effects of the AC inactivation by cooling on neuronal activity in subcortical structures were performed in the medial geniculate body (Villa et al., 1991, Antunes and Malmierca, 2011). In the IC it has been demonstrated that the AC cooling altered the ability of IC neurons in guinea pigs to localize the sound source in space based on interaural level differences (Nakamoto et al., 2008), altered the temporal and/or the spike response to the concurrent, monaural harmonic complexes (Nakamoto et al., 2010) and modified the stimulus-specific adaptation (Anderson and Malmierca, 2013). In these studies the neuronal activity was analyzed in the whole IC.

5.2.2. Effects of AC inactivation on individual time segments of the response

AC inactivation influenced individual time segments of the response to BBN stimulation differently. The changes in the onset part of the responses (10-20 ms after stimulus onset) were much smaller than the changes in the last 10 ms of the responses (60-70 ms after stimulus onset). Similar results, i.e., more pronounced changes in the firing rate (increase or decrease) in the later part of the responses in comparison with the onset parts were demonstrated by Popelař et al. (2003) during AC inactivation by tetrodotoxin. On the contrary, Anderson and Malmierca (2013) found mostly changes in magnitude of the onset responses; however, these authors recorded and evaluated preferentially the onset-responding neurons due to their strong SSA, which might have influenced the overall result. In the present study, we observed changes of both the onset and the offset parts of the responses, but the onset changes were much smaller than changes of the offset parts. We assume that the onset part of the response represents the incoming afferent activity from the subcollicular

structures whereas the later, sustained part of the response arises from the processing of neuronal activity within the IC that can be modulated by cortical descending fibers.

5.2.3. Effect of AC inactivation on the DCIC and CIC neurons

In the present study the inactivation of the AC in rats resulted in an increase of the spontaneous and evoked activity in the majority of IC neurons. The results indicate that AC cooling produces an excitatory-inhibitory dis-balance on the level of the IC in favor of a more expressed excitation and suppressed inhibition. In guinea pigs, Nakamoto et al. (2008) also observed increased or decreased neuronal activity in the IC during AC inactivation, but in a larger portion of neurons the responses were suppressed rather than enhanced (82 vs. 50 neurons). However, the authors found no difference between the effects of AC cooling in the CIC and ECIC.

The recording approach used in our study enabled us to record neuronal activity from the DCIC and CIC, not from the ECIC. The portion of neurons expressing the increase of neuronal activity during cortical inactivation was similar in the DCIC (63.4%) as in the CIC (60.0%). The cortico-collicular projection has been previously shown to be glutamatergic (Feliciano and Potashner, 1995). The projections terminate more densely on the DCIC and ECIC neurons (Druga and Syka, 1984b, Druga and Syka, 1984a, Druga et al., 1997), but a small amount of projections also directly target the CIC (Saldana et al., 1996, Winer et al., 1998). However, these glutamatergic projections activate intracollicular circuits that are mostly inhibitory and propagate throughout the entire IC (Malmierca et al., 2005, Hernandez et al., 2006). Therefore, the CC projections may finally possess predominantly inhibitory effects on IC neurons and elimination of these projections by AC cooling may result in the increase of response magnitude of many IC neurons.

The effects of AC cooling on neurons recorded in the area located between the DCIC and CIC at a depth of 300-500 μm in the IC was minimal even though CFs of neurons recorded in this area by electrode spots 4 and 5 are not beyond the dorso-ventral gradient of neuronal CFs. We suppose that the neurons recorded in the depth 300-500 μm in the IC probably belonged to functionally unspecific transition zone between the DCIC and CIC.

5.2.4. Effects of AC inactivation on neuronal adaptation

AC cooling resulted not only in an increase in the spontaneous and evoked activity in the majority of IC neurons, but also in the suppression of post-excitatory inhibition and changes in neuronal adaptation resulting in an increase in the ability to respond to individual

clicks in a series of clicks with a fast repetition rate. The most prominent effect of the AC cooling was a significantly larger response accompanied by a higher degree of synchronization to high click repetition rates, occurred in 90 % of IC neurons studied.

Neuronal adaptation to fast repeated stimuli is a characteristic of the standard adaptation phenomenon resulting from intrinsic properties of the neuron. The effects of AC cooling on higher level adaptation, stimulus-specific adaptation (SSA), which is dependent on the history of stimulation, was studied by Anderson and Malmierca (2013) and reviewed by Malmierca et al. (2015). The authors demonstrated that significant changes in SSA sensitivity during AC cooling were observed in only half of IC neurons. These results demonstrated that higher level SSA, occurring in the midbrain (IC), thalamus (MGB) and AC, could be linked to auditory memory, recognition of acoustic objects and auditory scene analysis (Escera and Malmierca, 2014) and it is less influenced by corticofugal pathways than the neuronal adaptation to fast repeated stimuli.

5.2.5. The function of the efferent system

Other studies focused on the function of the corticofugal efferent system used several approaches based typically on either activation or inactivation of the cortico-collicular projections. Both situations represent different experimental situations. Whereas electrical stimulation of the AC stimulates nerve fibers that target individual cells in the IC, AC inactivation changes the excitatory-inhibitory balance influencing lower auditory structures. Most of the previous experiments investigating the effects of the AC cooling on neuronal activity in subcortical structures were performed in the medial geniculate body (Villa et al., 1991, Antunes and Malmierca, 2011). In the IC it has been demonstrated that the AC cooling altered the ability of IC neurons in guinea pigs to localize the sound source in space based on interaural level differences (Nakamoto et al., 2008), altered the temporal and/or the spike response to the concurrent, monaural harmonic complexes (Nakamoto et al., 2010) and modified the stimulus-specific adaptation in rats (Anderson and Malmierca, 2013). Nakamoto et al. (2008) observed increased or decreased neuronal activity in the IC during AC inactivation in guinea pigs, but in a larger portion of neurons the responses were suppressed rather than enhanced (82 vs. 50 neurons).

Silencing of the cortico-collicular projections can be reached not only by cooling procedure, which was applied in this study, but also by application of chemical substances (like lidocaine, muscimol or TTX) or by cortical lesion, which - in contrast to previous two methods - has a permanent impact on the auditory circuitry. Results of our previous studies

investigating the role of the cortico-tectal descending system using long term pharmacological inactivation of the AC in rats with tetrodotoxin (TTX) (Popelar et al., 2003, Nwabueze-Ogbo et al., 2002), demonstrated that during AC inactivation the amplitude of click-evoked IC responses and the firing rate of IC neurons increased, decreased or did not change in comparison with control conditions. Similar effects of AC inactivation on the IC neuronal activity were observed in the present study using a cooling procedure.

5.3. Acoustical enrichment-induced plasticity in rat auditory cortex

Our results show that an acoustical enrichment during the sensitive phase of postnatal development positively influences the representation of basic stimuli in the auditory cortex, improving the stability of the rate code and the reliability and reproducibility of the temporal code. Importantly, the effect is permanent and can still be seen in adult animals. So, the developmental intervention introduces long-lasting consequences rather than temporary alterations which disappear shortly after the return of the organism to standard conditions. This result confirms and extends the outcomes of our previous study on the inferior colliculus (Bures et al., 2014), in which developmentally-enriched animals exhibited permanent changes of neuronal responsiveness, while the animals exposed to the same stimulation in adulthood showed only minor and temporary improvements.

It is known from previous studies that maturation of the central auditory system is shaped by input to the developing nuclei. The sound-evoked activity controls the refinements of the structure of neuronal network (Ouda et al., 2016, Kandler and Gillespie, 2005, Sanes and Takacs, 1993, Lu et al., 2014), which in turn results in functional refinements and maturation of neuronal responsiveness and representation of the stimulus (Zhang et al., 2001, Chang et al., 2005, Bures et al., 2014, Bures et al., 2017), hence altering the input will also alter the development of the system. Despite considerable uncertainty as to what effect a specific stimulation will have, it appears that the resulting state of the system relates to spectral and temporal characteristics of the acoustic input.

5.3.1. Acoustic enriched environment composition

The effect of sound environment on the development of the auditory system is explored most profoundly for primitive analytic stimuli such as tones or noise (Zhang et al., 2002, Chang and Merzenich, 2003, Chang et al., 2005, Zhang et al., 2001, Jiang et al., 2015, Nakahara et al., 2004, Miyakawa et al., 2013, Oliver et al., 2011). An opposite extreme is

represented by works which have used a mixture of selected natural and artificial sounds as a component of a multimodal enriching environment, comprising acoustic, visual, motor, and behavioural features (Engineer et al., 2004, Percaccio et al., 2005, Bose et al., 2010, Nichols et al., 2007). The former approach allows to associate the observed results with particular features of the environment, yet it is mostly unnatural and sometimes oversimplified. The latter approach better mimicks natural conditions, but it is difficult to distinguish the effects of individual environmental factors.

We aimed to locate our experiments in an intermediate position within this continuum, using a complex, yet well-defined enriching environment targeted exclusively to auditory perception. The stimulus is wideband, spanning the whole hearing range of the animals, it is modulated both in frequency and in amplitude, and it is random in many aspects (amplitude envelope, spectral envelope, temporal changes of spectral envelope). The sound was originally developed in such a way that its complex modulated character resembles natural sounds, yet it is not species-specific or meaningful and does not repeat itself. The complex modulated background is complemented with several randomly occurring target sounds with different spectral complexities which are in some cases bound to a reward release.

5.3.2. Effects of the enriched acoustic environment (AEE) on the neuronal representation of intensity and frequency

The current study extends our investigations of the IC neurons (Bures et al., 2014). Similarly as in the IC neurons, the cortical neurons of enriched animals had lower excitatory thresholds, indicating an increased sensitivity to faint sounds. This interpretation is also supported by the significantly lower hearing thresholds examined using the auditory brainstem responses. The result agrees with the finding of (Engineer et al., 2004); (Jiang et al., 2015), on the other hand, observed no significant impact of an enrichment on the minimal thresholds of the A1 units. The AC neurons in the enriched rats exhibited slightly lower evoked activity, which is in accordance with Yang et al. (2014), but in contradiction to our IC results and to (Engineer et al., 2004), who reported an increased evoked activity in the enriched animals. As in Bureset al. (2014), (Engineer et al., 2004), or Yang et al. (2014), complex AEE lead to narrower frequency tuning. Furthermore, the AC neurons of the enriched rats had a higher proportion of monotonic rate-intensity functions – similarly as in the IC (Bures et al., 2014).

5.3.3. Improved stability of the rate-based stimulus representation

Stimuli of different sound levels will result in different evoked spike counts; however, for the difference to be detectable, it must be large enough not to be masked by the spiking variability (Colburn et al., 2003, Silver, 2010). The reduced spike count variance observed in the enriched animals thus suggests an improved discrimination ability of sound level changes. Furthermore, the variance decreases as the stimulus intensity increases further from the threshold, and reaches a shallow minimum of around 60 dB SPL. This may relate to the average SPL of the exposure stimulation which was 55 dB SPL for the background modulated noise and 60 dB SPL for the target stimuli. As the animals were motivated to discriminate between different types of stimuli to obtain a reward, it may be that the minimum observed variance corresponds to the level of the behaviorally most important sounds.

5.3.4. Influence of the AEE on the selectivity of the AC neurons responses to modulated stimuli

There are only a few studies that deal with the influence of the AEE on the selectivity of the AC neurons to frequency and amplitude modulation. Furthermore, the reported results are relatively ambiguous, showing a high dependence on the precise setting of the environmental conditions. In our present work, the perception of the AM noise was similar in the enriched and control groups, possibly due to the prevalence of AM sounds in the natural environment, so that the control group wasn't completely deprived of the AM stimulation. Periodically frequency-modulated tones, on the other hand, are rarer and even rat vocalizations are minimally modulated in frequency (Portfors, 2007, Brudzynski, 2009, Ouda et al., 2016b). It therefore appears that the addition of an FM stimulus during the development of the auditory system had a more prominent impact on the perception of the FM tones in the enriched animals. FM-MTFs were significantly different in the two experimental groups, the low-pass cut-off frequencies being moved to the higher values in the enriched animals. This allows the AC neurons in the enriched animals to follow the FM tones with higher modulation frequencies. Despite the fact that only one particular FM tone was associated with the reward; FM-MTFs differed in a wide range of modulation frequencies, probably thanks to the complex modulated character of the background rippled noise.

Temporal coding employs precise positioning of individual spikes in time, which may potentially carry larger information content than the rate code, and furthermore the information is conveyed almost immediately (Tiesinga et al., 2008). Considering also the neuronal populations, if a group of neurons projecting to another neuron produces spike

patterns that are well-aligned in time, the higher synchrony will improve the detection of the signal. We studied the temporal acuity using two measures: the vector strength quantifying the synchronization of spikes with sound period, and van Rossum distance quantifying the similarity of individual evoked patterns. The neurons in the enriched animals exhibited an improved synchronization with temporally structured stimuli – amplitude-modulated noise, frequency-modulated tones, and click trains. The observed higher vector strength values indicate that the evoked spikes are positioned more precisely within the period of the signal modulation (in the case of amplitude-modulated noise and frequency-modulated tones) or repetition (in the case of click trains).Results suggest that the enriched animals might have a better ability to detect and discriminate temporally varying stimuli. The proportion of significantly phase-locking neurons is not different in the two groups.

Reproducibility and self-consistency of firing patterns as a response to a given stimulus may play an important role in stimulus detection and discrimination tasks, particularly in complicated listening conditions such as a noisy environment. The smaller van Rossum distances of firing patterns to a repetitive stimulus in the enriched group indicate that the individual neuronal responses are more similar to each other, thus encoding more precisely or reliably the respective stimulus. This fact may relate to the experimental paradigm in which the enriched animals were motivated to discriminate several similar stimuli to obtain a reward. Smaller van Rossum distances after an acoustic training have also been observed by Cheng et al. (2017).

5.3.5. Probable sources of the AEE-induces alterations

The sources of the described alterations caused by the AEE during early development arise from both structural and physiological changes in the neurons both in the cortex and at subcortical levels. A study of (Bose et al., 2010) showed that a complex enriched environment led to an increased basal dendritic length and an increased spine density in both apical and basal dendrites of A1 layer 2/3 neurons; at the same time, enhanced glutamatergic synaptic transmission was observed in these neurons (Nichols et al., 2007). Significant increases in inhibitory $GABA_A$ receptor α1, β3 subunits; excitatory NMDA receptor NR2A, NR2B subunits, AMPA receptor GluR2 subunit protein expression, and in the ratios of $GABA_A$α1/$GABA_A$α3 and NR2A/NR2B, were described in the A1 after acoustic enrichment (Cai et al., 2010). Rearing animals in a moderate-level noise environment during the CP had the opposite effects, manifested in a less mature (infantile) state of adult A1 with less $GABA_A$ α1 and β2/3 subunits, and NMDA receptor NR2a and NR2b producing, followed by reduced

cortical expression of brain-derived neurotrophic factor (BDNF), which promotes the formation of the inhibition (Zhou et al., 2011).

5.3.6. Role of the AEE in the human early postnatal development

The finding that an acoustic environment during early development may have profound and permanent effects on the state of the auditory system is also relevant for human neonatal and infant medicine. For children, the early auditory surrounding plays a crucial role in the language acquisition process (Newport, 2003, Kuhl, 2010, Friederici, 2012). Experimental and clinical experiences with cochlear implantation show that the optimal outcome for auditory performance results only from implantation during the first 1-3 years of life (Niparko et al., 2010, Geers and Sedey, 2011, Kral and O'Donoghue 2010). Language learning is the easiest in early life and even regular passive exposure to a foreign language, without its active usage during early childhood, results in a more native-like accent than when the subject learns the language in adulthood (Au et al., 2002). The connection between congenital hearing loss, severe otitis media in early childhood and the development of speech disorders, is also well established (Wertzner et al., 2012, Gravel and Wallace, 1998, Laws and Hall, 2014, Keogh et al., 2010, Samelli et al., 2017).

6. Conclusions

6.1. Intrinsic electrical properties of pyramidal neurons in the core and belt areas of the auditory cortex in rat

- Layer V pyramidal neurons in the core and belt areas of the AC significantly differ in their intrinsic electrical properties, in particular the membrane time constant and input resistance.
- Pyramidal neurons in the belt area of the AC are less excitable than the core neurons due to a elevated shunting conductance active at resting membrane potential.
- Constitutively active HCN1 and HNC2 channels contribute to the excitability of layer V pyramidal neurons in the core as well as belt areas of the AC.
- Increased density of I_h in layer V pyramidal neurons from the AC belt area affects their firing properties: prolongs the latency of single action potentials and decreases jitter of high frequency spikes.
- *Diversity of intrinsic electrical properties of layer V AC pyramidal neurons could be an important factor contributing to different sound-evoked responses.*

6.2. Corticofugal modulation of the neuronal responses in the inferior colliculus of rat

- Inactivation of the AC using a cooling procedure did not alter frequency tuning and thresholds of the inferior colliculus neurons, but significantly modulated their spontaneous and sound-evoked neuronal activity.
- AC inactivation results in a significant increase of spontaneous and sound-evoked neuronal activity in almost half of the IC neurons. Modulatory effect of AC cooling was apparent also in lower post-excitatory suppression, emphasized off-responses and synchronization to click train stimulation.
- Effects of cortical inactivation were observed in the dorsal cortex of the IC as well as in the central part of the IC.
- Characteristics of the neuronal activity in the IC recovered within one hour after the cooling cessation.
- *Observed effects point to a weaker inhibition as a consequence of a reduced activation of the intrinsic GABAergic network within the IC after AC inactivation. It suggests*

that corticofugal pathways can provide an effective control of the neuronal activity in the dorsal cortex and the central part of the IC.

6.3. Acoustical enrichment-induced plasticity in rat auditory cortex

- Acoustically enriched environment during the critical period of postnatal development influences basic properties of neuronal receptive fields in the auditory cortex. In particular, the AEE lowers the excitatory thresholds, sharpens the frequency selectivity, reduces the maximum response strength and lowers the proportion of non-monotonic RLFs.
- The AEE also affects the processing of temporally structured stimuli (amplitude and frequency modulated sounds).
- Enriched environment presented shortly after the onset of hearing has the power to improve the stability of evoked cortical responses and to lower the variance of spike rates in response to a repetitive stimulus.
- Temporal acuity of individual spikes expressed by synchronization and similarity indexes (vector strength and van Rossum distance, respectively) was significantly amended in the enriched animals compared to the controls.
- Changes in neuronal responsiveness are retained to adulthood, suggesting that they had their origin in developmental processes, presumably shaping the properties of excitatory and inhibitory synaptic transmission.
- *The observed changes suggest that complex acoustic environment may have positive implications for the individual's ability to detect and discriminate sounds, especially in complex listening environments.*

7. Summary

Auditory cortex (AC) is the ultimate target of afferent auditory pathways and plays a crucial role in the perception and localization of complex sounds. In the thesis were investigated and discussed three aspects of the AC function: diversity of the intrinsic passive and active electrical properties of core and belt AC neurons, the modulatory function of the descending connections from the auditory cortex to the inferior colluculus and the effect of a complex acoustical environment applied during the critical period on the responsiveness of auditory cortex neurons in rats.

7.1. Intrinsic electrical properties of pyramidal neurons in the core and belt areas of the auditory cortex in rat

The AC comprises the core and surrounding belt regions that substantially differ in terms of their cytoarchitecture, connectivity, and in their sound-evoked responses. To reveal possible differences in intrinsic electrical properties of neurons in core and belts regions whole cell patch-clamp recordings from layer V pyramidal neurons in acute AC slices isolated from young adult rats were performed. The data indicate that at resting membrane potential the pyramidal neurons from core AC are more excitable than those from the belt. Their time membrane constants and input resistances were significantly increased compared to those in the belt region. Accordingly, core pyramidal neurons generated action potentials with shorter latencies and lower rheobases. Observed differences result from an elevated constitutive shunting conductance activated in belt neurons at the resting membrane potential. We have identified the HCN channels as a mediator for this elevated conductance in the belt pyramidal neurons. Analysis of voltage-dependence and gating kinetics of HCN-mediated I_h currents suggested a combination of several HCN channel subtypes to be functional in pyramidal neurons. Consistently, both single-cell RT-qPCR and immunohistochemistry analyses revealed the HCN1 and HCN2 as two major subtypes expressed by pyramidal neurons of both auditory areas. Experimental blockade of I_h hyperpolarized pyramidal neurons, increased their input resistances, reduced the rheobase and delay of action potentials generated by pyramidal neurons; all effects were significantly more prominent in the belt compare to the core region. This indicated that I_h is an important factor regulating the spiking of layer V pyramidal neurons in the belt regions. Furthermore, I_h generated a depolarization sag in the voltage responses to hyperpolarizing current steps injected into pyramidal neurons. The activation kinetics of the sag was fast enough to shorten the duration of the after-hyperpolarization phase

of action potentials in the belt neurons. Consistently, the jitter of steady-state action potentials evoked by repetitive current stimuli was significantly reduced in belt pyramidal neurons compared to their core counterparts. This suggests that I_h could help to maintain the persistent firing of neurons from the belt region. Our data supports the view that the *in vivo* observed diversity in spiking patterns of core and belt neurons could be at least partially attributable to differences in their intrinsic electrical properties.

7.2. Corticofugal modulation of the neuronal responses in the inferior colliculus of rat

There are powerful pathways descending from the auditory cortex to the inferior colliculus, yet their function is not fully understood. To examine functional impact of corticofugal projections on the neuronal activity in the IC we used a reversible cortical inactivation, achieved by cooling of the auditory cortex. Investigating the depth profile of the temperature in the AC during cooling documented that the temperature in the deep layers of the AC (layers V and VI) dropped within 2 min after the start of cooling to a temperature around 15 ºC, i.e. low enough to block the neuronal activity in these layers.

Extracellular single-unit or multi-unit activity was recorded in the IC with a 16-channel multielectrode introduced into the IC along the dorso-ventral axis, allowing for the simultaneous recording of activity from neurons of different characteristic frequencies in the DCIC and CIC. Recording of the IC neuronal activity during a pre-cooling period was compared to IC activity during cooling of the AC and also after the cooling. The frequency selectivity and thresholds of the inferior colliculus neurons did not show any changes during the AC cooling period. In contrary, AC cooling produced in more than half of the IC neurons a significant increase in the spontaneous activity and in magnitude of the sound-evoked response. Changes in the neuronal activity were observed in the dorsal cortex as well as in the central nucleus of the IC, while changes in the transition zone between DCIC and CIC were minimal. The AC inactivation did not influence the initial (onset) part of the responses to acoustical stimuli, whereas the end of the sustained part of the responses and the off responses were significantly amplified. AC inactivation resulted also in a reduction of the post-excitatory suppression and in a pronounced enhancement of the responses to fast click-repetition rate stimuli. The response parameters recovered to the pre-cooling levels after cessation of the cooling within ~1 hour.

The results demonstrate that corticofugal pathways impose tonic regulatory, mostly inhibitory effects upon the IC activity. AC thus can provide an effective control of the neuronal activity in the dorsal cortex and the central part of the IC.

7.3. Acoustical enrichment-induced plasticity in rat auditory cortex

It is well known that auditory experience during early development shapes response properties of AC neurons, affecting tonotopical arrangement, response thresholds and strength, or frequency selectivity. Our results show that rearing rat pups in a complex AEE leads to an improved representation of complex sounds in the AC when recorded later in adulthood, influencing spectral and temporal characteristics and also the reliability of neuronal responses. The acoustic enrichment comprised a continuous wide-band amplitude-modulated rippled noise with varying periodic spectral envelope complemented with several types of randomly occurring acoustic target signals, one of which triggered a reward release. The AEE was presented at moderate intensity (55 dB SPL, target stimuli at 60 dB SPL) 12 hours a day during the critical period of the auditory system development (between postnatal days 14 and 28). The application of the AEE resulted in lower excitatory thresholds and better frequency selectivity of AC neurons. These changes were nonspecific and present in the whole range of neuronal characteristic frequencies. Importantly, the acoustic enrichment resulted in increased reliability of neuronal representation of stimuli based both on the rate and the temporal codes. For a repetitive stimulus, the neurons in the AEE-exposed rats exhibited a lower spike count variance, indicating a more stable rate coding. The reduced variance was present both during the strong onset reaction and during the sustained part of the neuronal response. Also at the level of timing of individual spikes, the discharge patterns showed a higher degree of similarity across stimulus repetitions: the computed van Rossum distances of different spike trains evoked by the same stimulus were significantly smaller in the enriched animals. Furthermore, the neurons followed more precisely the temporal course of the stimulus, as manifested by better phase-locking (higher vector strength values) to frequency- and amplitude-modulated sounds.

The results point at importance of the complex acoustical stimulation during developmental period for formation of neural circuits providing effective processing of relevant acoustical stimuli. Besides basic alterations of the receptive fields, the acoustic environment during the critical period of postnatal development permanently affects also the stochasticity, reproducibility, and fine structure of neuronal spiking patterns.

8. Souhrn

Sluchová kůra (AC) je konečným cílem aferentních sluchových drah a hraje klíčovou roli ve vnímání a lokalizaci složitých zvuků. V předložené práci jsou zkoumány a diskutovány tři aspekty funkce sluchové kůry na modelu potkana: i) diverzita vnitřních pasivních a aktivních elektrických vlastností korových neuronů v centrální oblasti sluchové kůry (označované jako core) a v oblasti periferního pásu (označované jako belt), ii) modulační funkce sestupných drah ze sluchové kůry do colliculu inferior (IC) a iii) vliv komplexní akustické stimulace v průběhu kritického období dozrávání sluchového systému na aktivitu sluchových neuronů.

8.1. Vnitřní elektrické vlastnosti pyramidových neuronů v centrální oblasti a v oblasti periferního pásu sluchové kůry u potkana.

V rámci AC lze rozlišit centrální oblast (core) a oblast periferního pásu (belt), které se od sebe podstatně liší, jak z hlediska jejich cytoarchitektury, konektivity tak i reakcí na zvukovou stimulaci. Možné rozdíly ve vnitřních elektrických vlastnostech neuronů v centrální oblasti a v oblasti periferního pásu pásů, byly studovány s využitím techniky patch-clamp na pyramidových neuronech páté vrstvy v akutních korových řezech izolovaných z mladých dospělých potkanů. Získané výsledky ukazují, že při hodnotách blízkých klidovému membránovému potenciálu jsou pyramidové neurony v centrální oblasti AC více excitabilní než neurony v oblasti periferního pásu. Jejich časové konstanty a hodnoty vstupní odporu byly významně vyšší než hodnoty u neuronů periferního pásu. Proto pyramidové neurony centrální oblasti generovaly akční potenciály s kratšími latencemi a měly nižší reobázi. Pozorované rozdíly jsou důsledkem zvýšené nespecifické (tzv. shunting) vodivosti v neuronech periferního pásu, která se projevuje při hodnotách blízkých klidovému membránovému potenciálu. Identifikovali jsme, že tato zvýšená vodivost zprostředkována neselektivními HCN (hyperpolarizací aktivované cyklické nukleotidy řízené) kanály pyramidových buněk periferního pásu. Analýza napěťové charakteristiky a kinetiky proudů zprostředkovaných HCN kanály (I_h), naznačila přítomnost několika podtypů kanálů HCN v pyramidových neuronech. Jak analýza pomocí jednobuněčné RT-qPCR, tak i imunohistochemická analýza shodně odhalily HCN1 a HCN2 jako dva hlavní podtypy HCN kanálů exprimovaných v pyramidových neuronech obou studovaných sluchových korových oblastí. Zablokování I_h vedlo u hyperpolarizovaných pyramidových neuronů ke zvýšení jejich vstupního odporu, snížení reobáze a zpoždění generovaných akčních potenciálů; všechny tyto účinky byly významně větší u neuronů periferního pásu v porovnání s neurony v centrální

oblasti AC. To naznačuje, že I_h je důležitým faktorem regulujícím generování akčních potenciálů pyramidovými neurony páté vrstvy v oblasti periferního pásu. I_h také způsoboval zrychlení návratu membránového potenciálu (tzv. depolarization sag) v napěťových odezvách pyramidových neuronů na stimulaci hyperpolarizačními proudy. Aktivační kinetika tohoto jevu byla dostatečně rychlá, aby se mohla projevit ve zkrácení doby trvání post-hyperpolarizační fáze akčních potenciálů u neuronů periferního pásu. V souladu s tím, byla u pyramidových neuronů periferního pásu zjištěna i výrazně nižší odchylka v časování (jitter) akčních potenciálů vyvolaných opakujícími se proudovými podněty ve srovnání s neurony centrální oblasti. To naznačuje, že I_h může pomoci udržovat spolehlivost časového vzoru neuronové aktivity u neuronů periferního pásu. Získané poznatky podporují názor, že rozdíly mezi odpověďmi neuronů centrální oblasti AC a neurony periferního pásu AC, pozorovány v *in vivo* experimentech, by mohly být přinejmenším částečně způsobeny rozdíly v jejich vnitřních elektrických vlastnostech.

8.2. Korová modulace neuronové aktivity v colliculus inferior u potkana

Existence sestupné dráhy ze sluchové kůry (auditory cortex, AC) do colliculu inferior (IC) je dobře známa, ale její funkce stále není ještě úplně objasněna. Pro zkoumání funkčního dopadu kortikofugálních projekcí na neuronovou aktivitu v IC jsme použili metodiku dočasného vyřazení sluchové kůry, kterého bylo dosaženo jejím chlazením. Měření hloubkového profilu teploty v AC během chlazení prokázalo, že teplota v hlubokých vrstvách AC (vrstvy V a VI) klesla po zahájení chlazení na teplotu kolem 15 °C a došlo tedy k potlačení neuronové aktivity v těchto vrstvách.

Extracelulární záznamy aktivity neuronů byly měřeny v IC s použitím 16-kanálové multielektrody zavedené do IC ve směru dorso-ventrální osy, což umožnilo současné měření aktivity neuronů s různými charakteristickými frekvencemi ve dvou podjádrech IC - v dorzální kůře (dorsal cortex of inferior colliculus, DCIC) a v centrálním jádře (central nucleus of inferior colliculus, CIC). Neuronová aktivita byla vždy snímána nejprve v době před chlazením a srovnávána s aktivitou IC během chlazení sluchové kůry a také po ukončení chlazení. Frekvenční selektivita a prahové hodnoty neuronů IC nevykazovaly žádné změny během chlazení AC. Chlazení AC se však projevilo ve významném zvýšení spontánní aktivity a velikosti odpovědí na zvukovou stimulaci u více než poloviny neuronů v IC. Změny v neuronové aktivitě byly pozorovány v obou sledovaných podjádrech IC - v dorzální kůře i v centrálním jádře, zatímco změny v přechodové zóně mezi DCIC a CIC byly minimální. Vyřazení sluchové kůry příliš neovlivnilo reakci neuronů na akustické podněty v počáteční

(onset) části odpovědi, zatímco pozdější ustálená (sustained) aktivita i reakce na konec podnětu (off) byla výrazně zesílena. Vyřazení AC se projevilo také v menší post-excitační inhibici aktivity po skončení zvukové stimulace a výrazném zesílení odpovědí na podněty složené z rychle se opakujících impulsů. Vlastnosti neuronové aktivity se vracely na úroveň před chlazení během cca 1 hodiny po ukončení chlazení.

Výsledky ukazují, že sestupná dráha ze sluchové kůry má tonický regulační efekt s převážné inhibičními účinky na neuronovou aktivitu v IC. AC tak může účinně ovlivňovat neuronovou aktivitu v dorzální kůře i centrální části IC.

8.3. Plasticita sluchové kůry vyvolaná akusticky obohaceným prostředím u potkana

Je známo, že zvuková stimulace v průběhu raného mládí ovlivňuje vlastnosti neuronů sluchové kůry, jejich tonotopické uspořádání, hodnoty prahů a také velikost reakce neuronů nebo jejich frekvenční selektivitu. Naše výsledky ukazují, že prostředí s komplexní akustickou stimulací u velmi mladých potkanů vede ke zlepšení reprezentace komplexních zvuků v AC, ovlivňuje spektrální a časové charakteristiky neuronů a také spolehlivost a reprodukovatelnost neuronových reakcí, přičemž tyto změny přetrvávají do dospělosti. Komplexní akustická stimulace zahrnovala kontinuální širokopásmové amplitudově a frekvenčně modulované zvukové pozadí doplněné o několik typů náhodně se vyskytujících odlišných zvukových signálů, z nichž jeden byl spojen s odměnou. Zvuková stimulace měla střední intenzitu (55 dB SPL, cílové stimuly pak 60 dB SPL) a byla prezentována12 hodin denně během kritického období vývoje sluchového systému u potkana (mezi 14. a 28. postnatálním dnem). Komplexní akustické prostředí vedlo k nižším excitačním prahům a lepší frekvenční selektivitě neuronů v AC. Tyto změny byly nespecifické a byly přítomny u neuronů v celém rozsahu charakteristických frekvencí. Zvuková stimulace se projevila i ve zvýšené spolehlivosti neuronové reprezentace zvukových podnětů jak z hlediska počtu akčních potenciálů, tak z hlediska časového kódování. Neurony u potkanů vystavených komplexní akustické stimulaci vykazovaly nižší variabilitu počtu akčních potenciálů pro opakující se zvukové podněty, což ukazuje na stabilnější kódování počtem akčních potenciálů (tzv. rate-code). Nižší rozptyly počtu akčních potenciálů byly přítomné jak během počáteční (onset) fáze odpovědi neuronu, tak i během pozdější ustálené (sustained) části neuronové odpovědi. Také na úrovni časování jednotlivých akčních potenciálů vykazovaly neurony zvířat z akusticky obohaceného prostředí vyšší míru podobnosti mezi odpověďmi na jednotlivé stimulace: vypočtené rozdíly dle van Rossumovy metriky byly u těchto zvířat

výrazně menší ve srovnání s kontrolami. Navíc aktivita neuronů přesněji sledovala časový průběh podnětu, což bylo patrné v lepší synchronizaci odpovědí neuronů s průběhem frekvenční i amplitudové modulace zvukových podnětů. Výsledky ukazují na význam komplexní akustické stimulace během kritické vývojové fáze pro formování neuronových obvodů sluchového systému a jejich schopnosti efektivně zpracovat relevantní akustické podněty. Kromě změn základních parametrů receptivních polí neuronů sluchové kůry akustické prostředí během kritického období postnatálního vývoje trvale ovlivňuje také náhodnost, reprodukovatelnost a detailní časovou strukturu neuronových odpovědí.

9. List of abbreviations

5-HT	5-hydroxytryptamine
AA	Anterior area
AAF	Anterior auditory field
ABR	Auditory brainstem response
AC	Auditory cortex
ACh	Acetylcholine
AChE	Acetylcholinesterase
AChR	Acetylcholine receptor
ADB	Anterodorsal belt field
ADF	Anterior dorsal field
ADP	Afterdepolarization phase
AEE	Acoustically enriched environment
AHP	Afterhyperpolarization phase
AI	Primary auditory area
ALA	Anterolateral area
Ald	dorsal region of the primary auditory field
AM	Amplitude modulated
AMPA	α-amino-3-hydroxy-5methylisoxazol-4-propionic acid
AMPAR	α-amino-3-hydroxy-5methylisoxazol-4-propionic receptor
AP	Action potential
AV	Anteroventral field
AVCN	Anteroventral Cochlear Nucleus
BBN	Broad band noise
BDNF	Brain derived neurotrophic factor
BW30	Bandwidth of the excitatory area 30dB above the threshold
CC	Cortico-collicular projections
cDNA	Complementary deoxyribonucleic acid
CF	Characteristic frequency
CIC	Central nucleus of inferior colliculus
CL	Caudolateral belt
CM	Caudomedial area
CN	Cochlear nucleus
CNS	Central nervous system

CoN	Cochlear nuclei
CPB	Caudal parabelt
CS	Central sulcus
D	Dorsal field
DAPI	4, 6-diamidino-2-phenylindole
DB	Dorsal belt field
dB	Decibel
DC	Direct current
DCB	Dorsocaudal belt
DCIC	Dorsal cortex of inferior colliculus
DCN	Dorsal cochlear nukleus
DLPFC	Dorsolateral prefrontal cortex
DNLL	Dorsal nucleus of the lateral lemniscus
DNQX	6,7-dinitroquinoxaline-2,3-dione
dMGN	Dorsal division of medial geniculate nucleus
DP	Dorsoposterior field
DRB	Dorsorostral belt
ECIC	External cortex of inferior colliculus
EP	Ectosylvian posterior
EPSCs	Excitatory postsynaptic currents
EPSP	Excitatory postsynaptic potentials
E_{rev}	Reverse potential
FM	Frequency modulated
G	Granule cell
GABA	y-aminobutyric acid
$GABA_AR$	y-aminobutyric acid receptor
GAD	Glutamic acid decarboxylase
G density	Conductance density
GIRK	G-protein-coupled inwardly-rectifying potassium channel
GluR	Ionotropic glutamate receptor
Glu	Glutamate
GluR	Glutamatergic receptor
H	Horizontal cell
HCG	Horizontal cell group
HCN	Hyperpolarization/cyclic nucleotide-gated cation

I_h	HCN-mediated current
IC	Inferior colliculus
IFC	Inferior frontal cortex
INLL	Intermediate nucleus of the lateral lemniscus
Ins	Insula
IPL	Intraparietal lobule
IPS	Intraparietal sulcus
K_{ir}	Inward rectifying potassium ion channel
LA	Lateral area
LL	Lateral lemniscus
LP	Lateroposterior area
LS	Lateral sulcus
M	Martinotti cell
MA	Medial area
mAChR	Muscarinic acetylcholine receptor
MAP2	Anti-microtubule-associated protein 2
MGB	Medial geniculate body
MLRs	Middle latency responses
MM	Mediomedial belt
mMGN	Medial division of medial geniculate nucleus
mRNA	Messenger ribonucleic acid
MTF	Modulation-transfer functions
nAChR	Nicotinic acetylcholine receptor
NGF	Nerve growth factor
NLL	Nuclei of the lateral lemniscus
NMDA	N-methyl-D-aspartate
NMDAR	N-methyl-D-aspartate receptor
ns	Non-significant
P	Pyramidal cell
PA	Posterior area
PAF	Posterior auditory field
PB	Phosphate buffer
PBS	Phosphate-buffered saline
PDB	Posterodorsal belt field
PDF	Posterior dorsal field

PFA	Paraformaldehyde
PL	Paralemniscal regions
PMC	Premotor cortex
PPF	Posterior pseudosylvian field
PSF	Posterior suprasylvian field
PSTH	Peri-stimulus time histogram
PVCN	Posterioventral cochlear nukleus
qPCR	Quantitative polymerase chain reaction
R-CPP	3-((R)-2-Carboxypiperazin-4-yl)-propyl-1-phosphonic acid
R_{in}	Input resistance
RIF	Rate-intensity function
RM	Rostromedial belt
RNA	Ribonucleic acid
RPB	Rostral parabelt
RT	Room temperature
RTL	Rostrotemporal lateral belt
RTM	Rostrotemporal medial belt
RTN	Reticular thalamic nucleus
RT-qPCR	Real-time quantitative polymerase chain reaction
S	Stellate cell
Sag	Nucleus sagulum
SD	Standard deviation
SEM	Standard error of the mean
SOC	Superior olivary complex
SPL	Sound pressure level
SR95531	Gabazine
SRAF	Suprarhinal auditory field
STA	Superior temporal area
STGr	Superior temporal gyrus
STS	Superior temporal sulcus
SSA	Stimulus-specific adaptation
T	Transitional belt area
Te	Temporal
TLC	Tectal longitudinal column
τ_m	Time constant

Tpt	Temporal lobe association cortex
TTX	Tetrodotoxin
V	Ventral field
$V_{1/2}$	half-maximum activation level
VAF	Ventral auditory field
VCN	Ventral cochlear nucleus
VCB	Ventrocaudal belt
VLPFC	Ventrolateral prefrontal cortex
VM	Ventromedial field
vMGN	Ventral division of medial geniculate nucleus
VNLL	Ventral nucleus of the lateral lemniscus
VP	Ventroposterior field
VRB	Ventrorostral belt
V_{rest}	Resting membrane potential
VS	Vector strength

10. References

1. AITKIN, L. 1986. *The Auditory Midbrain,* Clifton, Humana Press.
2. ALMOG, M. & KORNGREEN, A. 2009. Characterization of Voltage-Gated Ca2+ Conductances in Layer 5 Neocortical Pyramidal Neurons from Rats. *Plos One,* 4.
3. ANDERSON, L. & MALMIERCA, M. 2013. The effect of auditory cortex deactivation on stimulus-specific adaptation in the inferior colliculus of the rat. *European Journal of Neuroscience,* 37**,** 52-62.
4. ANOMAL, R., DE VILLERS-SIDANI, E., MERZENICH, M. & PANIZZUTTI, R. 2013. Manipulation of BDNF Signaling Modifies the Experience-Dependent Plasticity Induced by Pure Tone Exposure during the Critical Period in the Primary Auditory Cortex. *Plos One,* 8.
5. ANTUNES, F. & MALMIERCA, M. 2011. Effect of Auditory Cortex Deactivation on Stimulus-Specific Adaptation in the Medial Geniculate Body. *Journal of Neuroscience,* 31**,** 17306-17316.
6. APONTE, Y., LIEN, C. C., REISINGER, E. & JONAS, P. 2006. Hyperpolarization-activated cation channels in fast-spiking interneurons of rat hippocampus. *Journal of Physiology-London,* 574**,** 229-243.
7. ARAMAKIS, V. B., BANDROWSKI, A. E. & ASHE, J. H. 1997. Muscarinic reduction of GABAergic synaptic potentials results in disinhibition of the AMPA/kainate-mediated EPSP in auditory cortex. *Brain Research,* 758**,** 107-117.
8. ASTON-JONES, G. & COHEN, J. D. 2005. An integrative theory of locus coeruleus-norepinephrine function: Adaptive gain and optimal performance. *Annual Review of Neuroscience,* 28**,** 403-450.
9. AU, T. K.-F., KNIGHTLY, L. M., JUN, S.-A. & OH, J. S. 2002. Overhearing a Language During Childhood. *Psychological Science,* 13**,** 238-243.
10. BAI, W. Z., ISHIDA, M. & ARIMATSU, Y. 2004. Chemically defined feedback connections from infragranular layers of sensory association cortices in the rat. *Neuroscience,* 123**,** 257-67.
11. BAJO, V. M., NODAL, F. R., BIZLEY, J. K., MOORE, D. R. & KING, A. J. 2007. The ferret auditory cortex: Descending projections to the inferior colliculus. *Cerebral Cortex,* 17**,** 475-491.
12. BAJO, V. M., NODAL, F. R., MOORE, D. R. & KING, A. J. 2010. The descending corticocollicular pathway mediates learning-induced auditory plasticity. *Nature Neuroscience,* 13**,** 253-U146.
13. BANNISTER, A. P. 2005. Inter- and intra-laminar connections of pyramidal cells in the neocortex. *Neuroscience Research,* 53**,** 95-103.
14. BEKKERS, J. M. & DELANEY, A. J. 2001. Modulation of excitability by alpha-dendrotoxin-sensitive potassium channels in neocortical pyramidal neurons. *Journal of Neuroscience,* 21**,** 6553-6560.
15. BENESOVA, J., RUSNAKOVA, V., HONSA, P., PIVONKOVA, H., DZAMBA, D., KUBISTA, M. & ANDEROVA, M. 2012. Distinct Expression/Function of Potassium and Chloride Channels Contributes to the Diverse Volume Regulation in Cortical Astrocytes of GFAP/EGFP Mice. *Plos One,* 7.
16. BENEYTO, M. & PRIETO, J. J. 2001. Connections of the auditory cortex with the claustrum and the endopiriform nucleus in the cat. *Brain Research Bulletin,* 54**,** 485-498.
17. BERARDI, N., PIZZORUSSO, T. & MAFFEI, L. 2000. Critical periods during sensory development. *Current Opinion in Neurobiology,* 10**,** 138-145.
18. BERGER, T., LARKUM, M. E. & LUSCHER, H. R. 2001. High I-h channel density in the distal apical dendrite of layer V pyramidal cells increases bidirectional attenuation of EPSPs. *Journal of Neurophysiology,* 85**,** 855-868.
19. BERGER, T., SENN, W. & LUSCHER, H. R. 2003. Hyperpolarization-activated current I-h disconnects somatic and dendritic spike initiation zones in layer V pyramidal neurons. *Journal of Neurophysiology,* 90**,** 2428-2437.
20. BERZAGHI, M. D., COOPER, J., CASTREN, E., ZAFRA, F., SOFRONIEW, M., THOENEN, H. & LINDHOLM, D. 1993. Cholinergic regulation of brain-derived neurotrophic factor (BDNF) and nerve-growth factor (NGF) but not neurotrophin-3 (NT-3) messenger-RNA levels in the developing rat hippocampus. *Journal of Neuroscience,* 13**,** 3818-3826.
21. BIALEK, W., RIEKE, F., DE RUYTER VAN STEVENINCK, R. & WARLAND, D. 1991. Reading a neural code. *Science,* 252**,** 1854-1857.
22. BIEL, M., WAHL-SCHOTT, C., MICHALAKIS, S. & ZONG, X. 2009. Hyperpolarization-activated cation channels: from genes to function. *Physiol Rev,* 89**,** 847-85.
23. BILLIMORIA, C. P., DICAPRIO, R. A., BIRMINGHAM, J. T., ABBOTT, L. F. & MARDER, E. 2006. Neuromodulation of Spike-Timing Precision in Sensory Neurons. *The Journal of Neuroscience,* 26**,** 5910-5919.
24. BIZLEY, J. K. & COHEN, Y. E. 2013. The what, where and how of auditory-object perception. *Nature Reviews Neuroscience,* 14**,** 693-707.
25. BIZLEY, J. K., NODAL, F. R., NELKEN, I. & KING, A. J. 2005. Functional organization of ferret auditory cortex. *Cerebral Cortex,* 15**,** 1637-1653.

26. BOSE, M., MUNOZ-LLANCAO, P., ROYCHOWDHURY, S., NICHOLS, J., JAKKAMSETTI, V., PORTER, B., BYRAPUREDDY, R., SALGADO, H., KILGARD, M., ABOITIZ, F., DAGNINO-SUBIABRE, A. & ATZORI, M. 2010. Effect of the Environment on the Dendritic Morphology of the Rat Auditory Cortex. *Synapse,* 64**,** 97-110.
27. BRODAL, P. 1972. CORTICOPONTINE PROJECTION IN CAT - PROJECTION FROM AUDITORY CORTEX. *Archives Italiennes De Biologie,* 110**,** 119-&.
28. BRUDZYNSKI, S. 2009. Communication of Adult Rats by Ultrasonic Vocalization: Biological, Sociobiological, and Neuroscience Approaches. *Ilar Journal,* 50**,** 43-50.
29. BURES, Z., BARTOSOVA, J., LINDOVSKY, J., CHUMAK, T., POPELAR, J. & SYKA, J. 2014. Acoustical enrichment during early postnatal development changes response properties of inferior colliculus neurons in rats. *European Journal of Neuroscience,* 40**,** 3674-3683.
30. BURES, Z., GRECOVA, J., POPELAR, J. & SYKA, J. 2010. Noise exposure during early development impairs the processing of sound intensity in adult rats. *European Journal of Neuroscience,* 32**,** 155-164.
31. BURES, Z., POPELAR, J. & SYKA, J. 2017. The effect of noise exposure during the developmental period on the function of the auditory system. *Hearing Research,* 352**,** 1-11.
32. CAI, R., ZHOU, X., GUO, F., XU, J., ZHANG, J. & SUN, X. 2010. Maintenance of enriched environment-induced changes of auditory spatial sensitivity and expression of GABA(A), NMDA, and AMPA receptor subunits in rat auditory cortex. *Neurobiology of Learning and Memory,* 94**,** 452-460.
33. CHANG, E., BAO, S., IMAIZUMI, K., SCHREINER, C. & MERZENICH, M. 2005. Development of spectral and temporal response selectivity in the auditory cortex. *Proceedings of the National Academy of Sciences of the United States of America,* 102**,** 16460-16465.
34. CHANG, E. & MERZENICH, M. 2003. Environmental noise retards auditory cortical development. *Science,* 300**,** 498-502.
35. CHEN, W. S. & BEAR, M. F. 2007. Activity-dependent regulation of NR2B translation contributes to metaplasticity in mouse visual cortex. *Neuropharmacology,* 52**,** 200-214.
36. CHENG, Y., JIA, G., ZHANG, Y., HAO, H., SHAN, Y., YU, L., SUN, X., ZHENG, Q., KRAUS, N., MERZENICH, M. & ZHOU, X. 2017. Positive impacts of early auditory training on cortical processing at an older age. *Proceedings of the National Academy of Sciences of the United States of America,* 114**,** 6364-6369.
37. COLBERT, C. & JOHNSTON, D. 1996. Axonal action-potential initiation and Na+ channel densities in the soma and axon initial segment of subicular pyramidal neurons. *Journal of Neuroscience,* 16**,** 6676-6686.
38. COLBURN, H., CARNEY, L. & HEINZ, M. 2003. Quantifying the information in auditory-nerve responses for level discrimination. *Jaro-Journal of the Association For Research in Otolaryngology,* 4**,** 294-311.
39. COOMBER, B., EDWARDS, D., JONES, S., SHACKLETON, T., GOLDSCHMIDT, J., WALLACE, M. & PALMER, A. 2011. Cortical Inactivation by Cooling in Small Animals. *Frontiers in Systems Neuroscience,* 5**,** 53.
40. COOMES, D. L., SCHOFIELD, R. M. & SCHOFIELD, B. R. 2005. Unilateral and bilateral projections from cortical cells to the inferior colliculus in guinea pigs. *Brain Research,* 1042**,** 62-72.
41. COX, C. L., METHERATE, R., WEINBERGER, N. M. & ASHE, J. H. 1992. Synaptic potentials and effects of amino-acid antagonists in the auditory cortex. *Brain Research Bulletin,* 28**,** 401-410.
42. DARROW, K. N., MAISON, S. F. & LIBERMAN, M. C. 2006. Cochlear efferent feedback balances interaural sensitivity. *Nature Neuroscience,* 9**,** 1474-1476.
43. DAY, M., CARR, D. B., ULRICH, S., ILIJIC, E., TKATCH, T. & SURMEIER, D. J. 2005. Dendritic excitability of mouse frontal cortex pyramidal neurons is shaped by the interaction among HCN, Kir2, and k(leak) channels. *Journal of Neuroscience,* 25**,** 8776-8787.
44. DE LA MOTHE, L. A., BLUMELL, S., KAJIKAWA, Y. & HACKETT, T. A. 2006. Thalamic connections of the auditory cortex in marmoset monkeys: core and medial belt regions. *J Comp Neurol,* 496**,** 72-96.
45. DE VILLERS-SIDANI, E., CHANG, E., BAO, S. & MERZENICH, M. 2007. Critical period window for spectral tuning defined in the primary auditory cortex (A1) in the rat. *Journal of Neuroscience,* 27**,** 180-189.
46. DEIS, R. P. & PRILUSKY, J. 1984. Participation of the hippocampus in the facilitatory effect of an exteroceptive stimulus on milk ejection. *Experimental Brain Research,* 55**,** 177-179.
47. DESJARDINS, A. E., LI, Y. X., REINKER, S., MIURA, R. M. & NEUMAN, R. S. 2003. The influences of Ih on temporal summation in hippocampal CA1 pyramidal neurons: a modeling study. *J Comput Neurosci,* 15**,** 131-42.
48. DIAMOND, I. T., JONES, E. G. & POWELL, T. P. S. 1969. Projection of auditory cortex upon the diencephalon and brain stem in cat. *Brain Research,* 15**,** 305-&.

49. DOUCET, J. R., MOLAVI, D. L. & RYUGO, D. K. 2003. The source of corticocollicular and corticobulbar projections in area Te1 of the rat. *Experimental Brain Research,* 153**,** 461-466.
50. DRINGENBERG, H. C., DAY, L. R. B. & CHOI, D. H. 2014. Chronic Fluoxetine Treatment Suppresses Plasticity (Long-Term Potentiation) in the Mature Rodent Primary Auditory Cortex In Vivo. *Neural Plasticity*.
51. DRUGA, R. & SYKA, J. 1984a. Ascending and descending projections to the inferior colliculus in the rat. *Physiologia Bohemoslovaca,* 33**,** 31-&.
52. DRUGA, R. & SYKA, J. 1984b. Projections from auditory structures to the superior colliculus in the rat. *Neuroscience Letters,* 45**,** 247-252.
53. DRUGA, R., SYKA, J. & RAJKOWSKA, G. 1997. Projections of auditory cortex onto the inferior colliculus in the rat. *Physiological Research,* 46**,** 215-222.
54. EHRET, G. & ROMAND, R. 1997. *The Central Auditory System,* New York |Oxford, Oxford University Press.
55. ENGINEER, N., PERCACCIO, C., PANDYA, P., MOUCHA, R., RATHBUN, D. & KILGARD, M. 2004. Environmental enrichment improves response strength, threshold, selectivity, and latency of auditory cortex neurons. *Journal of Neurophysiology,* 92**,** 73-82.
56. ESCERA, C. & MALMIERCA, M. 2014. The auditory novelty system: An attempt to integrate human and animal research. *Psychophysiology,* 51**,** 111-123.
57. FELICIANO, M. & POTASHNER, S. J. 1995. Evidence for a glutamatergic pathway from the guinea pig auditory cortex to the inferior colliculus. *Journal of Neurochemistry,* 65**,** 1348-1357.
58. FITZPATRICK, D. C. & HENSON, O. W. 1994. Cell types in the moustached bat auditory cortex. *Brain Behavior and Evolution,* 43**,** 79-91.
59. FRIEDERICI, A. 2012. The cortical language circuit: from auditory perception to sentence comprehension. *Trends in Cognitive Sciences,* 16**,** 262-268.
60. GARCIA-OSCOS, F., TORRES-RAMIREZ, O., DINH, L., GALINDO-CHARLES, L., PADILLA, E. A. P., PINEDA, J. C., ATZORI, M. & SALGADO, H. 2015. Activation of 5-HT Receptors Inhibits GABAergic Transmission by Pre-and Post-Synaptic Mechanisms in Layer II/III of the Juvenile Rat Auditory Cortex. *Synapse,* 69**,** 115-127.
61. GEALDOR, M., FREEMAN, S., LI, G. & SOHMER, H. 1993. Development of hearing in neonatal rats - air and bone conducted ABR thresholds. *Hearing Research,* 69**,** 236-242.
62. GEERS, A. E. & SEDEY, A. L. 2011. Language and Verbal Reasoning Skills in Adolescents With 10 or More Years of Cochlear Implant Experience. *Ear and Hearing,* 32**,** 39S-48S.
63. GELFAND, S. A. 2010. *Hearing : an introduction to psychological and physiological acoustics,* London, Informa Healthcare.
64. GRAVEL, J. & WALLACE, I. 1998. Language, speech, and educational outcomes of otitis media. *Journal of Otolaryngology,* 27**,** 17-25.
65. GRECOVA, J., BURES, Z., POPELAR, J., SUTA, D. & SYKA, J. 2009. Brief exposure of juvenile rats to noise impairs the development of the response properties of inferior colliculus neurons. *European Journal of Neuroscience,* 29**,** 1921-1930.
66. HACKETT, T. A. 2011. Information flow in the auditory cortical network. *Hear Res,* 271**,** 133-46.
67. HARRIS, N. C. & CONSTANTI, A. 1995. Mechanism of block by ZD 7288 of the hyperpolarization-activated inward rectifying current in guinea pig substantia nigra neurons in vitro. *Journal of Neurophysiology,* 74**,** 2366-2378.
68. HE, C., CHEN, F., LI, B. & HU, Z. 2014. Neurophysiology of HCN channels: From cellular functions to multiple regulations. *Progress in Neurobiology,* 112**,** 1-23.
69. HE, J., HASHIKAWA, T., OJIMA, H. & KINOUCHI, Y. 1997. Temporal integration and duration tuning in the dorsal zone of cat auditory cortex. *J Neurosci,* 17**,** 2615-25.
70. HEFFNER, H. E. & HEFFNER, R. S. 1990. Effect of bilateral auditory cortex lesions on absolute thresholds in japanese macaques. *Journal of Neurophysiology,* 64**,** 191-205.
71. HEIL, P., RAJAN, R. & IRVINE, D. R. F. 1994. Topographic representation of tone intensity along the isofrequency axis of cat primary auditory cortex. *Hearing Research,* 76**,** 188-202.
72. HEIL, P., SCHEICH, H., BUDINGER, E. & KONIG, R. 2005. *The Auditory Cortex: A Synthesis of Human and Animal Research*, Taylor & Francis.
73. HENDELMAN, W. 2005. *Atlas of functional neuroanatomy*, CRC Press.
74. HERBERT, H., ASCHOFF, A. & OSTWALD, J. 1991. Topography of projections from the auditory cortex to the inferior colliculus in the rat. *J Comp Neurol,* 304**,** 103-22.
75. HERNANDEZ, O., REES, A. & MALMIERCA, M. 2006. A GABAergic component in the commissure of the inferior colliculus in rat. *Neuroreport,* 17**,** 1611-1614.
76. HOHMANN, C. F. & BERGER-SWEENEY, J. 1998. Cholinergic regulation of cortical development and plasticity - New twists to an old story. *Perspectives on Developmental Neurobiology,* 5**,** 401-425.

77. HOHMANN, C. F., POTTER, E. D. & LEVEY, A. I. 1995. Development of muscatinic receptor subtypes in the forebrain of the mouse. *Journal of Comparative Neurology,* 358**,** 88-101.
78. HONSA, P., PIVONKOVA, H., HARANTOVA, L., BUTENKO, O., KRISKA, J., DZAMBA, D., RUSNAKOVA, V., VALIHRACH, L., KUBISTA, M. & ANDEROVA, M. 2014. Increased Expression of Hyperpolarization-Activated Cyclic Nucleotide-Gated (HCN) Channels in Reactive Astrocytes Following Ischemia. *Glia,* 62**,** 2004-2021.
79. HUANG, Z. J., KIRKWOOD, A., PIZZORUSSO, T., PORCIATTI, V., MORALES, B., BEAR, M. F., MAFFEI, L. & TONEGAWA, S. 1999. BDNF regulates the maturation of inhibition and the critical period of plasticity in mouse visual cortex. *Cell,* 98**,** 739-755.
80. HUGGENBERGER, S., VATER, M. & DEISZ, R. A. 2009. Interlaminar differences of intrinsic properties of pyramidal neurons in the auditory cortex of mice. *Cereb Cortex,* 19**,** 1008-18.
81. HUTSLER, J. J. & GAZZANIGA, M. S. 1996. Acetylcholinesterase staining in human auditory and language cortices: Regional variation of structural features. *Cerebral Cortex,* 6**,** 260-270.
82. JAASKELAINEN, I. P. & AHVENINEN, J. 2014. Auditory-Cortex Short-Term Plasticity Induced by Selective Attention. *Neural Plasticity*.
83. JARAMILLO, S. & ZADOR, A. M. 2011. The auditory cortex mediates the perceptual effects of acoustic temporal expectation. *Nature Neuroscience,* 14**,** 246-U340.
84. JEN, P. H. S., SUN, X. D. & CHEN, Q. C. 2001. An electrophysiological study of neural pathways for corticofugally inhibited neurons in the central nucleus of the inferior colliculus of the big brown bat, Eptesicus fuscus. *Experimental Brain Research,* 137**,** 292-302.
85. JENKINS, W. M. & MERZENICH, M. M. 1984. Role of cat primary auditory cortex for sound localisation behavior. *Journal of Neurophysiology,* 52**,** 819-847.
86. JIANG, C., XU, X., YU, L., XU, J. & ZHANG, J. 2015. Environmental enrichment rescues the degraded auditory temporal resolution of cortical neurons induced by early noise exposure. *European Journal of Neuroscience,* 42**,** 2144-2154.
87. KAAS, J. H. & HACKETT, T. A. 1998. Subdivisions of auditory cortex and levels of processing in primates. *Audiology and Neuro-Otology,* 3**,** 73-85.
88. KAHLE, W., FROTSCHER, M. & SPITZER, G. 2003. *Color atlas of human anatomy. Volume 3, Volume 3,* Stuttgart; New York, Thieme.
89. KALATSKY, V. A., POLLEY, D. B., MERZENICH, M. M., SCHREINER, C. E. & STRYKER, M. P. 2005. Fine functional organization of auditory cortex revealed by Fourier optical imaging. *Proceedings of the National Academy of Sciences of the United States of America,* 102**,** 13325-13330.
90. KANDLER, K. & GILLESPIE, D. 2005. Developmental refinement of inhibitory sound-localization circuits. *Trends in Neurosciences,* 28**,** 290-296.
91. KASE, D., INOUE, T. & IMOTO, K. 2012. Roles of the subthalamic nucleus and subthalamic HCN channels in absence seizures. *Journal of Neurophysiology,* 107**,** 393-406.
92. KAUR, S., LAZAR, R. & METHERATE, R. 2004. Intracortical pathways determine breadth of subthreshold frequency receptive fields in primary auditory cortex. *Journal of Neurophysiology,* 91**,** 2551-2567.
93. KAWASE, T. & LIBERMAN, M. C. 1993. Antimasking effects of the olivocochlear reflex. 1. Enchancement of compound action potentials to masked tones. *Journal of Neurophysiology,* 70**,** 2519-2532.
94. KELLY, J. B. 1980. Effects of auditory cortical lesions on sound localisation by the rat. *Journal of Neurophysiology,* 44**,** 1161-1174.
95. KELLY, J. B. & KAVANAGH, G. L. 1986. Effects of auditory cortical lesions on pure-tone sound localisation by the albino rat. *Behavioral Neuroscience,* 100**,** 569-575.
96. KEOGH, T., KEI, J., DRISCOLL, C. & KHAN, A. 2010. Children with Minimal Conductive Hearing Impairment: Speech Comprehension in Noise. *Audiology and Neuro-Otology,* 15**,** 27-35.
97. KOCH, U. & GROTHE, B. 2003. Hyperpolarization-activated current (I-h) in the inferior colliculus: Distribution and contribution to temporal processing. *Journal of Neurophysiology,* 90**,** 3679-3687.
98. KRAL, A. 2013. Auditory critical periods: a review from system's perspective. *Neuroscience,* 247**,** 117-133.
99. KRAL, A., HARTMANN, R., TILLEIN, J., HEID, S. & KLINKE, R. 2001. Delayed maturation and sensitive periods in the auditory cortex. *Audiology and Neuro-Otology,* 6**,** 346-362.
100. KRAL , A. & O'DONOGHUE , G. M. 2010. Profound Deafness in Childhood. *New England Journal of Medicine,* 363**,** 1438-1450.
101. KRAL, A. & PALLAS, S. 2010. *Development of the Auditory Cortex*.
102. KRESS, G., DOWLING, M., MEEKS, J. & MENNERICK, S. 2008. High threshold, proximal initiation, and slow conduction velocity of action potentials in dentate granule neuron mossy fibers. *Journal of Neurophysiology,* 100**,** 281-291.

103. KUHL, P. 2010. Brain Mechanisms in Early Language Acquisition. *Neuron,* 67**,** 713-727.
104. LAWS, G. & HALL, A. 2014. Early hearing loss and language abilities in children with Down syndrome. *International Journal of Language & Communication Disorders,* 49**,** 333-342.
105. LIBERMAN, M. C. & BROWN, M. C. 1986. Physiology and anatomy of single olivocochlear neurons in the cat. *Hearing Research,* 24**,** 17-36.
106. LINDEN, J. F. & SCHREINER, C. E. 2003. Columnar transformations in auditory cortex? A comparison to visual and somatosensory cortices. *Cerebral Cortex,* 13**,** 83-89.
107. LOMBER, S., PAYNE, B. & HOREL, J. 1999. The cryoloop: an adaptable reversible cooling deactivation method for behavioral or electrophysiological assessment of neural function. *Journal of Neuroscience Methods,* 86**,** 179-194.
108. LU, H., SYKA, J., CHIU, T. & POON, P. 2014. Prolonged sound exposure has different effects on increasing neuronal size in the auditory cortex and brainstem. *Hearing Research,* 314**,** 42-50.
109. MA, X. F. & SUGA, N. 2001a. Corticofugal modulation of duration-tuned neurons in the midbrain auditory nucleus in bats. *Proceedings of the National Academy of Sciences of the United States of America,* 98**,** 14060-14065.
110. MA, X. F. & SUGA, N. 2001b. Plasticity of bat's central auditory system evoked by focal electric stimulation of auditory and/or somatosensory cortices. *Journal of Neurophysiology,* 85**,** 1078-1087.
111. MAGEE, J. C. 1998. Dendritic hyperpolarization-activated currents modify the integrative properties of hippocampal CA1 pyramidal neurons. *Journal of Neuroscience,* 18**,** 7613-7624.
112. MAGEE, J. C. 1999a. Dendritic I-h normalizes temporal summation in hippocampal CA1 neurons. *Nature Neuroscience,* 2**,** 508-514.
113. MAGEE, J. C. 1999b. Dendritic I-h normalizes temporal summation in hippocampal CA1 neurons (vol 2, pg 508, 1999). *Nature Neuroscience,* 2**,** U9-U9.
114. MAI, J. K. & PAXINOS, G. 2011. *The Human Nervous System*, Elsevier Science.
115. MAISON, S. F. & LIBERMAN, M. C. 2000. Predicting vulnerability to acoustic injury with a noninvasive assay of olivocochlear reflex strength. *Journal of Neuroscience,* 20**,** 4701-4707.
116. MALMIERCA, M., HERNANDEZ, O. & REES, A. 2005. Intercollicular commissural projections modulate neuronal responses in the inferior colliculus. *European Journal of Neuroscience,* 21**,** 2701-2710.
117. MALMIERCA, M. S., ANDERSON, L. A. & ANTUNES, F. M. 2015. The cortical modulation of stimulus-specific adaptation in the auditory midbrain and thalamus: a potential neuronal correlate for predictive coding. *Frontiers in Systems Neuroscience,* 9.
118. MANUNTA, Y. & EDELINE, J. M. 2004. Noradrenergic induction of selective plasticity in the frequency tuning of auditory cortex neurons. *Journal of Neurophysiology,* 92**,** 1445-1463.
119. MARKOVITZ, C. D., TANG, T. T. & LIM, H. H. 2013. Tonotopic and localized pathways from primary auditory cortex to the central nucleus of the inferior colliculus. *Frontiers in Neural Circuits,* 7.
120. MARTINS, A. R. O. & FROEMKE, R. C. 2015. Coordinated forms of noradrenergic plasticity in the locus coeruleus and primary auditory cortex. *Nature Neuroscience,* 18**,** 1483-+.
121. MELTZER, N. E. & RYUGO, D. K. 2006. Projections from auditory cortex to cochlear nucleus: A comparative analysis of rat and mouse. *Anatomical Record Part a-Discoveries in Molecular Cellular and Evolutionary Biology,* 288A**,** 397-408.
122. MERCHAN, M., AGUILAR, L. A., LOPEZ-POVEDA, E. A. & MALMIERCA, M. S. 2005. The inferior colliculus of the rat: Quantitative immunocytochemical study of GABA and glycine. *Neuroscience,* 136**,** 907-925.
123. MESULAM, M. M., MUFSON, E. J., LEVEY, A. I. & WAINER, B. H. 1983a. Cholinergic innervation of cortex by the basal forebrain - cyto-chemistry and cortical connections of the septal area, diagonal band nuclei, nucleus basalis (substantia innominata), and hypothalamus in the rhesus-monkey. *Journal of Comparative Neurology,* 214**,** 170-197.
124. MESULAM, M. M., MUFSON, E. J., WAINER, B. H. & LEVEY, A. I. 1983b. Central cholinergic pathway in the rat - an overview based on an alternative nomenclature (CH1-CH6). *Neuroscience,* 10**,** 1185-1201.
125. METHERATE, R. & HSIEH, C. Y. 2003. Regulation of glutamate synapses by nicotinic acetylcholine receptors in auditory cortex. *Neurobiology of Learning and Memory,* 80**,** 285-290.
126. MITANI, A. & SHIMOKOUCHI, M. 1985. Neuronal connections in the primary auditory cortex - an electrophysiological study in the cat. *Journal of Comparative Neurology,* 235**,** 417-429.
127. MITANI, A., SHIMOKOUCHI, M., ITOH, K., NOMURA, S., KUDO, M. & MIZUNO, N. 1985. Morphology and laminar organization of electrophysiologically identified neurons in the primary auditory cortex in the cat. *Journal of Comparative Neurology,* 235**,** 430-447.

128. MITANI, A., SHIMOKOUCHI, M. & NOMURA, S. 1983. Effects of stimulation of the primary auditory cortex upon colluculogeniculate neurons in the inferior colliculus of the cat. *Neuroscience Letters,* 42**,** 185-189.
129. MIYAKAWA, A., GIBBONI, R. & BAO, S. 2013. Repeated exposure to a tone transiently alters spectral tuning bandwidth of neurons in the central nucleus of inferior colliculus in juvenile rats. *Neuroscience,* 230**,** 114-120.
130. MOMIN, A., CADIOU, H., MASON, A. & MCNAUGHTON, P. A. 2008. Role of the hyperpolarization-activated current I-h in somatosensory neurons. *Journal of Physiology-London,* 586**,** 5911-5929.
131. MOORE, D. R. 2002. Auditory development and the role of experience. *British Medical Bulletin,* 63**,** 171-181.
132. MOOSMANG, S., BIEL, M., HOFMANN, F. & LUDWIG, A. 1999. Differential distribution of four hyperpolarization-activated cation channels in mouse brain. *Biological Chemistry,* 380**,** 975-980.
133. MULDERS, W. & ROBERTSON, D. 2000. Evidence for direct cortical innervation of medial olivocochlear neurones in rats. *Hearing Research,* 144**,** 65-72.
134. MØLLER, A. R. 2000. *Hearing: Its Physiology and Pathophysiology*, Academic Press.
135. NAKAHARA, H., ZHANG, L. & MERZENICH, M. 2004. Specialization of primary auditory cortex processing by sound exposure in the "critical period". *Proceedings of the National Academy of Sciences of the United States of America,* 101**,** 7170-7174.
136. NAKAMOTO, K., JONES, S. & PALMER, A. 2008. Descending projections from auditory cortex modulate sensitivity in the midbrain to cues for spatial position. *Journal of Neurophysiology,* 99**,** 2347-2356.
137. NAKAMOTO, K., SHACKLETON, T. & PALMER, A. 2010. Responses in the Inferior Colliculus of the Guinea Pig to Concurrent Harmonic Series and the Effect of Inactivation of Descending Controls. *Journal of Neurophysiology,* 103**,** 2050-2061.
138. NAKAMOTO, K. T., MELLOTT, J. G., KILLIUS, J., STOREY-WORKLEY, M. E., SOWICK, C. S. & SCHOFIELD, B. R. 2013. Ultrastructural examination of the corticocollicular pathway in the guinea pig: a study using electron microscopy, neural tracers, and GABA immunocytochemistry. *Frontiers in Neuroanatomy,* 7.
139. NAUNDORF, B., WOLF, F. & VOLGUSHEV, M. 2006. Unique features of action potential initiation in cortical neurons. *Nature,* 440**,** 1060-3.
140. NETTER, F. 2014. *Atlas of Human Anatomy*, Saunders.
141. NEWPORT, E. L. 2003. Language development, critical periods in. *In:* NADEL, L. (ed.) *Encyclopedia of Cognitive Science.* Nature Publishing Group.
142. NICHOLS, J., JAKKAMSET'RI, V., SALGADO, H., DINH, L., KILGARD, M. & ATZORI, M. 2007. Environmental enrichment selectively increases glutamatergic responses in layer II/III of the auditory cortex of the rat. *Neuroscience,* 145**,** 832-840.
143. NIETO-DIEGO, J. & MALMIERCA, M. S. 2016. Topographic Distribution of Stimulus-Specific Adaptation across Auditory Cortical Fields in the Anesthetized Rat. *Plos Biology,* 14.
144. NIPARKO, J., TOBEY, E., THAL, D., EISENBERG, L., WANG, N., QUITTNER, A., FINK, N., TEAM, C. I. & TEAM, C. I. 2010. Spoken Language Development in Children Following Cochlear Implantation. *Jama-Journal of the American Medical Association,* 303**,** 1498-1506.
145. NOLAN, M., DUDMAN, J., DODSON, P. & SANTORO, B. 2007. HCN1 channels control resting and active integrative properties of stellate cells from layer II of the entorhinal cortex. *Journal of Neuroscience,* 27**,** 12440-12451.
146. NOLAN, M. F., MALLERET, G., DUDMAN, J. T., BUHL, D. L., SANTORO, B., GIBBS, E., VRONSKAYA, S., BUZSAKI, G., SIEGELBAUM, S. A., KANDEL, E. R. & MOROZOV, A. 2004. A behavioral role for dendritic integration: HCN1 channels constrain spatial inputs to distal dendrites memory and plasticity at of CA1 pyramidal neurons. *Cell,* 119**,** 719-732.
147. NWABUEZE-OGBO, F., POPELAR, J. & SYKA, J. 2002. Changes in the acoustically evoked activity in the inferior colliculus of the rat after functional ablation of the auditory cortex. *Physiological Research,* 51**,** S95-S104.
148. OLIVER, D., IZQUIERDO, M. & MALMIERCA, M. 2011. Persistent effects of early augmented acoustic environment on the auditory brainstem. *Neuroscience,* 184**,** 75-87.
149. OLIVER, D. L., WINER, J. A., BECKIUS, G. E. & SAINTMARIE, R. L. 1994. Morphology of GABAergic neurons in the inferior colliculus of the cat. *Journal of Comparative Neurology,* 340**,** 27-42.
150. OUDA, L., BURIANOVA, J., BALOGOVA, Z., LU, H. & SYKA, J. 2016a. Structural changes in the adult rat auditory system induced by brief postnatal noise exposure. *Brain Structure & Function,* 221**,** 617-629.

151. OUDA, L., JILEK, M. & SYKA, J. 2016b. Expression of c-Fos in rat auditory and limbic systems following 22-kHz calls. *Behavioural Brain Research,* 308**,** 196-204.
152. PANDYA, P. K., RATHBUN, D. L., MOUCHA, R., ENGINEER, N. D. & KILGARD, M. P. 2008. Spectral and temporal processing in rat posterior auditory cortex. *Cerebral Cortex,* 18**,** 301-314.
153. PATESTAS, M. A. & GARTNER, L. P. 2016. *A Textbook of Neuroanatomy*, Wiley.
154. PAVLOV, I., SCIMEMI, A., SAVTCHENKO, L., KULLMANN, D. M. & WALKER, M. C. 2011. Ih-mediated depolarization enhances the temporal precision of neuronal integration. *Nat Commun,* 2**,** 199.
155. PAXINOS, G. 2004. *The rat nervous system,* Amsterdam ; Boston, Elsevier Academic Press.
156. PENHUNE, V. 2011. Sensitive periods in human development: Evidence from musical training. *Cortex,* 47**,** 1126-1137.
157. PERALES, M., WINER, J. A. & PRIETO, J. J. 2006. Focal projections of cat auditory cortex to the pontine nuclei. *Journal of Comparative Neurology,* 497**,** 959-980.
158. PERCACCIO, C., ENGINEER, N., PRUETTE, A., PANDYA, P., MOUCHA, R., RATHBUN, D. & KILGARD, M. 2005. Environmental enrichment increases paired-pulse depression in rat auditory cortex. *Journal of Neurophysiology,* 94**,** 3590-3600.
159. PERCACCIO, C., PRUETTE, A., MISTRY, S., CHEN, Y. & KILGARD, M. 2007. Sensory experience determines enrichment-induced plasticity in rat auditory cortex. *Brain Research,* 1174**,** 76-91.
160. PHILPOT, B. D., SEKHAR, A. K., SHOUVAL, H. Z. & BEAR, M. F. 2001. Visual experience and deprivation bidirectionally modify the composition and function of NMDA receptors in visual cortex. *Neuron,* 29**,** 157-169.
161. POLLEY, D. B., READ, H. L., STORACE, D. A. & MERZENICH, M. M. 2007. Multiparametric auditory receptive field organization across five cortical fields in the albino rat. *Journal of Neurophysiology,* 97**,** 3621-3638.
162. POPELAR, J., NWABUEZE-OGBO, F. & SYKA, J. 2003. Changes in neuronal activity of the inferior colliculus in rat after temporal inactivation of the auditory cortex. *Physiological Research,* 52**,** 615-628.
163. PORTFORS, C. 2007. Types and functions of ultrasonic vocalizations in laboratory rats and mice. *Journal of the American Association For Laboratory Animal Science,* 46**,** 28-34.
164. PROFANT, O., BURIANOVA, J. & SYKA, J. 2013. The response properties of neurons in different fields of the auditory cortex in the rat. *Hearing Research,* 296**,** 51-59.
165. PUJOL, R. & IRVING, S. 2016. Auditory brain. *In:* PUJOL, R. (ed.) *Journey into the World of Hearing.* www.cochlea.eu.
166. RAUSCHECKER, J. P. 1999. Auditory cortical plasticity: a comparison with other sensory systems. *Trends in Neurosciences,* 22**,** 74-80.
167. RAUSCHECKER, J. P., TIAN, B., PONS, T. & MISHKIN, M. 1997. Serial and parallel processing in rhesus monkey auditory cortex. *J Comp Neurol,* 382**,** 89-103.
168. REALE, R. A. & IMIG, T. J. 1983. Auditory cortical field projections to the basal ganglia of the cat. *Neuroscience,* 8**,** 67-86.
169. RECANZONE, G. H. 2000. Response profiles of auditory cortical neurons to tones and noise in behaving macaque monkeys. *Hearing Research,* 150**,** 104-118.
170. RIVIER, F. & CLARKE, S. 1997. Cytochrome oxidase, acetylcholinesterase, and NADPH-diaphorase staining in human supratemporal and insular cortex: Evidence for multiple auditory areas. *Neuroimage,* 6**,** 288-304.
171. ROBERTS, R. C. & RIBAK, C. E. 1987. An electrron-microscopic study of GABAergic neurons and terminals in the central nucleus of the inferior colliculus of the rat. *Journal of Neurocytology,* 16**,** 333-345.
172. ROBINSON, R. B. 2003. Hyperpolarization-activated cation currents: From molecules to physiological function. *Annual Review of Physiology,* 65**,** 453-480.
173. ROGER, M. & ARNAULT, P. 1989. Anatomical study of the connections of the primary auditory area in the rat. *J Comp Neurol,* 287**,** 339-56.
174. ROMANSKI, L. M., BATES, J. F. & GOLDMAN-RAKIC, P. S. 1999. Auditory belt and parabelt projections to the prefrontal cortex in the rhesus monkey. *J Comp Neurol,* 403**,** 141-57.
175. ROMANSKI, L. M. & LEDOUX, J. E. 1993. Information cascade from primary auditory cortex to the amygdala - corticocortical and corticoamygdaloid projections of temporal cortex in the rat. *Cerebral Cortex,* 3**,** 515-532.
176. RUTKOWSKI, R. G., MIASNIKOV, A. A. & WEINBERGER, N. M. 2003. Characterisation of multiple physiological fields within the anatomical core of rat auditory cortex. *Hearing Research,* 181**,** 116-130.
177. RYBALKO, N., SUTA, D., NWABUEZE-OGBO, F. & SYKA, J. 2006. Effect of auditory cortex lesions on the discrimination of frequency-modulated tones in rats. *European Journal of Neuroscience,* 23**,** 1614-1622.

178. RYBALKO, N., SUTA, D., POPELAR, J. & SYKA, J. 2010. Inactivation of the left auditory cortex impairs temporal discrimination in the rat. *Behavioural Brain Research,* 209**,** 123-130.
179. RYBALKO, N. & SYKA, J. 2001. Susceptibility to noise exposure during postnatal development in rats. *Hearing Research,* 155**,** 32-40.
180. RYUGO, D. K., FAY, R. R. & POPPER, A. N. 2010. *Auditory and Vestibular Efferents*, Springer New York.
181. SACCO, C. B., TARDIF, E., GENOUD, C., PROBST, A., TOLNAY, M., JANZER, R. C., VERNEY, C., KRAFTSIK, R. & CLARKE, S. 2009. GABA receptor subunits in human auditory cortex in normal and stroke cases. *Acta Neurobiologiae Experimentalis,* 69**,** 469-493.
182. SALDANA, E. 2015. All the Way from the Cortex: a Review of Auditory Corticosubcollicular Pathways. *Cerebellum,* 14**,** 584-596.
183. SALDANA, E., FELICIANO, M. & MUGNAINI, E. 1996. Distribution of descending projections from primary auditory neocortex to inferior colliculus mimics the topography of intracollicular projections. *Journal of Comparative Neurology,* 371**,** 15-40.
184. SALLY, S. L. & KELLY, J. B. 1988. ORGANIZATION OF AUDITORY-CORTEX IN THE ALBINO-RAT - SOUND FREQUENCY. *Journal of Neurophysiology,* 59**,** 1627-1638.
185. SAMELLI, A., RONDON-MELO, S., RABELO, C. & MOLINI-AVEJONAS, D. 2017. Association between language and hearing disorders - risk identification. *Clinics,* 72**,** 213-217.
186. SANCHEZ-ALONSO, J. L., HALLIWELL, J. V. & COLINO, A. 2008. ZD 7288 inhibits T-type calcium current in rat hippocampal pyramidal cells. *Neuroscience Letters,* 439**,** 275-280.
187. SANES, D. & TAKACS, C. 1993. Activity-dependent refinement of inhibitory connections. *European Journal of Neuroscience,* 5**,** 570-574.
188. SANTORO, B., LIU, D. T., YAO, H., BARTSCH, D., KANDEL, E. R., SIEGELBAUM, S. A. & TIBBS, G. R. 1998. Identification of a gene encoding a hyperpolarization-activated pacemaker channel of brain. *Cell,* 93**,** 717-729.
189. SCHEICH, H., BRECHMANN, A., BROSCH, M., BUDINGER, E., OHL, F. W., SELEZNEVA, E., STARK, H., TISCHMEYER, W. & WETZEL, W. 2011. Behavioral semantics of learning and crossmodal processing in auditory cortex: The semantic processor concept. *Hearing Research,* 271**,** 3-15.
190. SCHOFIELD, B. R. 2009. Projections to the inferior colliculus from layer VI cells of auditory cortex. *Neuroscience,* 159**,** 246-258.
191. SCHOFIELD, B. R. & CANT, N. B. 1999. Descending auditory pathways: Projections from the inferior colliculus contact superior olivary cells that project bilaterally to the cochlear nuclei. *Journal of Comparative Neurology,* 409**,** 210-223.
192. SCHREINER, C. E. & WINER, J. A. 2007. Auditory cortex mapmaking: principles, projections, and plasticity. *Neuron,* 56**,** 356-65.
193. SCHULLER, G., COVEY, E. & CASSEDAY, J. H. 1991. Auditory pontine gray connections and response properties in the horseshoe bat. *European Journal of Neuroscience,* 3**,** 648-662.
194. SHAH, M. 2014a. Cortical HCN channels: function, trafficking and plasticity. *Journal of Physiology-London,* 592**,** 2711-2719.
195. SHIDELER, K. K. & YAN, J. 2010. M-1 muscarinic receptor for the development of auditory cortical function. *Molecular Brain,* 3.
196. SIEGEL, A. & SAPRU, H. N. 2011. *Essential neuroscience,* Philadelphia, Wolters Kluwer/Lippincott Williams & Wilkins Health.
197. SILVER, R. 2010. Neuronal arithmetic. *Nature Reviews Neuroscience,* 11**,** 474-489.
198. SLATER, B., WILLIS, A. & LLANO, D. 2013. Evidence for layer-specific differences in auditory corticocollicular neurons. *Neuroscience,* 229**,** 144-154.
199. SMITH, P. H. & POPULIN, L. C. 2001. Fundamental differences between the thalamocortical recipient layers of the cat auditory and visual cortices. *Journal of Comparative Neurology,* 436**,** 508-519.
200. STERIADE, M. 2000. Corticothalamic resonance, states of vigilance and mentation. *Neuroscience,* 101**,** 243-276.
201. STIEBLER, I., NEULIST, R., FICHTEL, I. & EHRET, G. 1997. The auditory cortex of the house mouse: left-right differences, tonotopic organization and quantitative analysis of frequency representation. *Journal of Comparative Physiology a-Sensory Neural and Behavioral Physiology,* 181**,** 559-571.
202. STRAKA, M. M., HUGHES, R., LEE, P. & LIM, H. H. 2015. Descending and tonotopic projection patterns from the auditory cortex to the inferior colliculus. *Neuroscience,* 300**,** 325-337.
203. STRAUSS, U., KOLE, M. H., BRAUER, A. U., PAHNKE, J., BAJORAT, R., ROLFS, A., NITSCH, R. & DEISZ, R. A. 2004. An impaired neocortical Ih is associated with enhanced excitability and absence epilepsy. *Eur J Neurosci,* 19**,** 3048-58.

204. SUGA, N. 2008. Role of corticofugal feedback in hearing. *Journal of Comparative Physiology a-Neuroethology Sensory Neural and Behavioral Physiology,* 194**,** 169-183.
205. SUN, W., MERCADO, E., WANG, P., SHAN, X. J., LEE, T. C. & SALVIA, R. J. 2005. Changes in NMDA receptor expression in auditory cortex after learning. *Neuroscience Letters,* 374**,** 63-68.
206. SUN, X. D., CHEN, Q. C. & JEN, P. H. S. 1996. Corticofugal control of central auditory sensitivity in the big brown bat, Eptesicus fuscus. *Neuroscience Letters,* 212**,** 131-134.
207. SWENSON, R. 2006. Review of clinical and functional neuroscience. *In:* HOLMES, G. (ed.) *Educational Review Manual in Neurology.* New York: Castle Connolly Graduate Medical Publishing.
208. SYKA, J. & POPELAR, J. 1984. Inferior colliculus in the rat - neuronal responses to stimulation of the auditory cortex. *Neuroscience Letters,* 51**,** 235-240.
209. SYKA, J., POPELAR, J., RYBALKO, N., NWABUEZE-OGBO, F. C., MAZELOVA, J. & SUTA, D. 2005. *Changes in auditory function following auditory cortex inactivation*.
210. SYKA, J., POPELÁŘ, J., DRUGA, R. & VLKOVÁ, A. 1988. Descending Central Auditory Pathway — Structure and Function. *In:* SYKA, J. & MASTERTON, R. B. (eds.) *Auditory Pathway: Structure and Function.* Boston, MA: Springer US.
211. TERREROS, G. & DELANO, P. H. 2015. Corticofugal modulation of peripheral auditory responses. *Frontiers in Systems Neuroscience,* 9.
212. THOMAS, H., TILLEIN, J., HEIL, P. & SCHEICH, H. 1993a. Functional organization of auditory cortex in the mongolian gerbil (Meriones unguiculatus). I. Electrophysiological mapping of frequency representation and distinction of fields. *Eur J Neurosci,* 5**,** 882-97.
213. TIAN, B. & RAUSCHECKER, J. P. 2004. Processing of frequency-modulated sounds in the lateral auditory belt cortex of the rhesus monkey. *Journal of Neurophysiology,* 92**,** 2993-3013.
214. TIESINGA, P., FELLOUS, J. & SEJNOWSKI, T. 2008. Regulation of spike timing in visual cortical circuits. *Nature Reviews Neuroscience,* 9**,** 97-109.
215. TORTEROLO, P., ZURITA, P., PEDEMONTE, M. & VELLUTI, R. A. 1998. Auditory cortical efferent actions upon inferior colliculus unitary activity in the guinea pig. *Neuroscience Letters,* 249**,** 172-176.
216. VAN WELIE, I., REMME, M. W. H., VAN HOOFT, J. A. & WADMAN, W. J. 2006. Different levels of I-h determine distinct temporal integration in bursting and regular-spiking neurons in rat. *Journal of Physiology-London,* 576**,** 203-214.
217. VILLA, A., ROUILLER, E., SIMM, G., ZURITA, P., DERIBAUPIERRE, Y. & DERIBAUPIERRE, F. 1991. Corticofugal modulation of the information processing in the auditory thalamus of the cat. *Experimental Brain Research,* 86**,** 506-517.
218. WAHL-SCHOTT, C. & BIEL, M. 2009. HCN channels: structure, cellular regulation and physiological function. *Cell Mol Life Sci,* 66**,** 470-94.
219. WALLACE, M. N., JOHNSTON, P. N. & PALMER, A. R. 2002. Histochemical identification of cortical areas in the auditory region of the human brain. *Experimental Brain Research,* 143**,** 499-508.
220. WALLACE, M. N., RUTKOWSKI, R. G. & PALMER, A. R. 2000a. Identification and localisation of auditory areas in guinea pig cortex. *Experimental Brain Research,* 132**,** 445-456.
221. WARR, W. B. 1980. Efferent components of the auditory system. *Annals of Otology Rhinology and Laryngology,* 89**,** 114-120.
222. WARREN, E. H. & LIBERMAN, M. C. 1989. Effecets of contralateral sound on auditory nerve responses.1. COntribution of cochlear efferents. *Hearing Research,* 37**,** 89-104.
223. WEEDMAN, D. L. & RYUGO, D. K. 1996a. Projections from auditory cortex to the cochlear nucleus in rats: Synapses on granule cell dendrites. *Journal of Comparative Neurology,* 371**,** 311-324.
224. WEEDMAN, D. L. & RYUGO, D. K. 1996b. Pyramidal cells in primary auditory cortex project to cochlear nucleus in rat. *Brain Research,* 706**,** 97-102.
225. WERTZNER, H. F., SANTOS, P. I. D. & PAGAN-NEVES, L. D. O. 2012. Tipos de erros de fala em crianças com transtorno fonológico em função do histórico de otite média. *Revista da Sociedade Brasileira de Fonoaudiologia,* 17**,** 422-429.
226. WILLIAMS, S. R. & STUART, G. J. 2000. Site independence of EPSP time course is mediated by dendritic I(h) in neocortical pyramidal neurons. *J Neurophysiol,* 83**,** 3177-82.
227. WINER, J. A. 1984. ANATOMY OF LAYER-IV IN CAT PRIMARY AUDITORY-CORTEX (AI). *Journal of Comparative Neurology,* 224**,** 535-567.
228. WINER, J. A. 2005. Decoding the auditory corticofugal systems. *Hearing Research,* 207**,** 1-9.
229. WINER, J. A., LARUE, D. T., DIEHL, J. J. & HEFTI, B. J. 1998. Auditory cortical projections to the cat inferior colliculus. *Journal of Comparative Neurology,* 400**,** 147-174.
230. WINER, J. A. & LEE, C. C. 2007. The distributed auditory cortex. *Hear Res,* 229**,** 3-13.
231. WOOD, K. C., TOWN, S. M., ATILGAN, H., JONES, G. P. & BIZLEY, J. K. 2017. Acute Inactivation of Primary Auditory Cortex Causes a Sound Localisation Deficit in Ferrets. *Plos One,* 12.

232. WU, X., LIAO, L. P., LIU, X. M., LUO, F., YANG, T. M. & LI, C. H. 2012. Is ZD7288 a selective blocker of hyperpolarization-activated cyclic nucleotide-gated channel currents? *Channels,* 6**,** 438-442.
233. XU, J., YU, L., CAI, R., ZHANG, J. & SUN, X. 2009. Early auditory enrichment with music enhances auditory discrimination learning and alters NR2B protein expression in rat auditory cortex. *Behavioural Brain Research,* 196**,** 49-54.
234. YAN, J. 2003. Canadian association of neuroscience review: Development and plasticity of the auditory cortex. *Canadian Journal of Neurological Sciences,* 30**,** 189-200.
235. YAN, J. & EHRET, G. 2001. Corticofugal reorganization of the midbrain tonotopic map in mice. *Neuroreport,* 12**,** 3313-3316.
236. YAN, J. & ZHANG, Y. F. 2005. Sound-guided shaping of the receptive field in the mouse auditory cortex by basal forebrain activation. *European Journal of Neuroscience,* 21**,** 563-576.
237. YEOMANS, J. S. & FRANKLAND, P. W. 1995. The acoustic startle reflex: Neurons and connections. *Brain Research Reviews,* 21**,** 301-314.
238. YEOMANS, J. S., LI, L., SCOTT, B. W. & FRANKLAND, P. W. 2002. Tactile, acoustic and vestibular systems sum to elicit the startle reflex. *Neuroscience and Biobehavioral Reviews,* 26**,** 1-11.
239. ZALOCUSKY, K. & DEISSEROTH, K. 2013. Optogenetics in the behaving rat: integration of diverse new technologies in a vital animal model. *Optogenetics.*
240. ZHANG, L., BAO, S. & MERZENICH, M. 2001. Persistent and specific influences of early acoustic environments on primary auditory cortex. *Nature Neuroscience,* 4**,** 1123-1130.
241. ZHANG, L., BAO, S. & MERZENICH, M. 2002. Disruption of primary auditory cortex by synchronous auditory inputs during a critical period. *Proceedings of the National Academy of Sciences of the United States of America,* 99**,** 2309-2314.
242. ZHANG, Y. F., HAMILTON, S. E., NATHANSON, N. M. & YAN, J. 2006. Decreased input-specific plasticity of the auditory cortex in mice lacking M-1 muscarinic acetylcholine receptors. *Cerebral Cortex,* 16**,** 1258-1265.
243. ZHOU, X. & MERZENICH, M. 2008. Enduring effects of early structured noise exposure on temporal modulation in the primary auditory cortex. *Proceedings of the National Academy of Sciences of the United States of America,* 105**,** 4423-4428.
244. ZHOU, X., PANIZZUTTI, R., DE VILLERS-SIDANI, E., MADEIRA, C. & MERZENICH, M. 2011. Natural Restoration of Critical Period Plasticity in the Juvenile and Adult Primary Auditory Cortex. *Journal of Neuroscience,* 31**,** 5625-5634.
245. ZILLES, K., PALOMERO-GALLAGHER, N., GREFKES, C., SCHEPERJANS, F., BOY, C., AMUNTS, K. & SCHLEICHER, A. 2002a. Architectonics of the human cerebral cortex and transmitter receptor fingerprints: reconciling functional neuroanatomy and neurochemistry. *European Neuropsychopharmacology,* 12**,** 587-599.
246. ZILLES, K., SCHLEICHER, A., PALOMERO-GALLAGHER, N., GEYER, S., GREFKES, C., CHOI, H., BOY, C. & BAUER, A. 2002b. Reconciling functional neuroanatomy and neurochemistry: Architectonics of the human cerebral cortex and transmitter receptor fingerprints. *European Neuropsychopharmacology,* 12**,** S11-S12.
247. ZILLES, K. & WREE, A. 1985. Cortex: areal and laminar structure. *In:* PAXINOS, G. (ed.) *The Rat Nervous System. Forebrain and Midbrain.* New York: Academic Press.
248. ZILLES, K., ZILLES, B. & SCHLEICHER, A. 1980. A quantitative approach to cytoarchitectonics.6. The areal pattern of the cortex of the albino-rat. *Anatomy and Embryology,* 159**,** 335-360.
249. ZNAMENSKIY, P. & ZADOR, A. M. 2013. Corticostriatal neurons in auditory cortex drive decisions during auditory discrimination. *Nature,* 497**,** 482-+.
250. ZONG, X. G., KRAUSE, S., CHEN, C. C., KRUGER, J., GRUNER, C., CAO-EHLKER, X., FENSKE, S., WAHL-SCHOTT, C. & BIEL, M. 2012. Regulation of Hyperpolarization-activated Cyclic Nucleotide-gated (HCN) Channel Activity by cCMP. *Journal of Biological Chemistry,* 287**,** 26506-26512.

11. List of author's publications

Publications related to the thesis:

With impact factor:

Popelář J., Šuta D., Lindovský J., Bureš Z., **Pysanenko K.**, Chumak T. and Syka J. Cooling of the auditory cortex modifies neuronal activity in the inferior colliculus in rats. Hearing Research, February 2016, Vol: 332, pp: 7–16. ISSN: 0378-5955. **IF: 2.906**

Pysanenko K. *, Bureš Z., Lindovský J. and Syka J., The effect of complex acoustic environment during early development on the responses of auditory cortex neurons in rats. Neuroscience, February 2018; Vol. 371, pp: 221-228. doi: 10.1016/j.neuroscience.2017.11.049. **IF: 3.277**

Lindovský J., **Pysanenko K.**, Popelář J. and Syka J. Fast tonotopy mapping of the rat auditory cortex with a custom-made electrode array. Physiological Research, submitted December 18, 2017; Refference number 933835. **IF: 1.461**

Bureš Z., **Pysanenko K.**, Lindovský J. and Syka J. Acoustical enrichment during early development improves response reliability in the adult auditory cortex of the rat. Neural Plasticity, submitted December 12, 2017; Refference number 5903720. **IF: 3.054**

Other author's publications:

With impact factor:

Hruskova B., Trojanova J., Kulik A., Kralikova M., **Pysanenko K.,** Bures Z., Syka J., O. Trussel L., and Turecek R. Differential distribution of glycine receptor subtypes at the rat calyx of Held synapse. The Journal of Neuroscience, November 2012, Vol. 32, Issue 47, pp: 17012-17024. ISSN: 0270-6474. **IF: 8.38**

* Corresponding author